ROTATION RATES OF ALGOL-TYPE BINARIES
FROM ABSORPTION LINE PROFILES

By

JAYDEEP MUKHERJEE

A DISSERTATION PRESENTED TO THE GRADUATE SCHOOL
OF THE UNIVERSITY OF FLORIDA IN PARTIAL FULFILLMENT
OF THE REQUIREMENTS FOR THE DEGREE OF
DOCTOR OF PHILOSOPHY

UNIVERSITY OF FLORIDA

1993

This dissertation is dedicated to my parents and to Dr. Deepak Chatterjee.

ACKNOWLEDGMENTS

A number of people have given me their time, support and guidance over the years that I have been here. I would like to express my gratitude to them and thank them for all their support.

First of all, I would like to thank the chairman of my committee, Dr. R.E. Wilson, who though being my advisor treated me as a friend and not a slaving graduate student. His patience and immense knowledge of binary stars made my thesis a very pleasant one. Also, our numerous tennis matches helped improve my game.

I would like to thank Dr. Oliver for all his help and for writing all those reference letters. I would also like to thank the other members of my committee, Dr. H. Smith, Dr. Dermott and Dr. Ghosh, for reading the thesis and for their constructive criticism. Special thanks go to Dr. Peters for making all the observations, which I have used in this thesis.

I would like to express my sincere appreciation to my fellow graduate student David Kaufmann, who time and again has helped me get out of a difficult spot. I thank him for his patience and understanding and for the long discussions on every topic that one can imagine, though just one victory in a tennis match would have been appreciated.

My special thanks go to the other graduate students especially, J.C. Liou, Damo Nair, Billy Cooke, and Sandra Clements. I would like to thank my office-mates Jane Morrison and Ricky Smart for putting up with me over the last three years.

Special thanks go as well to the department secretaries, Debra Hunter and Anne Elton, for their help with grants and for sending all those reference letters.

TABLE OF CONTENTS

LIST OF TABLES

LIST OF FIGURES

Abstract of Dissertation Presented to the Graduate School
of the University of Florida in Partial Fulfillment of the
Requirements for the Degree of Doctor of Philosophy

ROTATION RATES OF ALGOL-TYPE BINARIES
FROM ABSORPTION LINE PROFILES

By

Jaydeep Mukherjee

December, 1993

Chairman: R.E. Wilson
Major Department: Astronomy

Rotational velocities of stars normally are determined from spectral line widths by

means of a calibration of width versus v *sin i* from suitable standards. Over the last

few years, it has been possible to extract rotation rates from light curves of binary

systems. The light curve model has been mainly used to compute theoretical light

curves, which is to say that it deals mainly with continuum radiation rather than line

radiation. However, the model can be used to predict the behavior of absorption lines.

The dissertation consists of modelling and fitting line profiles generated by a program

that includes the main local broadening mechanisms (damping, thermal, rotational and

micro-turbulent broadening, etc.) and binary star effects (gravity and limb darkening,

ellipsoidal variation, rotational distortion, etc.).

Previous estimates of rotation from line profiles assumed that all or most other

broadening effects are negligible compared to rotational broadening. This means that

the previous methods are at their best for fast rotators and at their worst for slow

rotators. However, it is for the slow and moderate rotators that information is most needed, because light curves are beginning to provide rotation rates for the fastest rotators, and the light curve method is best for fast rotation.

Knowledge of rotation rates of mass transferring binaries will be useful in gathering information on mass transfer rates and the general mass transfer process and hence on the nature of close binary star evolution. It will also help us ascertain how well rotational velocities can be determined from light curves. Finally, it will help us establish the statistical distributions of Algol rotations, including how many systems are close to, or in, double contact (both components filling up their limiting lobes, one Roche and the other rotational).

CHAPTER 1
INTRODUCTION

Overview of the Problem

Traditional methods for determining stellar rotation rates from absorption line profiles neglect most or all other broadening mechanisms. They are subjective and do not provide standard error estimates. Previous models also neglected effects such as gravity darkening, limb darkening, reflection, tidal distortion, and eclipses. The measurement of line profiles can provide much information about a stellar atmosphere. It can tell about element abundances, surface gravity, and turbulence. Due to developments in detectors such as CCDs it is possible to get high resolution spectra, which is very important if one wants to analyze line profiles.

One of the most important fundamental parameters of a star is its rate of axial rotation (surface rotation). This parameter affects the shape of the star and the distribution of light over the surface. By analyzing eclipsing binary systems, both photometrically and spectroscopically, and combining the results, one can get values of fundamental astrophysical parameters such as mass, radius, and luminosity. To ensure accurate determinations of these fundamental parameters one must have accurate light curve solutions. This can be achieved by treating all the parameters correctly, including rotation.

One parameter that can be obtained from light curve solutions is the rate of axial rotation. However, this determination may not be easy in practice because of correlations of the rotation parameter with other parameters. It is difficult to discuss the

1

correlations, but previous work by various authors has shown that rotation rates can be strongly determined for some fast rotators. For slow rotators and in-between cases one has to rely on line profile analysis, which is the subject of this dissertation.

Knowledge of rotation rates yields important information on the evolutionary status of a star. In particular, if there is a binary system in which one of the components is rotating rapidly and there is evidence of a gas stream between components, which implies a slow rate of mass transfer, one can infer that there was a recent large-scale mass and angular momentum transfer. If there is a binary system where the components are in synchronous rotation and there is evidence of circumstellar matter around one of the components, as in the case of some Algol-type binaries, one can infer that the component was once in rapid rotation but tidal braking has slowed the rotation to near synchronism. There are cases of binary systems in which one of the components is surrounded by a thick accretion disk. In this case, the system is in a rapid phase of mass transfer and possibly the gainer of this mass is in rapid rotation. Thus statistics of primary star rotation, especially of Algol types, will provide information on the mass transfer process and therefore on close binary evolution.

Roche Lobes

For binary star systems the idea of level surfaces (equipotentials) is used to define the shapes of the stars. In the case of synchronous rotation, the largest equipotential surface that completely encloses one star or the other is the one that includes the inner Lagrangian (L_1) point (see Figure 1). At this point, the sum of the two forces (gravitational and centrifugal) equals zero. The volume enclosed by the equipotential

surface which passes through the L_1 point is called the Roche lobe. The whole system is assumed to have uniform angular rotation about the center of mass.

If one considers a system in which star 1 is filling up its Roche lobe and star 2 is not (i.e., a semidetached system), then, if star 1 tries to expand (due to evolution) there will be mass transfer onto the second star. This is because at the balance point the material from the lobe-filling star faces a vacuum and will flow toward the second star. Actually, the material in the whole photosphere faces a vacuum, but everywhere, except at the balance point, the outward pressure is balanced by the inward effective gravity and so the star does not expand (except slowly due to evolution). However, the balance point is a null point of effective gravity, and so there is nothing to stop the flow of matter from star 1 to star 2 in a small region around L_1 (see Figure 1).
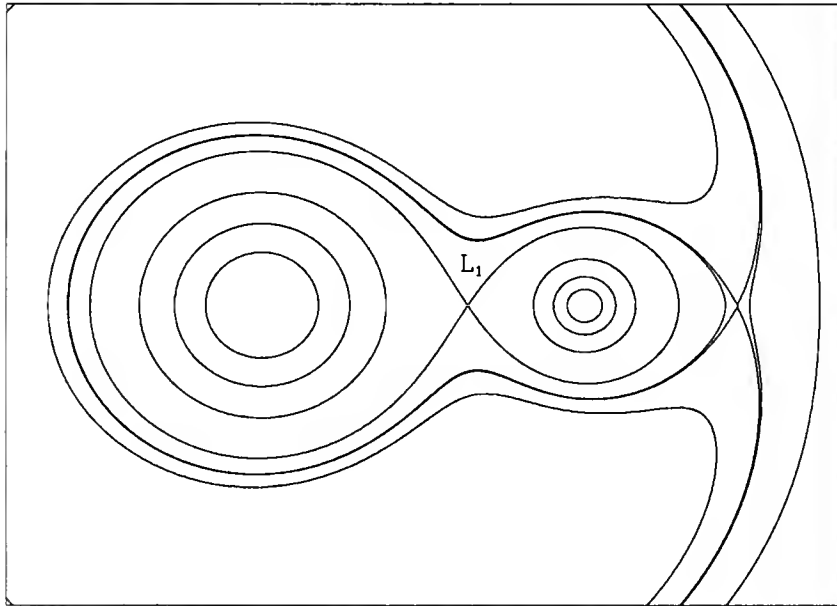
Figure 1: Equipotential diagram (mass ratio = 0.25)

Mass transfer will continue until there is pressure equilibrium across the balance point, when there will be no more need for mass transfer and the stars will be able to support a common envelope (<u>overcontact</u> system). If the system extends still further out, it can reach outer contact. The equipotential, which includes the outer Lagrangian point, L_2, will limit the size of the system as a whole because L_2 is a null point of effective gravity and material can flow from the system at this point. If the two masses are equal, one could get another outer contact surface on the left hand side (behind the higher mass star), but if $m_1 > m_2$ this configuration could never be reached since mass escapes from L_2. L_2 is at a lower potential than L_3 and is always behind the lower mass star.

In defining these categories, certain assumptions have to be made. They are as follows:

i. The stars are point masses. (Real stars are very centrally condensed, even on the main sequence, and as they evolve they become more condensed.)

ii. Orbits are circular. In many close binaries, tidal effects will circularize the orbits, under commonly found circumstances.

iii. The stars rotate synchronously, at least near their surfaces. This often is a valid assumption, unless there is an active spin-up or spin-down mechanism such as mass transfer. However, there are models that take asynchronism into account.

iv. Radiation pressure can be neglected. This effect can be added if necessary and should not pose a problem unless the radiation comes from outside the star.

If the mass receiving star rotates faster than synchronously, the balance point moves closer to the star, thus shrinking the limiting lobe. If one star has filled its Roche lobe

and the other has filled its rotational lobe, the binary is called a <u>double contact</u> system (Wilson, 1979).

Algols

The primary star is a main sequence star in the hydrogen burning stage and is chemically uniform or nearly so. The secondary is a subgiant and usually is the larger star, with a helium enriched core. The mass ratio (m_2/m_1) ranges from about 0.1 to 0.35. In Algol type systems the primary (m_1) is the higher mass star. Star 2 is more evolved, usually a subgiant, except in very short period Algols. Originally, m_2 was the more massive star, filled up its Roche lobe, and transferred mass to the other star. Thus m_1 became more massive, leading to the Algol stage where it is now stable against mass transfer. The light curves of Algols have deep eclipses, which make them easy to discover.

Relation Between W Ser Systems and Algols

When mass transfer (M.T.) occurs in a close binary system, the matter expelled by the mass losing component can gain an appreciable amount of angular momentum along its path to the other component, and in typical Algols it begins with considerable angular momentum. The accreting part can cause the gainer to rotate faster than synchronously. It is found that quite a large fraction of angular momentum can be converted into rotational angular momentum (Wilson and Stothers, 1975). Calculations show that the secondary has to accrete only 5 to 10 percent of its original mass in order to spin up to its break-up rotational velocity (Packet 1981). The mass that is transferred early in the rapid phase is quickly assimilated by the original secondary (present primary), which

is spun up at the surface and to some extent internally. When the surface rotation rate reaches the limiting rate (i.e., the limiting velocity for which the surface gravity goes to zero for at least one point at the surface), no further accretion is possible and the accreting material has to accumulate into a thick geometrical disk. Such a system is a W Ser-type system (ex. RX Cas, SX Cas, β Lyr, W Ser). This is a class of binaries that was introduced by Plavec (1980). These systems are transferring mass at a relatively high rate, probably on the order of 10^{-6}–10^{-4} solar masses per year. W Ser stars show spectacular spectroscopic behavior due to large-scale ejection of matter from the system, as well as rotation and eclipse effects by circumstellar rings or disks and flow of gas from an evolved component into the ring or the disk. However, the thick and opaque disks make observations of W Ser systems very difficult.

One can learn more by looking at systems in which the rapid phase of mass transfer (R.P.M.T.) is just ending or has just ended. They can be recognized by the rapid rotation of their more massive components. These are called Rapidly Rotating Algols (RRAs). Some examples of RRAs are AQ Peg, RZ Sct and RW Per. This term was introduced by Wilson et al. (1985). It is presumed that after tidal braking has acted for a sufficient interval, RRAs will become normal Algol systems. Thus it seems reasonable to assume that the W Ser systems are in double contact and that some of the RRAs may be in double contact.

CHAPTER 2
ROTATIONAL VELOCITIES

The four basic methods for measuring axial rotation of stars are as follows:

1. Rotational modulation of light

2. Rossiter effect

3. Light curve analysis

4. Spectral line profile analysis

Rotational Modulation of Light

Apart from the sun and a few other stars (α Ori), none of the stars can be resolved as stellar disks. However, one can determine the rotation period of a nonuniform surface by studying the periodic changes in light that it produces. Slettebak (1985) divided this work into two categories: (a) study of a variable continuous spectrum as star spots appear and disappear on the rotating disk, and (b) measurements of the variation in strength of emission lines (e.g., Ca II, H and K) that arise in plages in a rotating chromosphere.

Rossiter Effect

As a star rotates, one of the limbs will be moving towards us and the other away from us. As a result the spectrum lines are normally symmetrically broadened by the Doppler effect. Assuming direct rotation, when one of the stars (star 1) is entering eclipse, one of its limbs is gradually covered by the eclipsing star (star 2). Thus lines from star 1 are fully broadened on one side only (Figure 2). When these lines are measured for the

determination of radial velocity, the center of density of the line will be shifted towards the broadened edge and away from the center of the symmetrical line. The measured center of the line is thus displaced towards the region of longer wavelengths. The radial velocities are then too large positively. When the star is emerging from eclipse, the receding limb is covered and the approaching limb is visible. Thus the measured center of the line is displaced towards the region of shorter wavelengths and the radial velocities are too large negatively. This is called the Rossiter effect (Rossiter, 1924).
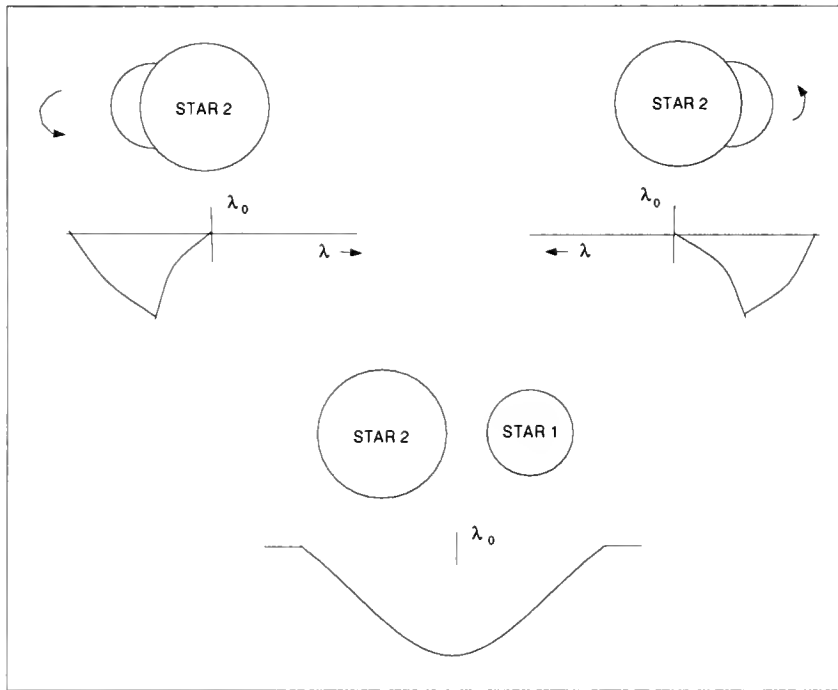
Figure 2: Rossiter effect (Twigg, 1979)

Twigg (1979) determined $V_{eq.}$ for 19 Algol systems by carefully analyzing the Rossiter effect. An example of a binary system showing the Rossiter effect is shown in Figure 3. He used Wilson and Devinney's (1971) light curve program for the analysis.

Twigg's procedure was iterative since a computer program for the simultaneous solution of photometric and spectroscopic data was not available then. He first used the light curve program to get a good fit with an assumed value F (see section on light curve analysis for a definition of F). Then the theoretical radial velocity curve was plotted against the observed one in order to check the amplitude of the Rossiter effect. If the initial guess of F and hence the amplitude of the Rossiter effect was incorrect, then light curve runs were carried out for another value of F, until the correct amplitude was achieved. Twigg then carried out a light curve differential correction solution for the new F.
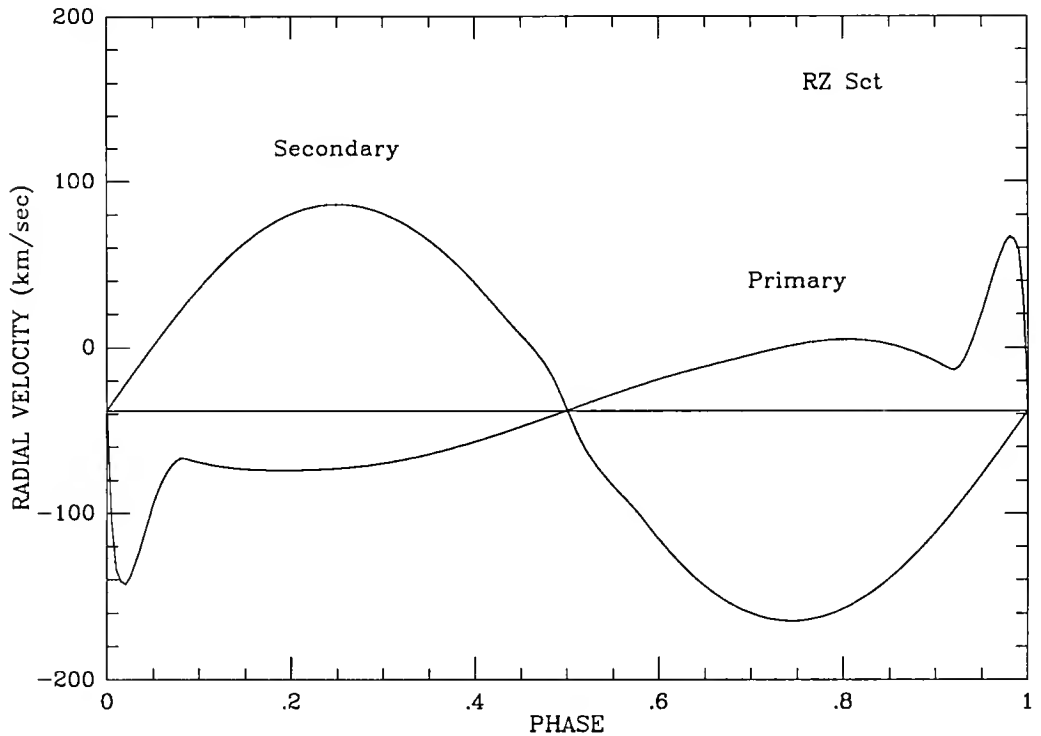
Figure 3: Radial velocity curve of a model of RZ Sct, showing the Rossiter effect.

Light Curve Analysis

Determination of rotation rates from light curves was introduced by Wilson (1979) and Wilson et al. (1985). Rotation affects the figure of a binary component and hence its surface brightness distribution. These rotational effects influence light curves. Rotation of the primary component will result in polar flattening, which in turn influences the shapes and depths of the eclipses. The brightness ratio of the primary to the secondary star also influences eclipse depths but is less obvious. If a component of a binary system is in rapid rotation it is less bright, seen equator on, than a slow rotator with the same mean effective temperature. As a result the tidally distorted secondary provides an increased fraction of the system light. Thus there is an increase in the observable ellipsoidal variation. Since the primary has polar flattening, the secondary intercepts relatively little of the primary's emission. This reduces the reflection effect. All these effects help in estimating the rotation rate, especially for fast rotation. Figure 4 shows light curves of RY Gem for both synchronous and nonsynchronous rotation.

One can compute light curves from given parameters using a light curve program (e.g., Wilson and Devinney, 1971, Wilson 1979). To compute the parameters from the observations one applies the method of differential corrections (Wilson and Devinney, 1971), using the expression for the total differential of the light values,

$$f(obs) \; - \; f(comp.) \; = \frac{\partial f}{\partial P_1} \, \Delta P_1 + \frac{\partial f}{\partial P_2} \Delta P_2 + \text{.......} + \frac{\partial f}{\partial P_n} \Delta P_n \qquad (2.1)$$

as the equation of condition for a linear least squares analysis. Here P_1, P_2,.....,P_n are adjustable parameters. The quantity *f(obs)* is a light value (i.e., relative flux) from

photometric observations. ΔP_1, ΔP_2, ...etc. are the parameter corrections which will be determined by least squares, and *f(comp.)* is to be computed from a light curve program. The derivatives, $\partial f / \partial P$, are to be found by

$$\frac{\partial f}{\partial P} = \frac{f(P + \frac{\Delta P}{2}) - f(P - \frac{\partial P}{2})}{\Delta P}.$$ (2.2)

The increments in P must be within a reasonable range (neither too small nor too large).

An important parameter is F, the ratio of spin angular speed to orbital angular speed. Although it is included in the list of parameters in the light curve model, one is not sure about the reliability of an estimated value of F obtained from a solution. The determination of F depends on how large the effects of rotation on the light curves are, and on how serious the correlations between F and the other parameters are. Wilson (1989b) has plotted rotational effects (polar flattening and equatorial dimming) vs. F/F(critical). It was seen that departures from the synchronous case grow slowly at first, reaching only about 18 percent of the full effect when F/F(critical) is 0.5. Previous work has shown that, at least for fast rotators, solutions for F often converge well. For known fast rotators the Differential Correction method usually will find a large value of F even when starting with a small value. For known slow rotators it finds small values even when starting with large values.

Rotation rates have been determined from light curves for RZ Sct (Wilson et al. 1985), U Sge and RY Per (Van Hamme and Wilson, 1986b), AW Peg, AQ Peg, and SW Cyg (Wilson and Mukherjee, 1988), RW Mon and RY Gem (Van Hamme and Wilson, 1990) and TT Hya (Van Hamme and Wilson, 1993). All the above systems, except for U Sge, are fast rotators. In order to test the reliability of a value of F, one must

compare it with rotation rates obtained from other methods such as line profile analysis and the Rossiter effect.
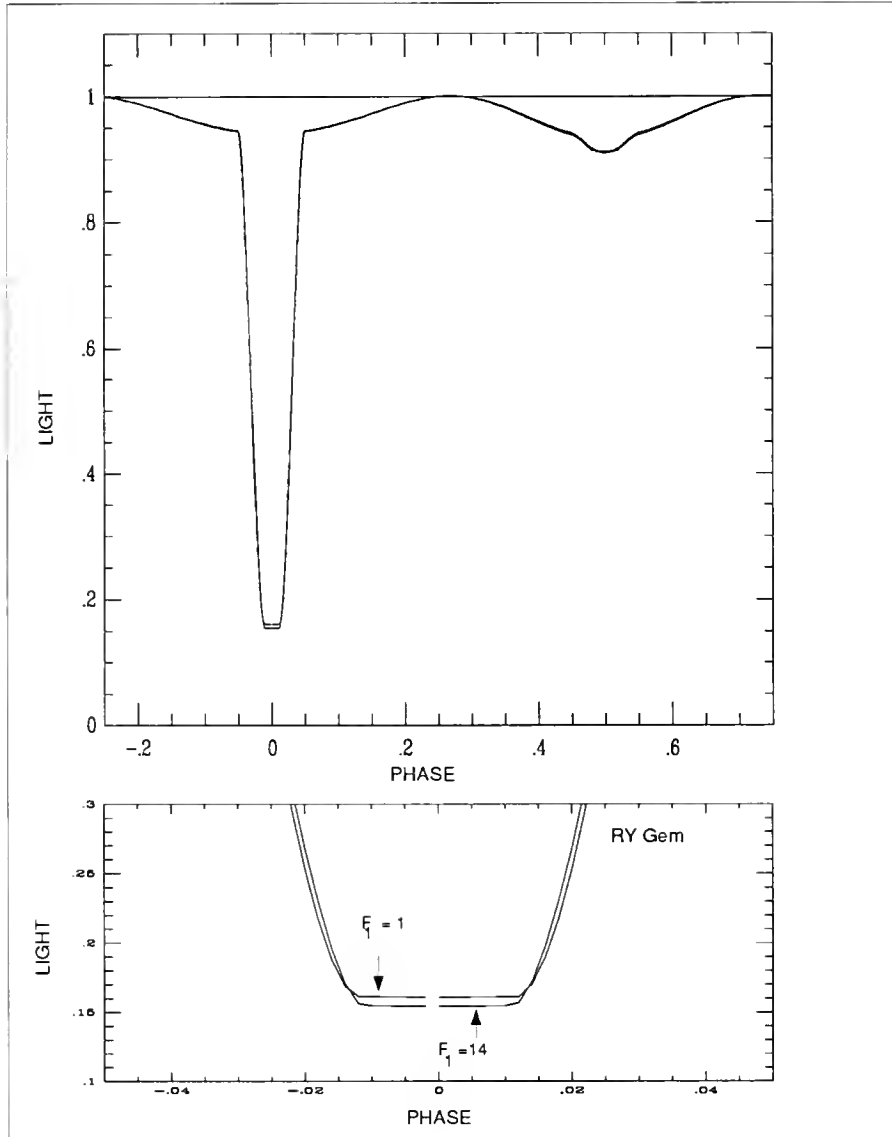
Figure 4: Figure showing light curves of RY Gem for both synchronous and nonsynchronous rotation.

Line Profile Analysis

Traditionally, the method used to obtain V_{eq} *sin i*, the projected equatorial rotational velocity of a star, is to match the observed profile of a spectral line with the corresponding profile of a standard star. The standard star is usually of the same spectral type and luminosity class as the observed star. This method may work for single stars but may have problems for binaries. The accuracy of V_{eq} *sin i* is the same as the reciprocal dispersion used in recording the spectrum. Thus to get accurate results one must have high resolution spectra.

Profile Fitting and Line-Width Measurements

Shapley and Nicholson (Slettebak, 1985) showed that an undarkened rotating stellar disk would broaden an infinitely sharp line into a semi-ellipse. Shajn and Struve (1929) developed a graphical method of computing rotationally broadened line profiles. The computed line profile is then compared with the observed line profile to give V *sin i*, the component of the rotational velocity in the line of sight. Following the graphical method of Shajn and Struve, Elvey (1930) determined the effect of axial rotation of a star on the contour of Mg II 4481. He assumed no limb darkening. Instead of using line profiles in the spectrum of the Moon as nonrotating lines, as had been done by Shajn and Struve, Elvey chose profiles from sharp-lined stars of early type. The computed contours were then compared with those observed in 59 stars of spectral classes O, B, A, and F.

Slettebak (Slettebak, 1985) and Slettebak and Howard (Slettebak, 1985) also used Shajn and Struve's graphical method, but included limb darkening effects to investigate stellar rotation in some 700 stars across the HR diagram. Collins (1974) calculated rotationally broadened line profiles for O9–F8 main sequence stars using the ATLAS

model atmosphere (Kurucz, 1970), taking into account the effects of limb darkening, gravity darkening and rotation.

Fourier Analysis

Fourier analysis of line profiles was introduced by Carroll (1933). The observed profile is a product of the transforms of the nonrotating profile and the rotational broadening function (Slettebak, 1985). Taking the Fourier transform of the observed profile and comparing the zeroes of the transform with the zeroes of the observed profile gives the value of v *sin i*. Gray (1976) has extended Carroll's method from a location of zeroes to a fitting of the entire transform.

Other Methods

Rucinski (1979) developed a line profile synthesis model where the spectral feature was assumed to have four lines (characterized by strength, d_i, and wavelength, λ_i), all broadened as Voigt profiles with the same damping constant 'a'. However he assumed that the primary star was spherical. Rucinski (1992) describes a method for determining the spectral-line broadening function based on simple linear mapping between sharp-line and broadline spectra. Anderson and Shu (1979) computed bolometric light curves and rotation broadening functions of contact binaries for a grid of values of mass ratio, filled fraction, and orbital inclination.

Vogt et al. (1987) describe a technique —Doppler imaging—for obtaining resolved images of certain rapidly rotating late-type spotted stars. There is a correspondence between wavelength position across a rotationally broadened spectral line and spatial position across the stellar disk. Cool spots on the surface of a rapidly rotating star produce distortions in the star's spectral lines. If the shapes of the spectral lines are

dominated by rotational Doppler broadening, as is the case with rapidly rotating stars, a high degree of correlation exists between the position of any distortion within a line profile and the position of the corresponding spot on the stellar surface. The above technique can therefore be modified to extract information on rotation.

Most of the previous modelling of line profiles assumed that all or most other broadening effects are negligible compared to rotational broadening. Thus the previous methods are at their best for fast rotators and at their worst for slow rotators. Since light curve analysis is beginning to provide rotation rates for the fastest rotators, information is most needed for the slow and moderate rotators.

Thus, one introduces a new method, which consists of modelling and fitting line profiles generated by a program that includes the main local broadening mechanisms (damping, thermal, rotational turbulent broadening, etc.) along with instrumental broadening and phase smearing, as well as binary star effects (tidal and rotational distortions, reflection effect, gravity darkening, limb darkening, etc.)

CHAPTER 3
THEORY OF ABSORPTION LINE PROFILES

Formation of Absorption Lines in Stellar Atmospheres

In the frequency range of an absorption line the absorption coefficient is composed of the coefficient of continuous absorption corresponding to bound-free and free-free transitions, added to the absorption coefficient corresponding to the discrete transition in question. Ionization results in bound-free transition and the acceleration of one charge as it passes close to another results in a free-free transition. Bound-bound transition gives rise to a spectral line. A point to note is that there is rarely a sharp transition between where the line absorption dominates the continuum absorption and vice versa. However for the development that follows it is assumed that a clear distinction does occur.

Equation of Radiative Transfer

Assume an axially symmetric radiation field that varies with θ but not with azimuthal angle ϕ. Energy crossing a differential area, dA, in time dt from the pencil of radiation in solid angle $d\Omega$ is given by

$$dE = I(\nu, x, \theta) \cos \theta \, d\Omega \, dt \, d\nu \, dA \qquad (3.1)$$

where

$I(\nu, x, \theta)$ is defined as the specific monochromatic intensity of radiation (ergs/cm^2/ sec/ Hz/ steradian)

ν is the frequency

16

x is the distance of the differential area dA from the surface, and

θ is the angle between the direction of the beam and the normal to the surface.

The difference between the amount of energy that emerges from the volume element and that incident must equal the amount created by emission from the material in the volume minus the amount absorbed. This is expressed by the equation of transfer, which is written as follows

$$\mu(\partial I_\nu/\partial \tau_\nu) = I_\nu - S_\nu \qquad (3.2)$$

where,

$\mu = \cos\theta$

τ_ν = optical depth, and

S_ν = source function = total emissivity/total opacity (ergs/cm^2/ sec/ Hz/ steradian)

The source function can be written as (Mihalas, 1978b)

$$S_\nu = \{[(1-\rho) + \varepsilon\beta_\nu]B_\nu + [\rho + (1-\varepsilon)\beta_\nu]J_\nu\}/(1+\beta_\nu) \qquad (3.3)$$

where,

$(1-\epsilon)$ refers to the fraction of photons absorbed that are scattered. Hence if $\epsilon = 1$, all emission is thermal (pure absorption) and if $\epsilon = 0$, then one has pure scattering.

ρ is defined as the ratio of continuum scattering coefficient to continuum opacity. If $\rho = 0$ there is no scattering in the continuum.

β_ν is defined as the ratio of line opacity to continuum opacity and can also be written as $\beta_0 H(a,\nu)$, $H(a,\nu)$ being the Hjerting function (see Chap. 5).

β_0 is defined as the ratio of line opacity to continuum opacity for a line with a Voigt profile (see page 30 in Chap. 3).

B_ν is the Planck's function

$J_\nu = \frac{1}{2} \int\limits_{-1}^{+1} I_\nu(\mu, \tau_\nu) d\mu$ and is known as the mean intensity.

Or, defining

$$\lambda_\nu = [(1 - \rho) + \varepsilon\beta_\nu]/(1 + \beta_\nu) \qquad (3.4)$$

the transfer equation becomes

$$\mu(\partial I_\nu/\partial\tau_\nu) = I_\nu - \lambda_\nu B_\nu - (1 - \lambda_\nu)J_\nu. \qquad (3.5)$$

The above equation is called the Milne-Eddington equation (Mihalas, 1978b). A point to note is that one assumes that line scattering is coherent and local thermal equilibrium holds. These are not accurate approximations.

The Milne-Eddington Model

Consider the Milne-Eddington equation under the assumptions that λ_ν, ε, and ρ are all constant with depth and that the Planck function B_ν is a linear function of the continuum optical depth τ (Mihalas, 1978c); i.e.,

$$B_\nu = a + b\tau = a + [b\tau_\nu/(1 + \beta_\nu)] = a + p_\nu\tau_\nu. \qquad (3.6)$$

Under these conditions an exact solution may be obtained (Chandrasekhar, 1947), but this solution differs only slightly from the approximate solution derived below.

Taking the zero-order moment of equation (3.5) one finds

$$dH_\nu/d\tau_\nu = J_\nu - (1 - \lambda_\nu)J_\nu - \lambda_\nu B_\nu = \lambda_\nu(J_\nu - B_\nu) \qquad (3.7)$$

where $H_\nu(\tau_\nu) = \frac{1}{2} \int\limits_{-1}^{+1} I_\nu(\tau_\nu, \mu)\mu d\mu$ and is called the Eddington flux. The first-order moment gives

$$\partial K_\nu/\partial\tau_\nu = H_\nu \qquad (3.8)$$

where $K_\nu = \frac{1}{2} \int\limits_{-1}^{+1} I_\nu(\tau_v, \mu)\mu^2 d\mu$ and is called the radiation pressure. Using the Eddington approximation $K_\nu = \frac{1}{3} J_\nu$ and substituting equation (3.8) for H_ν into equation (3.7), one obtains (Mihalas, 1978a)

$$\frac{1}{3}(\partial^2 J_\nu/\partial\tau_\nu^2) = \lambda_\nu(J_\nu - B_\nu) = \frac{1}{3}[\partial^2(J_\nu - B_\nu)/\partial\tau_\nu^2]. \qquad (3.9)$$

The solution to the above equation is (Mihalas, 1978c)

$$J_\nu = a + p_\nu\tau_\nu + (p_\nu - \sqrt{3}\,a)exp[-\sqrt{3\lambda_\nu}\,\tau_\nu]/[\sqrt{3} + \sqrt{3\lambda_\nu}]. \qquad (3.10)$$

Assuming that on a mean optical depth scale (Mihalas, 1978d),

$$B_\nu(\tau) = B_\nu(T_0) + (\partial B_\nu/\partial\tau)_0\tau = B_0 + B_1\tau \qquad (3.11)$$

and using the Eddington-approximation result for the grey temperature distribution, namely

$$T^4 = T_0^4(1 + 3/2\tau) \qquad (3.12)$$

one can show that (Mihalas, 1978d)

$$B_1 = \frac{3}{8}X_0 B_0, \qquad (3.13)$$

where

$$X_0 = u_0/(1 - e^{-u_0}) \qquad (3.14)$$

and

$$u_0 = (h\nu/kT_0). \qquad (3.15)$$

Thus the parameters in equation (3.6) are

$$a = B_0$$

$$b = \frac{3}{8}X_0 B_0(\bar{\kappa}/\kappa), \qquad (3.16)$$

where

$\bar{\kappa}$ = mean opacity, and κ = monochromatic continuum opacity

and

$$p_\nu = \frac{3}{8} X_0 B_0 (\bar{\kappa}/\kappa)/(1 + \beta_\nu). \tag{3.17}$$

Center-to-Limb Variation

The specific intensity at x=0 emergent at frequency ν, at an angle $\theta = cos^{-1}\mu$, is given by (Mihalas, 1978e)

$$I_\nu(0, \mu) = \int_0^\infty S_\nu(\tau_\nu) e^{-(\tau_\nu/\mu)} \mu^{-1} d\tau_\nu$$

$$= \int_0^\infty [B_\nu + (1 - \lambda_\nu)(J_\nu - B_\nu) exp(-\tau_\nu/\mu) \mu^{-1} d\tau_\nu \tag{3.18}$$

where the form of S_ν has been taken from equation (3.5). Substituting from equation (3.10) one gets

$$I_\nu(0, \mu) = (a + p_\nu \mu) + \{[(p_\nu - \sqrt{3}a)(1 - \lambda_\nu)]/[\sqrt{3}(1 + \lambda_\nu)(1 + \sqrt{3\lambda_\nu}\mu)]\}. \tag{3.19}$$

In the continuum, $\beta_\nu = 0$, hence

$$I_c(0, \mu) = a + b\mu + \frac{[(b - \sqrt{3}a)\rho]}{[\sqrt{3}(1 + \sqrt{(1 - \rho)})(1 + \sqrt{3(1 - \rho)}\mu)]}. \tag{3.20}$$

If there is no continuum scattering i.e., $\rho = 0$ then

$$I_c(0, \mu) = a + b\mu . \tag{3.21}$$

The residual intensity is given by

$$r_\nu(\mu) = I_\nu(0, \mu)/I_c(0, \mu) \tag{3.22}$$

and the absorption depth

$$a_\nu(\mu) = 1 - r_\nu(\mu) \,.$$

<div align="right">(3.23)</div>

For a pure absorption line, $\varepsilon = 1, \lambda_\nu = 1$ and the residual intensity is given by

$$r_\nu(\mu) = [1 + (b/a)\mu/(1 + \beta_\nu)]/[1 + (b/a)\mu] \,.$$

<div align="right">(3.24)</div>

Line Broadening Mechanisms

Natural Line Broadening

If a photon passes very close to a bound electron, the electron will oscillate in response to the photon's electric field. Classical broadening occurs because the bound electron can oscillate in frequencies not exactly at resonance. Thus a radiating atom emits a damped wave that gradually dies out, or it emits a wave of fixed frequency ν for a short time interval. If either kind of wave is Fourier analyzed, it is found that it is not monochromatic but consists of a narrow range of frequencies (Aller, 1963).

Quantum mechanically, although each emitted quantum has a precise energy E and frequency ν, the atomic energy levels themselves are actually fuzzy. This is due to Heisenberg's principle. According to that principle, $\Delta E \Delta t \sim h$ where ΔE is the energy width of the level and Δt is the lifetime of the energy level. The lifetime of a ground level is very long, hence ΔE is very small and the level is quite sharp. For an excited level, Δt is small, hence ΔE will be relatively large. Since the transition can take place from any part of the broadened level, the observed spectral line will be slightly widened (Aller, 1963).

Let the line absorption coefficient be denoted by α. Then from classical electro-dynamics one gets

$$\alpha = (e^2/mc)[(\gamma/4\pi)/\{(\Delta\nu^2) + (\gamma/4\pi)^2\}] \qquad (3.25)$$

The above equation is called the dispersion profile. γ is called the damping constant.

From classical dipole emission (Carpenter et al., 1984),

$$\gamma_{classical} = 0.22 \times 10^{16}/\lambda^2 \; (sec^{-1}) \; ; \; \lambda \; in \; A \; . \qquad (3.26)$$

In the above equation, γ_c is called the classical damping factor because it fixes the rate at which oscillations are damped as a result of the radiation process. The classical damping constant is usually smaller by an order of magnitude than inferred from observations and a quantum mechanical interpretation must be made.

If the transitions take place between two excited levels (u and l), the transitions from those levels will result in the broadening of the line and the value of γ will have the form (Collins, 1989a)

$$\gamma_r = \sum_{E_i < E_l} A_{li} + \sum_{E_i < E_u} A_{uj} \; , \qquad (3.27)$$

where

A_{li} = transition probability from level l (lower level) to level i.

A_{ui} = transition probability from level u (upper level) to level j.

One can also have broadening by electron collisions (γ_e). Then $\gamma = \gamma_r + \gamma_e$, although γ_e is always much smaller than γ_r.

Collisional Broadening

Interaction of neighboring particles with the absorbing atoms also can result in the broadening of spectral lines. Usually the particles are charged and their potential will interact with that of the atomic nucleus and thus perturb the energy levels of the atom (Collins, 1989b). The net result of all these perturbations is to broaden the spectral line. As in the case of radiation damping, one gets an absorption coefficient of the form

$$\alpha_\nu = (e^2/mc)\{[(\gamma_c/4\pi)]/[(\Delta\nu)^2 + (\gamma_c/4\pi)^2]\} \tag{3.28}$$

Here γ_c is the collisional damping constant.

If one takes into account simultaneous radiation and collisional damping, then the form of the absorption coefficient remains the same, except one has to introduce $\gamma = \gamma_c + \gamma_r + \gamma_e$. Thus,

$$\alpha_\nu = (e^2/mc)\{[(\gamma/4\pi)]/[(\Delta\nu)^2 + (\gamma/4\pi)^2]\} \tag{3.29}$$

Here α_ν is the absorption coefficient per oscillator.

So far the absorption coefficient has been given for an oscillator. To find the absorption coefficient per atom one has to find an expression that relates the number of oscillators $\bar{n}$ to the number of atoms or ions n in the state from which the transition begins. One introduces a quantity called the oscillator strength f ($\bar{n}=fn$). Thus the oscillator strength f gives the number of classical oscillators that reproduce the absorbing action of one atom in the given line. Therefore the absorption cross section per atom is given by

$$\alpha_\nu = (e^2 f/mc)\{[(\gamma/4\pi)]/[(\Delta\nu)^2 + (\gamma/4\pi)^2]\} \tag{3.30}$$

Radiation damping is of primary importance for strong lines in low density media. However in most cases collisional damping is significant.

Thermal Broadening

Another process that leads to the broadening of lines is the Doppler effect, brought about by the motion of the absorbing and emitting atoms. Even if damping by radiation or collision were absent, the absorption line would still be broadened due to the velocities of atoms or ions taking part in the absorption process (Ambartsumyan, 1958). The absorption cross section per atom due to the thermal process can be written as

$$\alpha_\nu = (\sqrt{\pi} e^2 f / mc\Delta\nu_D)[exp\{-(\Delta\nu)^2/(\Delta\nu_D)^2\}] \qquad (3.31)$$

where,

$\Delta\nu_D$ = Doppler width = $(\nu/c)\sqrt{2kT/m}$

m = mass of the atom considered

k = Boltzmann's constant

T = temperature

If both damping and thermal broadening are significant, a spectral line will have a core that is dominated by Doppler broadening while its wings are dominated by the damping profile.

Turbulence

Introduction. Motions of photospheric gas on a scale large compared to atomic dimensions but small compared to the size of the star are called turbulence. Turbulence alters the line profiles in a stellar spectrum through Doppler displacements. If one assumes that these turbulent velocities have a velocity distribution similar to the

distribution of thermal velocities (i.e., Gaussian), the resulting velocity distribution is again given by a Gaussian with a reference velocity

$$\xi_0^2 = \xi_{thermal}^2 + \xi_{turbulence}^2 \cdot \tag{3.32}$$

Therefore,

$$\Delta\nu_D = (\nu/c)\sqrt{(2kT/m) + \xi_{turbulence}^2} \tag{3.33}$$

and

$$\alpha_\nu = (\sqrt{\pi}e^2 f/mc\Delta\nu_D)\{exp - [(\Delta\nu)^2/(\Delta\nu_D)^2]\} \cdot \tag{3.34}$$

Turbulence is characterized by the Reynold's number (Gray, 1988) and is defined by the product of density, average flow velocity, and linear dimensions across the tube containing the flow, divided by the viscosity. If this number exceeds 1000, turbulence is expected. It is difficult to estimate the Reynold's number for a stellar atmosphere. Gray (1988) made some numerical calculations and came up with a number around 3×10^{13}. Such numbers indicate that a stellar atmosphere is certainly turbulent. Beckers describes turbulence as a word used "to describe motions which cause line broadening and changes in line saturation (curve of growth effects) but which are otherwise intangible as a specific kind of motion because of the absence of additional information such as spatial resolution, characteristic line profiles, line shifts, etc." (1980, p. 85). According to Beckers (1980), turbulence in astrophysics may have nothing or little to do with hydrodynamic turbulence. In astrophysics, turbulence can include convection, waves, stellar winds, large-scale flow patterns and even stellar rotation if the spectral resolution is insufficient to identify the characteristics of any of these non-thermal motions. The

observed velocity fields are better understood from the point of view of macroturbulence and microturbulence, which are the extremes of the cell-size spectrum.

Microturbulence. If the resolution of spectra is low, as in the early days, then one is limited to measuring equivalent width. One needs high resolution spectra to study line profiles. Equivalent width (W) is a measure of the total line strength and is defined as $W = \int\limits_0^\infty \frac{(F_c - F_\nu)}{F_c}$ where F_c and F_ν denote the continuum fluxes (before any instrumental distortion). W is the width of a perfectly black, rectangular absorption line having the same integrated strength as the real line. Early work found that curves of growth did not saturate as expected from theory. Struve and Elvey (1934) and others simply enhanced the thermal broadening beyond that corresponding to the known temperature, and this developed into the concept of microturbulence.

These velocities are much smaller than rotational velocities or turbulence dispersion. Strong lines are desaturated due to microturbulence such that the equivalent width increases. Weak lines reflect the Gaussian shape of the thermal and microturbulent velocity distributions (Gray, 1988). For weak lines, the opacity is small and hence a photon's mean free path is almost the same as the thickness of the line-forming region in the photosphere. Each absorbed photon displays the Doppler shift for the turbulent velocity of the material where it is absorbed (Gray, 1976). Microturbulence delays saturation by Doppler shifting the absorption over a wider spectral band (i.e. reducing τ_ν at each ν). In order to minimize thermal broadening, one should select lines from the heaviest possible elements. In practice, however, one has to select unblended lines, which is a more important criterion. Elements showing hyperfine structure also should be avoided. If there are other factors affecting the saturation portion then it becomes

difficult to measure the microturbulent velocity (ξ). Some of these are listed by Gray (1988):

i.   Non-LTE and $T(\tau)$ effects

ii. Systematic f-value errors

iii. Errors in damping constants: quite frequently the damping constant is stronger than expected according to classical theory.

iv. Zeeman splitting: magnetic broadening of the line absorption coefficient will delay saturation.

v.   Hyperfine structure

Recent investigations by Gray (1988) show that ξ increases with luminosity, but within any given luminosity class there is no strong change in ξ with effective temperature. For main sequence stars, a value of 1 km/sec is supported by some solar studies. However, others find higher values for ξ of about 3 km/sec (I. Furenlid, 1976). For dwarfs, a slight increase from 1.0 km/sec to $\approx$ 1.5 km/sec may occur with increasing effective temperature. A much larger temperature dependence was found using the older results reviewed by Gehren (1980).

Macroturbulence. If a cell of gas is significantly larger than the length corresponding to unit optical depth, it produces a specific intensity spectrum of its own, and that spectrum will be Doppler shifted according to the velocity of the cell. By assumption there is no differential motion within or across this cell, hence no change in the line absorption coefficient. This is the concept of macroturbulence (Gray, 1988).

In a review paper, Huang and Struve (1960) describe macroturbulent velocity as a geometrical effect rather than a physical effect. Thus macroturbulence has no effect on

the equivalent width. In general, one velocity is used to describe both types although it is very difficult to single out one characteristic velocity. The only way macroturbulence can be detected is from profiles. However, even at relatively high resolution, rotational broadening and macroturbulent broadening may not be separable.

Rotation

Due to rotation, one half of the star moves away from us, while the other half moves toward us. The component of motion in the direction of the line of sight is $v_y = v_r(\theta)sin\phi$, where $v_r(\theta)$ is the rotational velocity for the colatitude θ. For rigid body rotation $v_r(\theta) = v_e sin\theta$ and the velocity component v_y along the line of sight is $v_y = v_e sin\phi sin\theta$, where v_e is the equatorial rotational velocity and ϕ is the longitude. v_y is constant for all points on the sphere for which $sin\phi sin\theta$ is constant.

Combining Radiation, Collisions, and Thermal Motion

All the above broadening processes take place simultaneously. If one considers any two of the absorption coefficients and imagine the first one to be synthesized by a series of delta functions, then each of the delta functions experiences the broadening of the second absorption coefficient. Thus the two distributions must be convolved together to obtain a combined result. If one expands this to include all the processes, one gets a multiple convolution,

$$\alpha_{total} = \alpha_{natural} * \alpha_{collisional} * \alpha_{thermal} . \qquad (3.35)$$

The first two coefficients have a dispersion profile. If two dispersion profiles are convolved one gets a new dispersion profile with a damping constant, $\gamma = \gamma_{natural} + \gamma_{collisional}$. To obtain the total absorption coefficient, one combines radiation, collisions

and thermal motion. Therefore,

$$\alpha_{total} = \pi e^2 f/mc\{(\gamma/4\pi^2)/[(\Delta\nu)^2 + (\gamma/4\pi)^2]\}$$

$$*\{[1/\sqrt{\pi}\Delta\nu_D]exp - [(\Delta\nu)^2/(\Delta\nu_D)^2]\} \ . \tag{3.36}$$

The convolution of the dispersion and Gaussian profile is called the Voigt function.

$$V(\Delta\nu, \Delta\nu_D, \gamma) = \{(\gamma/4\pi^2)/[(\Delta\nu)^2 + (\gamma/4\pi)^2]\}$$

$$*\{(1/\sqrt{\pi}\Delta\nu_D)exp - [(\Delta\nu)^2/(\Delta\nu_D)^2]\} \ . \tag{3.37}$$

The Voigt function is normalized to unit area.

$$V(\Delta\nu, \Delta\nu_D, \gamma) = \int_{-\infty}^{+\infty} \{(\gamma/4\pi^2)/[(\Delta\nu - \Delta\nu_1)^2 + (\gamma/4\pi)^2]\}$$

$$\times \{(1/\sqrt{\pi}\Delta\nu_D)exp - [(\Delta\nu_1/\Delta\nu_D)^2]\}d\Delta\nu_1. \tag{3.38}$$

Let

$$v = \Delta\nu/\Delta\nu_D \quad and \quad a = (\gamma/4\pi)/\Delta\nu_D. \tag{3.39}$$

The quantity a is different from the one described on page 19. Therefore,

$$V(a,v) = (1/\sqrt{\pi}\Delta\nu_D)(a/\pi) \int_{-\infty}^{+\infty} (e^{-y^2})/[(v - y)^2 + a^2]dy \tag{3.40}$$

where

$$y = (\nu - \nu_0)/\Delta\nu_D. \tag{3.41}$$

The Hjerting function $H(a,v)$ (Hjerting, 1938) is closely related to $V(a,v)$ as shown below.

$$V(a,v) = (1/\sqrt{\pi}\Delta\nu_D)H(a,v) \ . \tag{3.42}$$

Therefore

$$\alpha_\nu = (\sqrt{\pi}e^2/mc)(f/\Delta\nu_D)H(a,v) \, . \tag{3.43}$$

Let

$$\alpha_0 = (\sqrt{\pi}e^2/mc)(f/\Delta\nu_D) \, . \tag{3.44}$$

Thus, (Gray, 1976)

$$\alpha_\nu = \alpha_0 H(a,v) \, . \tag{3.45}$$

Instrumental Broadening

Assuming that the spectrometer is receiving strictly monochromatic radiation, the profile recorded by scanning the spectrum will have a finite width due to the effects of diffraction, slit width, and other causes such as aberrations. It is considered adequate to adopt a Gaussian profile for instrumental broadening.

If the energy distribution of the source as a function of λ is a triangular function $\delta(\lambda - \lambda_0)$ centered on the wavelength λ_0, the recorded spectrum will be a curve representing a function $\phi(\lambda' - \lambda)$. Then by definition $\phi(\lambda')$ is the instrumental profile of the spectrometer. The narrower the instrumental profile, the less the recorded curve $R(\lambda')$ departs from the true spectral energy distribution $R(\lambda)$ of the source. Therefore the recorded function is the convolution of the source function and the instrumental profile (Bousquet, 1971),

$$R(\lambda') = \int\limits_0^\infty R(\lambda)\phi(\lambda' - \lambda)d\lambda. \tag{3.46}$$

CHAPTER 4
DATA REDUCTION

Observations

The observations were made at the Kitt Peak National Observatory by Dr. Geraldine J. Peters from 1989 to 1991. The Coude Feed telescope with Camera 5 and the TI3 CCD detector was used to observe Algol systems in the spectral range $\lambda\lambda 4400$–4550. In order to study depth effects in the rotation one needs lines formed under a range of excitation energy. Two such lines are He I ($\lambda 4471$) and Mg II ($\lambda 4481$).

Corrections

The observed wavelengths must be corrected for the orbital revolution and axial rotation of the Earth. Since the observations were taken at a particular phase, the primary star's velocity around the center of mass can be computed by the light curve program as part of the synthesized velocity. Hence the observations need only to be corrected for the Earth's rotation and revolution. To compute the sun-earth system corrections one needs to know the time of observation (sidereal time), the co-ordinates of the star, the latitude and longitude of the observatory and the longitude of the Sun, which, is defined as the angle at the Earth between the direction of the Sun and the direction of the Vernal Equinox.

Correction for Earth's Rotation

For an observer on the Earth's equator at some point x, the eastward velocity of x

is $V(x)$ =circumference/seconds per sidereal day. If R is the radius of the earth, then

$$V(x) = 2\pi R/86164 = 0.47 \; km/sec \tag{4.1}$$

The velocity is reduced by a factor $cos \; \phi$, where ϕ is the observer's latitude. Therefore,

$$V(x) = 0.47 \cos \phi \; km/sec \tag{4.2}$$

A star's radial velocity will be affected by the earth's rotation. If V is the velocity of a star towards the west due to the eastward velocity of the observer at latitude ϕ, then the component of V which is in the direction of the star is given by (Birney, 1991),

$$V_d = 0.47 \cos \phi \cos \delta \sin \tau \; km/sec \tag{4.3}$$

where

δ = declination of the star, and

τ = hour angle of the star

Correction for Orbital Motion of the Earth

The observed radial velocity will also be affected by the earth's motion around the Sun. This is corrected by calculating the earth's orbital velocity and then finding the magnitude of the component of the velocity in the direction of the star. First an expression is found in terms of the star's ecliptic coordinates, celestial latitude, β, and longitude, λ. It is then transformed to an expression in terms of the star's equatorial coordinates, declination and right ascension.

The heliocentric orbital velocity of the earth (V_e) is obtained from the FORTRAN subroutine BARVEL (Stumpff, 1980). In terms of the star's ecliptic coordinates, the

component of the earth's orbital velocity (V_y) in the direction of the star S is given by (Birney, 1991)

$$V_y = -V_\epsilon \cos\beta \sin(\odot - \lambda) \qquad (4.4)$$

where

β and λ are the ecliptic coordinates of a star at S, and

$\odot$ = celestial longitude of the Sun = angle at the earth between the direction of the Sun and the direction of the Vernal Equinox.

In this equation the negative sign has been included to maintain the convention that the radial velocity is positive when the distance between the source and the observer is increasing.

Corrections in Right Ascension and Declination

One now has to convert the star's ecliptic coordinates to equatorial coordinates. The last term in eq. (4.4) can be written as

$$\sin(\odot - \lambda) = \sin\odot \cos\lambda - \cos\odot \sin\lambda \qquad (4.5)$$

After multiplying both sides by $\cos\beta$ and rearranging one gets

$$\cos\beta \sin(\odot - \lambda) = \cos\beta \cos\lambda \sin\odot - \cos\beta \sin\lambda \cos\odot \qquad (4.6)$$

$$V_y = -V_\epsilon(\cos\beta \cos\lambda \sin\odot - \cos\beta \sin\lambda \cos\odot) \qquad (4.7)$$

Thus one has to find expressions for ($\cos\beta\cos\lambda$) and ($\cos\beta\sin\lambda$).

The components of any vector in the ecliptic system (E) can be transformed to the equator system (Q) by pre–multiplying with $R_1(\epsilon)$, which is a matrix that rotates a coordinate system by the angle ϵ on the x-axis. Therefore,

$$\hat{x}^E(\lambda, [90 - \beta]) = R_1(\epsilon)\hat{x}^Q(\alpha, [90 - \delta]) \tag{4.8}$$

The present value of ϵ is approximately $23°27'$

$$\begin{pmatrix} \sin(90 - \beta)\cos\lambda \\ \sin(90 - \beta)\sin\lambda \\ \cos(90 - \beta) \end{pmatrix} = \begin{pmatrix} 1 & 0 & 0 \\ 0 & \cos\epsilon & \sin\epsilon \\ 0 & -\sin\epsilon & \cos\epsilon \end{pmatrix} \begin{pmatrix} \sin(90 - \delta)\cos\alpha \\ \sin(90 - \delta)\sin\alpha \\ \cos(90 - \delta) \end{pmatrix} \tag{4.9}$$

$$\begin{pmatrix} \cos\beta\cos\lambda \\ \cos\beta\sin\lambda \\ \sin\beta \end{pmatrix} = \begin{pmatrix} \cos\delta\cos\alpha \\ \cos\epsilon\cos\delta\sin\alpha + \sin\epsilon\sin\delta \\ \cos\epsilon\sin\delta - \sin\epsilon\cos\delta\sin\alpha \end{pmatrix} \tag{4.10}$$

The inverse relation is as follows

$$\hat{x}^Q(\alpha, [90 - \delta]) = R_1(-\epsilon)\hat{x}^E(\lambda, [90 - \beta]) \tag{4.11}$$

$$\begin{pmatrix} \cos\delta\cos\alpha \\ \cos\delta\sin\alpha \\ \sin\delta \end{pmatrix} = \begin{pmatrix} 1 & 0 & 0 \\ 0 & \cos\epsilon & -\sin\epsilon \\ 0 & \sin\epsilon & \cos\epsilon \end{pmatrix} \begin{pmatrix} \cos\delta\cos\alpha \\ \cos\delta\sin\alpha \\ \sin\delta \end{pmatrix} \tag{4.12}$$

From eq. (4.10)

$$\cos\beta\sin\lambda = \cos\epsilon\cos\delta\sin\alpha + \sin\epsilon\sin\delta \tag{4.13}$$

and,

$$\cos\beta\cos\lambda = \cos\delta\cos\alpha \tag{4.14}$$

Substituting eq. (4.13) and (4.14) in eq. (4.7) one gets, (Birney, 1991)

$$V_y = -V_e\{\cos\alpha\cos\delta\sin\odot - \cos\odot(\sin\delta\sin\epsilon + \cos\delta\cos\epsilon\alpha)\}$$

$$= -V_e\{\cos\delta\cos\alpha\sin\odot - \cos\odot\sin\delta\sin\epsilon - \cos\odot\cos\delta\cos\epsilon\sin\alpha\}$$

(4.15)

If V_M is the measured radial velocity before any corrections have been applied, and if V_R is the radial velocity with respect to the sun, then $V_R = V_M + V_d + V_y$. Once this velocity is known the shift in the wavelength can be calculated.

Observed Algol-Type Systems

Table 1 lists the binaries whose line profiles have been analyzed here. In this table the term "noisy lines" refers to those for which the spectral distributions have large scatter, whether due to observational noise or to large numbers of spectral lines. Any blending is usually with lines of the same star because Algol-type secondary stars are much less luminous than the primaries. The term "clean lines" refers to those which are reasonably free of scatter and blending. The resolution of the CCD as it was used is 0.15 Angstroms per pixel.

Table 1 : Stars observed by G.J. Peters

CLEAN LINES		BLENDED & NOISY LINES	
RZ Cas	β Per	S Cnc	TU Mon
TV Cas	Y Psc	U Cep	RW Per
S Equ	U Sge	SW Cyg	RY Per
RW Mon	Z Vul	RY Gem	RZ Sct
DM Per			

CHAPTER 5
METHOD OF ANALYSIS

Introduction

The line profile program has been combined with the light curve program (Wilson and Devinney, 1971), which normally generates light and velocity curves, but now is used for its computation of surface quantities within a physical binary star system. The line profile code generates an absorption line profile, given the damping constant, the effective number of absorbers along the line of sight, the micro-turbulent velocity, and the rotation rate.

Light Curve Code

This code computes light curves from given parameters (Wilson and Devinney, 1971), which are listed in Table 2. It computes light and radial velocities for each component for a given phase or a range of phases. As a part of its calculation it also computes the radial velocity and the intensity at angle θ relative to the outward normal direction (limb darkening law) of the elemental surface areas. Since the line profile (LP) code requires $\cos \theta$ (θ = aspect angle) and the local flux, both of which are calculated in the light curve (LC) code, it is very important to have a good photometric solution. The light curve code is used as a subroutine in the line profile code, which is described in the next section. The light curve code includes binary effects such as tidal and rotational distortions, reflection effect, gravity darkening, and limb darkening.

Table 2: List of parameters for the LC code

PARAMETER	DESCRIPTION
F_1, F_2	Ratio of spin angular speed to mean orbital angular speed for each component
i	Orbital inclination in degrees
ϕ_0	Phase shift : This parameter permits a phase shift of the computed light curves by an arbitrary amount. It is the phase at which primary conjunction would occur if the longitude of periastron (ω) were 90°. It is not the actual phase of primary conjunction unless the longitude of periastron equals 90° or the eccentricity (e) equals 0.
e	Orbital eccentricity
ω	Longitude of periastron (orbit of star 1) in degrees
g_1, g_2	Gravity darkening exponent for each component with value unity corresponding to classical (Von Zeipel) darkening (i.e. for stars with radiative envelopes)
A_1, A_2	Bolometric albedos of the components having values of 1.0 for radiative envelopes and 0.5 for convective envelopes.
P	Period in days
T_1, T_2	Mean surface temperatures of the components in Kelvins
Ω_1, Ω_2	Modified surface potential for each star, which specifies a surface of constant potential energy

Table 2– – (Continued)

PARAMETER	DESCRIPTION
q	Mass ratio (m_2/m_1)
a	Semi-major axis of the relative orbit ($a_1 + a_2$) in solar radii
V_γ	System velocity in km/sec
x_1, x_2	'Linear cosine law' limb darkening coefficients
L_1, L_2	Monochromatic luminosities of the stars at a particular wavelength. It is a 4π steradian light output, and hence it will be about 4π times as large as the computed (output) light of the model star, which is per steradian
l_3	Amount of third light present at a specified wavelength in the same unit as the computed light values.

Line Profile Code

The line profile code (LPDC) generates an absorption line profile as an array of wavelength and residual flux, given the line profile parameters listed in Table 3 along with the light curve parameters listed in Table 2. The other input quantities are listed in Table 4. All the parameters and input quantities are identified according to their FORTRAN names. The parameter fitting procedure is described later in this chapter. A flow chart of the code is shown in Figure 5.
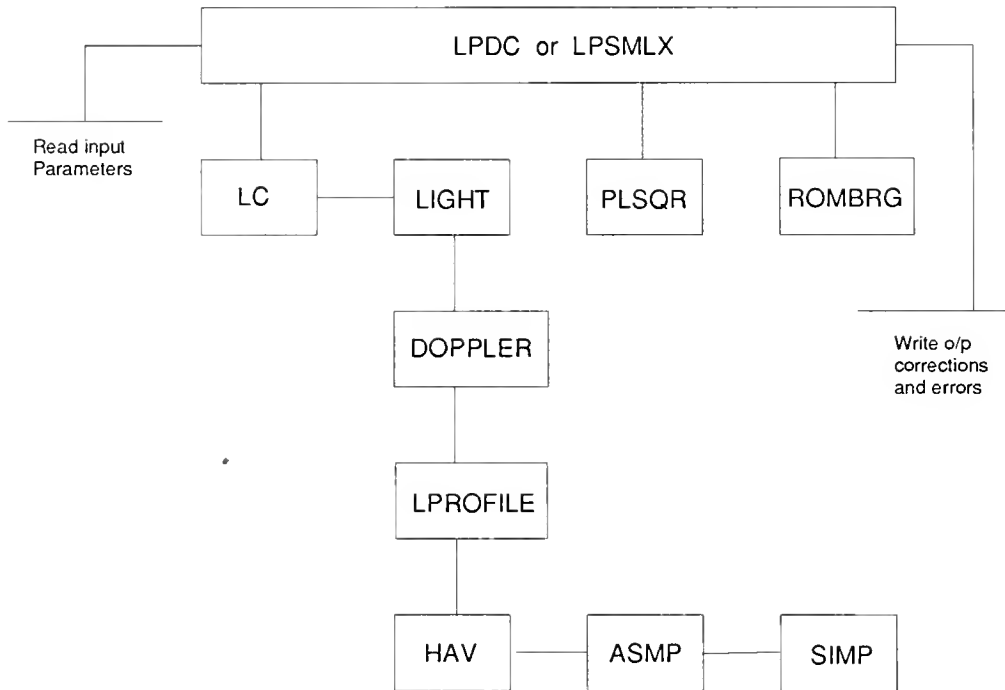
Figure 5: Flow chart of the Line Profile code

Table 3: Line Profile parameters

PARAMETERS (FORTRAN names)	DESCRIPTION
TEFF	Effective temperature
Nf	No. of absorbers along the line of sight
GAM	Damping constant (radiative + collisional)
TV	Micro-turbulent velocity (km/sec)
F1	Ratio of angular rotation speed to orbital angular speed for the primary star
RHOO	Ratio of continuum scattering coefficient to continuum opacity (ρ=0: No continuum scattering)
EPSILON	Fraction of the line emission due to thermal processes. ($\epsilon = 0$: Pure scattering) ($\epsilon = 1$: Pure absorption)

Table 4: Other input quantities for the Line Profile code

I/P QUANTITIES	DESCRIPTION
LAMBDA	Rest Wavelength in Angstrom Units
M	Atomic Weight of Element Producing the Line
INSTBR	Full width at half maximum of the Instrumental Profile
PHAS1	Phase at the beginning of observations
PHAS2	Phase at the midpoint of observations
PHAS3	Phase at the end of observations

Doppler Subroutine

This subroutine is called for each surface element by the LIGHT subroutine in the LC code. The central wavelength and the value of cos θ are inputs to this subroutine, which in turn calls the LINEPROF subroutine for each observed wavelength in the line profile. The central wavelength for each surface element will be different from the rest wavelength and will differ according to the velocity of each element. At each wavelength, LINEPROF calculates the residual intensity. Thus the output of DOPPLER is an array of wavelength and residual intensity for each area of the star.

Lineprof Subroutine

The input to this subroutine consists of the central wavelength, effective temperature, damping constant, micro-turbulent velocity, the number of absorbers along the line of sight, the atomic weight of the element producing the line, ratio of continuum scattering coefficient to continuum opacity, the fraction of line emission due to thermal processes, and the wavelength at which the residual intensity is to be calculated. One of the other inputs is the limb darkening factor, which is provided by the LIGHT subroutine. The output is the residual intensity at the wavelength specified.

The decrease in continuum strength as one approaches the limb of the apparent stellar disk is called limb darkening. For a spherical star, the outward normal direction corresponds to $\theta = 0^o$, or $\cos \theta = 1$. The ratio $I(\theta)/I(0)$, which gives the intensity at angle θ relative to the outward normal direction, is referred to as the limb darkening law. A rough approximation to real limb darkening is given by $I(\theta) = I(0)(1 - x + x \cos \theta)$. The coefficient x (provided by the light curve data file) used in the linear limb darkening equation is obtained from tables (e.g. Al Naimiy, 1978). These values are wavelength and temperature dependent. Limb darkening also affects line strengths. Figure 6 shows how limb darkening changes the line profile (pure absorption line). For a pure absorption line as the limb is approached, the line vanishes.

Figure 7 shows how the intrinsic line profile changes as the effective temperature, number of absorbers, damping constant and the micro-turbulent velocity are changed. Here one is assuming a pure absorption line. Figure 8 shows the variation of the intrinsic line profile when the parameters ρ and ϵ (see Table 3) are changed.
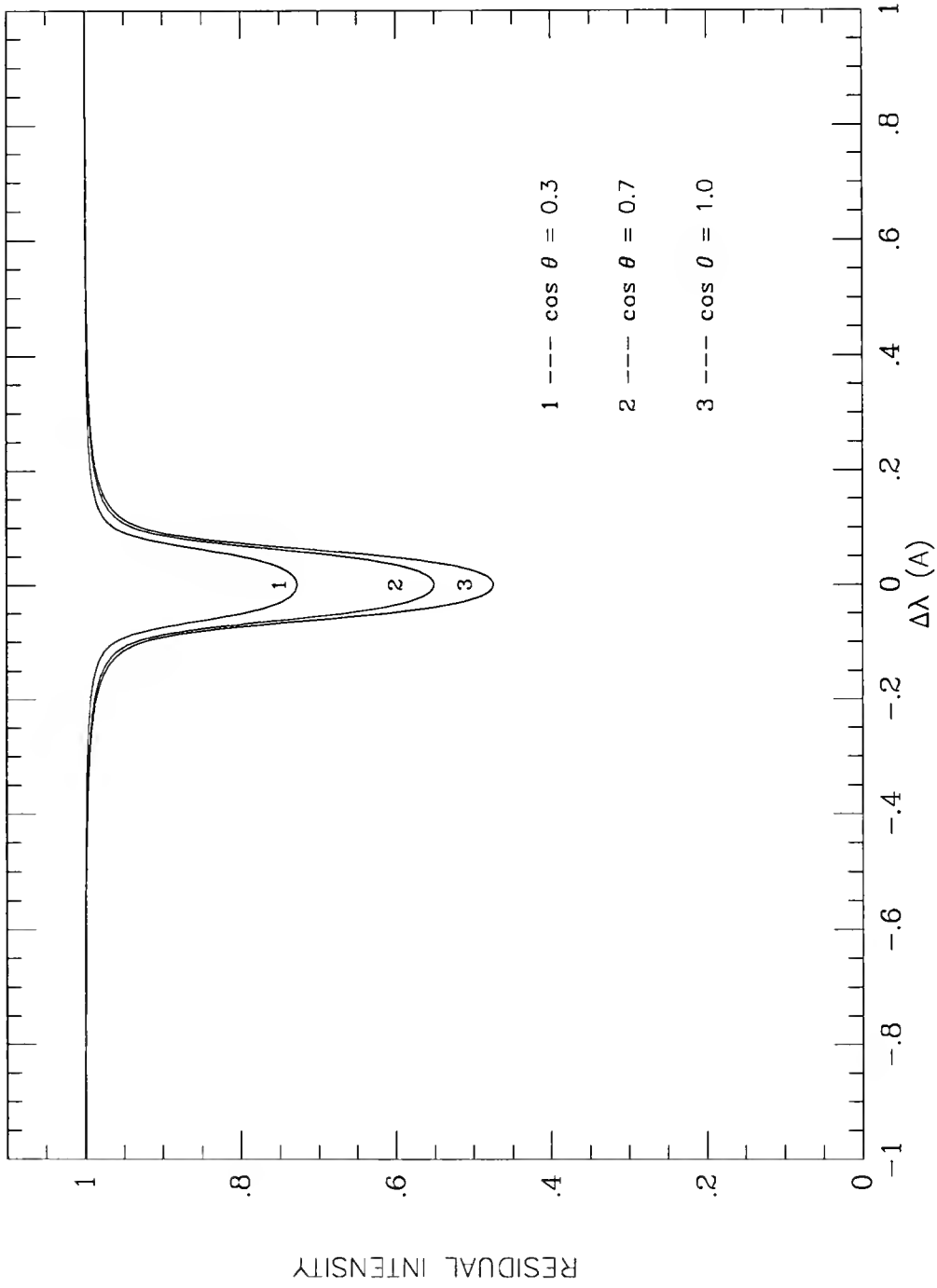
Figure 6: Variation in line profiles (pure absorption lines) due to limb darkening
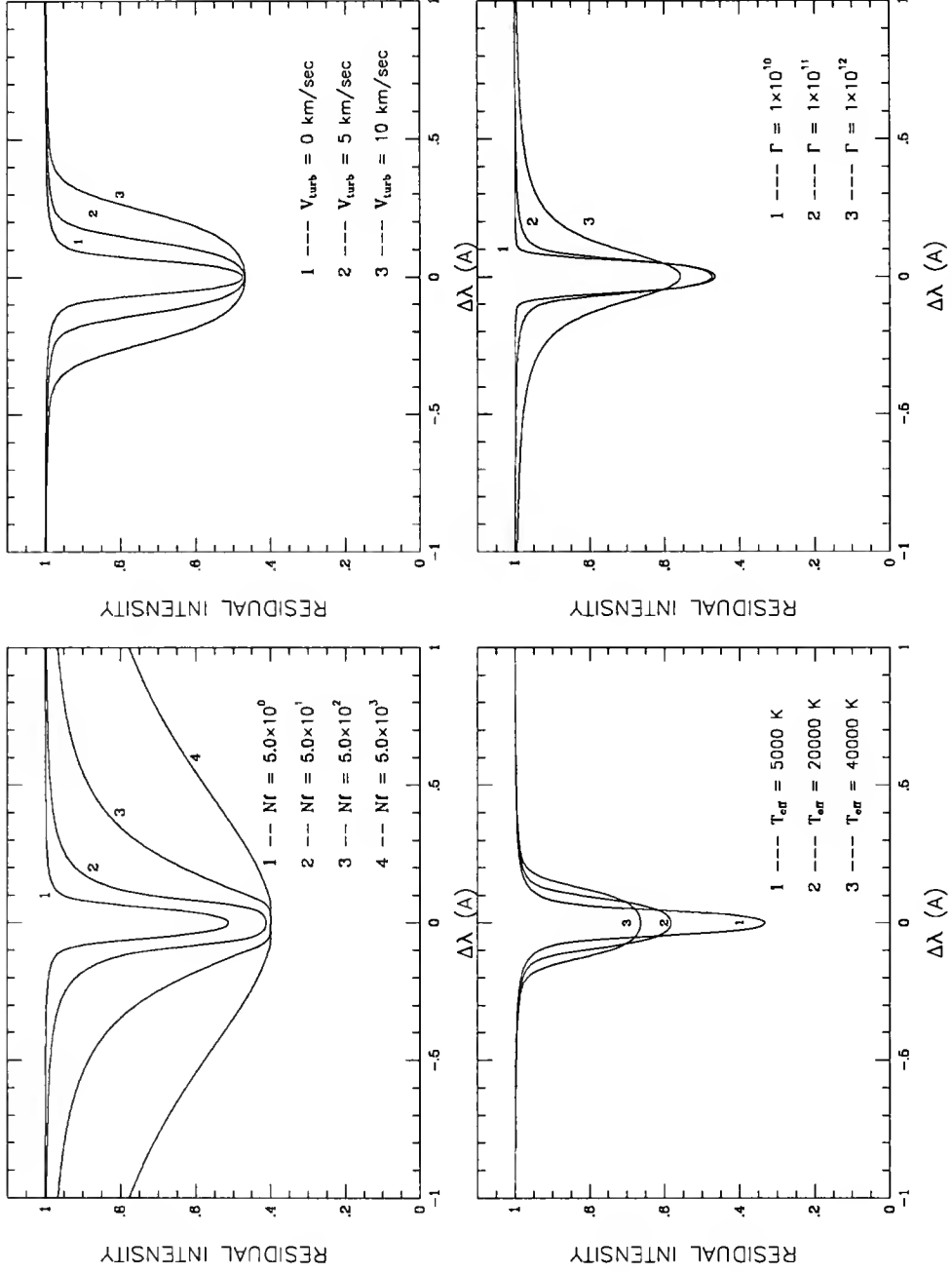
Figure 7: Variation in the intrinsic line profile by changing, clockwise from lower left, the effective temperature, number of absorbers, micro–turbulent velocity and the damping constant.
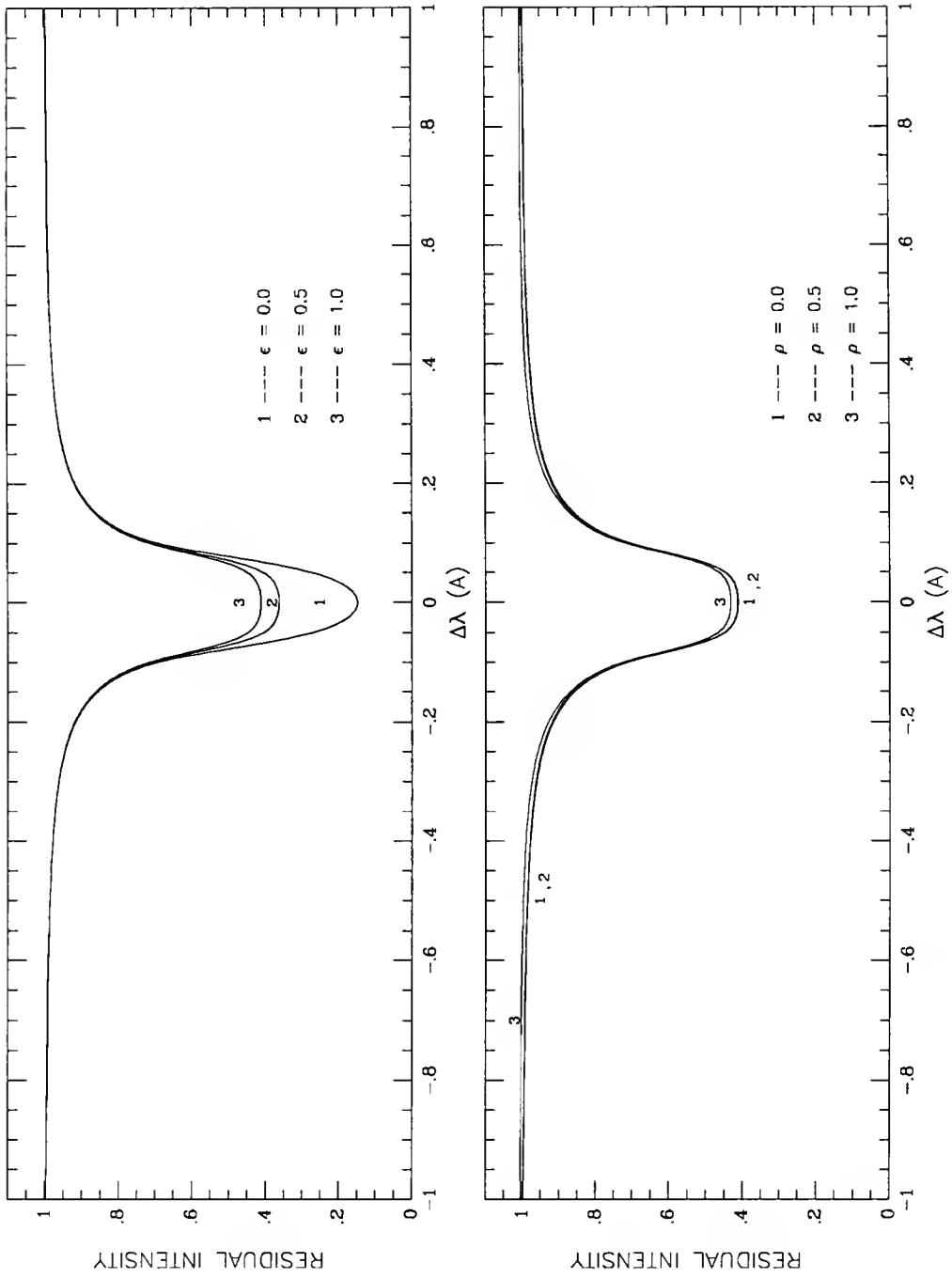
Figure 8: Variation in the intrinsic line profile by changing ρ and ϵ

Hav Subroutine
_____

This subroutine calculates the Voigt function $H(a,v)$. The function alone shapes

the absorption line, and accurate values of $H(a,v)$ are required to generate line profiles.

The function is given by the following expression (Aller, 1953)

$$H(a,v) = \frac{a}{\pi} \int\limits_{-\infty}^{+\infty} \frac{\exp(-y^2)}{a^2 + (v-y)^2} dy \qquad (5.1)$$

where,

$a = \frac{\Gamma}{4\pi \Delta\nu_D}$, and

Γ = damping constant (natural + collisional)

$\Delta\nu_D$ = Doppler width

v = frequency departure from the center of the line in units of Doppler width

$= \frac{\Delta\nu}{\Delta\nu_D}$

Much work on this problem has been done by Finn and Mugglestone (1965) and

Hummer(1965). This function has also been calculated by Hjerting (1938) who provided

a table of $H(a,v)$ for a up to 0.5 and v up to 5. Harris (1948) gives a table which

contains the coefficients of the Taylor expansion of $H(a,v)$ as a power series in a . For

small values of v and a ($v < 2.75$ and $a < 0.2$) one uses the Taylor series (Harris, 1948)

$$H(a, v) = H_0(v) + aH_1(v) + a^2 H_2(v) + a^3 H_3(v) + a^4 H_4(v),$$

where

$$H_0(v) = e^{-v^2}$$

$$H_1(v) = -\frac{2}{\sqrt{\pi}}[1 - 2vF(v)]$$

$$H_2(v) = (1 - 2v^2)e^{-v^2} \tag{5.2}$$

$$H_3(v) = -\frac{2}{\sqrt{\pi}}[\frac{2}{3}(1 - v^2) - 2v(1 - \frac{2}{3}v^2)F(v)]$$

$$H_4(v) = (\frac{1}{2} - 2v^2 + \frac{2}{3}v^4)e^{-v^2}$$

$$and \ F(v) = e^{-v^2} \int_0^\infty e^{t^2} dt$$

If $v > 2.75$ (for all values of a, except $a = 0$)

$$H(a, v) = \int_{-\infty}^{+\infty} \frac{e^{-y^2}}{a^2 + (v - y)^2} dy \tag{5.3}$$

We have truncated the limits to [-7,7]. The above integral is evaluated using Simpson's rule.

Finn and Mugglestone (1965) have shown that $H(a, v)$ can be written as

$$H(a, v) = e^{-v^2} + \frac{2a}{\sqrt{\pi}}[-1 + 2ve^{-v^2} \int_0^v e^{x^2} dx]$$

$$+ \frac{1}{\sqrt{\pi}} \int_0^\infty [e^{-ax} - 1 + ax]e^{-x^2/4} \cos(vx)dx \tag{5.4}$$

If $a = 0$

$$H(0, v) = e^{-v^2} \tag{5.5}$$

If $v = 0$

$$H(a,0) = 1 - \frac{2a}{\sqrt{\pi}} + \frac{1}{\sqrt{\pi}} \int\limits_0^\infty (e^{-ax} - 1 + ax)e^{-x^2/4}dx \qquad (5.6)$$

Thus the integration was divided into five parts according to the values of a and v. These five divisions are as follows:

i. $\quad a = 0.$ (equation 5.5)

ii. $\quad v = 0.$ (equation 5.6)

iii. $\quad v \geq 2.75$ (equation 5.3)

iv. $\quad v < 2.75$ and $a \geq 0.2$ (equation 5.3)

v. $\quad v < 2.75$ and $a \leq 0.2$ (equation 5.2)

Figures 9 and 10 show the broadening function $H(a,v)$ as a function of a and v respectively.

Light Subroutine

The LIGHT subroutine is a part of the light curve program. This subroutine calls the DOPPLER subroutine for each surface elemental area. In turn the DOPPLER subroutine calls the LINEPROF subroutine. Thus for each area we have a line profile. The next step is to weigh and sum them accordingly. This is all done in the LIGHT subroutine. As mentioned earlier, since each element has an associated velocity due to the rotation of the star, its central wavelength will be Doppler shifted. One must account for the possibility that the star might rotate faster than synchronously. This is where the F_1 parameter (in the case of the primary star) comes into effect. The velocity of each element, with respect to the center of the star, is multiplied by F_1.
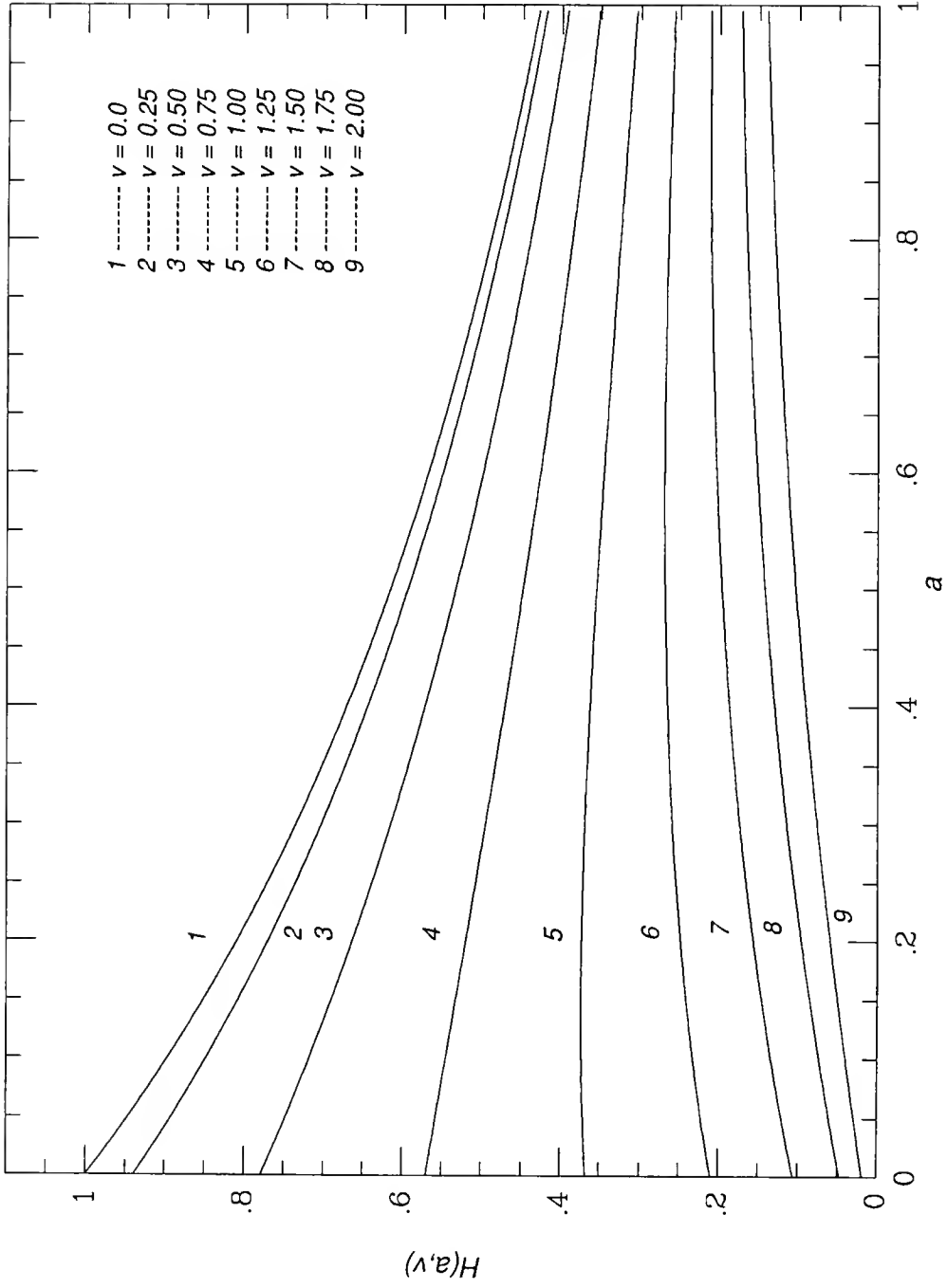
Figure 9: $H(a,v)$ as a function of a for various values of v
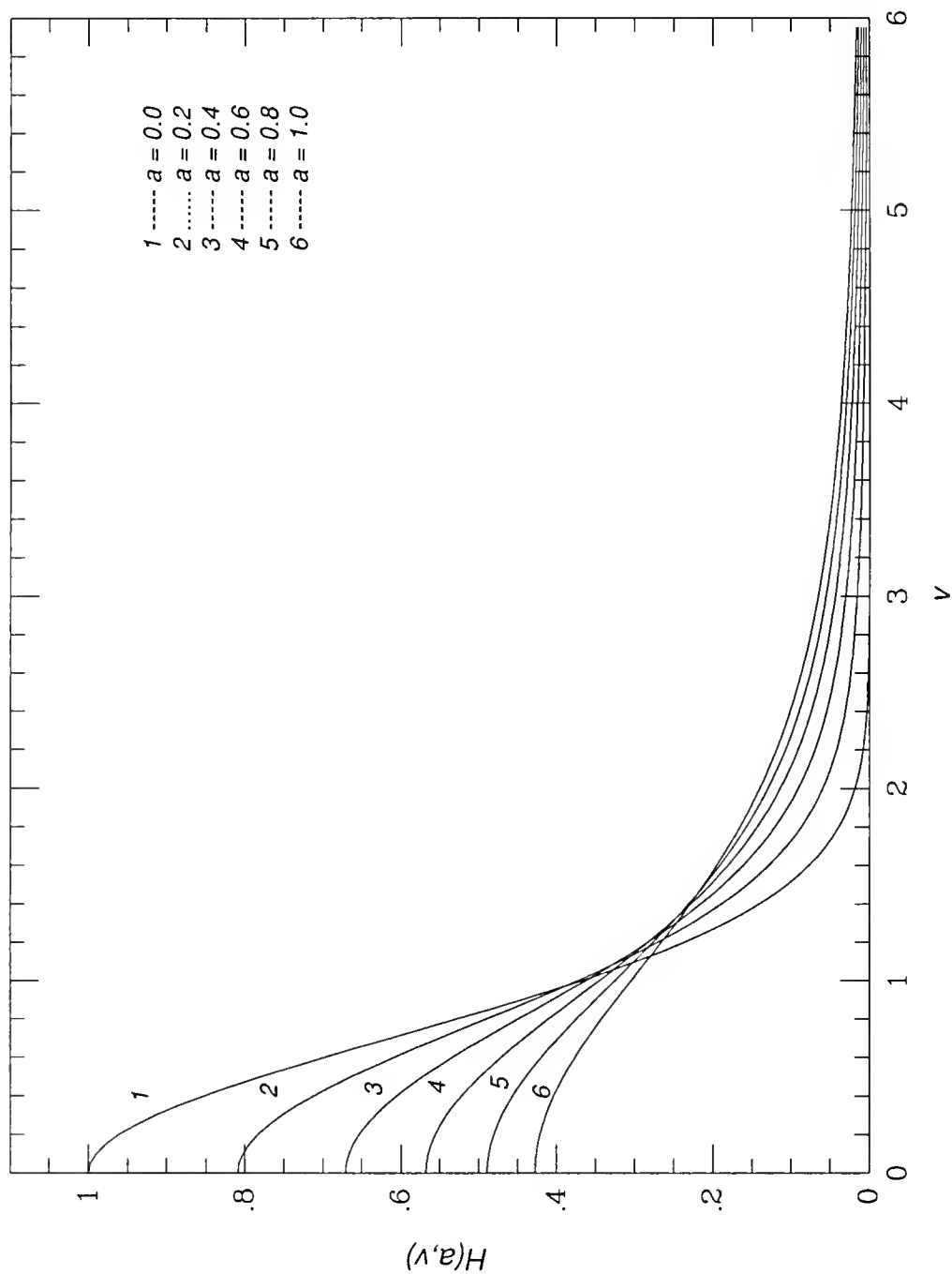
Figure 10: $H(a,v)$ as a function of v for various values of a

Figure 11 shows intrinsic line profile shifts due to rotation for two cases, one for asynchronous rotation and one for synchronous rotation ($F_1 = 1$). Figure 12 shows the line profile for the entire star, again one for the synchronous case and the other for the non synchronous case. In all these cases instrumental broadening has not been taken into account. The convolution of the line profile with the instrumental profile is described in the next subsection.
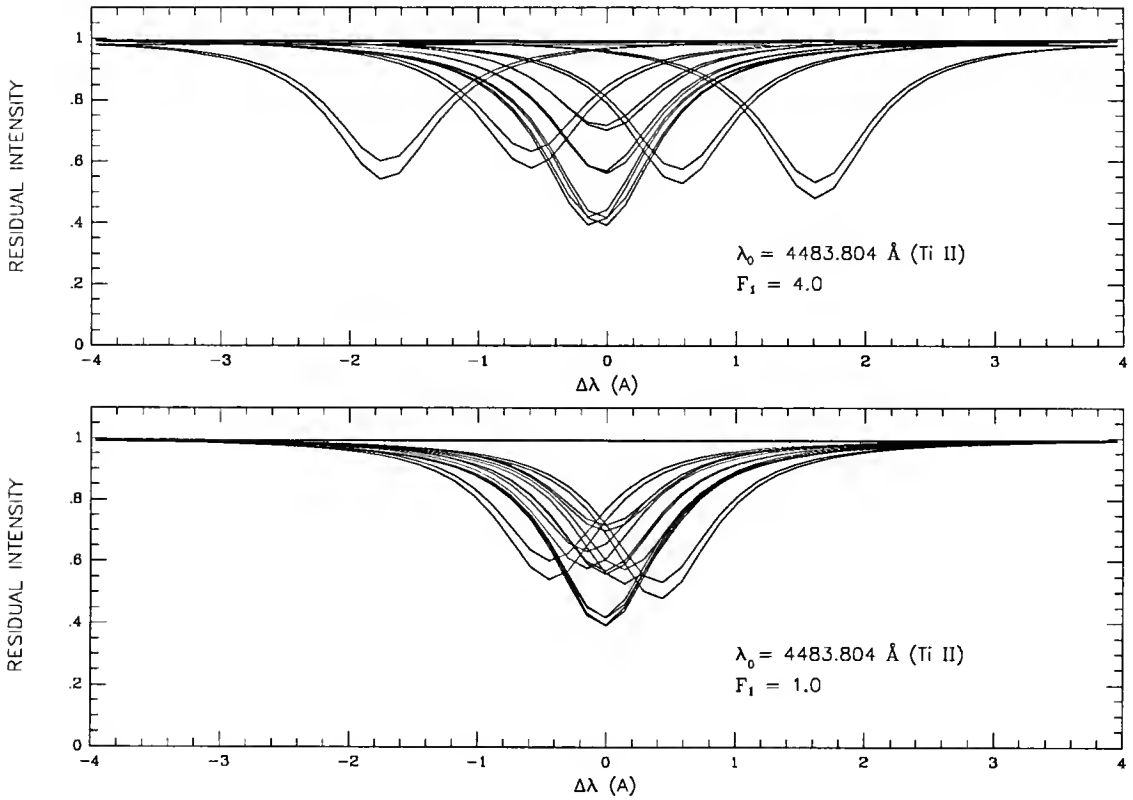
Figure 11: Intrinsic line profiles for synchronous (below) and non synchronous cases. The line profiles are choppy because they were calculated using a very small grid to illustrate the effect of non synchronous rotation.
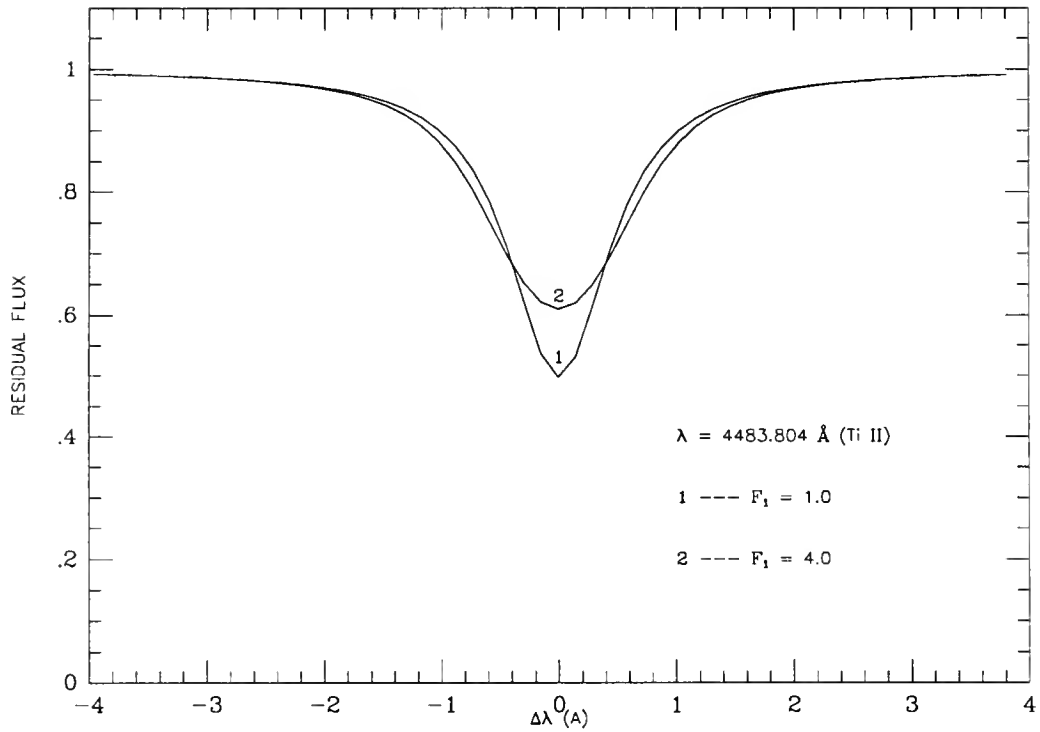
Figure 12: Line profile for the entire star for synchronous and non synchronous cases.

Instr Subroutine

The instrumental profile is represented in the program by a Gaussian. It is given in terms of full width at half maximum (FWHM). The instrumental profile depends on the instrument. The resolution for a 2–pixel line width for the CCD setting used was 0.30 A. This means that an infinitely sharp line that strikes just one pixel will appear 0.15 A wide. Thus the FWHM in our case would be 0.15 A.

Figure 13 shows instrumental profiles of various widths. The idealized theoretical line profile is to be convolved with the instrumental profile. If the line profile before convolution is broad, then the resultant line profile after convolution is not significantly different, so convolution with a broad line has little effect on the overall profile.

The INSTR subroutine convolves the idealized line profile with the instrumental profile. The line profile is an array of residual flux as a function of $\Delta\lambda$. However this array is not tabulated finely enough. Thus it is necessary to fit a smoothing function to the line profile over some range of wavelength. The smoothing function used was a polynomial of degree three. The coefficients of the polynomial are obtained by least squares.
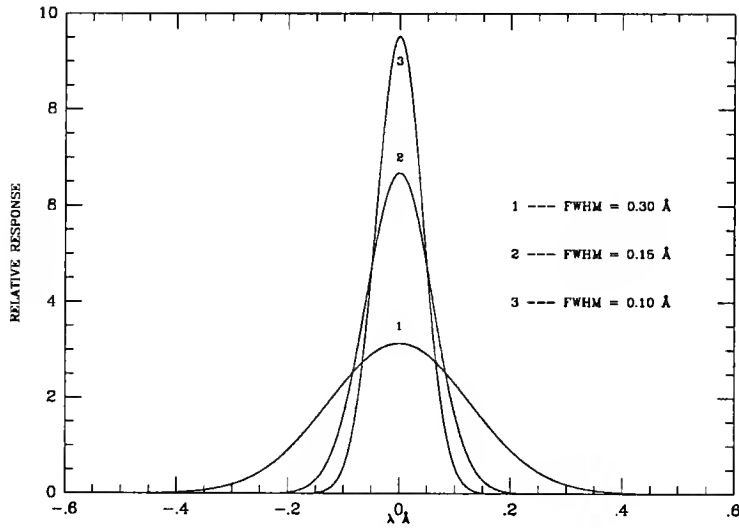
Figure 13: Instrumental profiles of various widths

Phase Smearing

The last stage of profile generation is to account for phase smearing. This is done by averaging computed profiles from the beginning and end of the observation interval. However if the observing interval is very small, it suffices to calculate the line profile at the phase corresponding to the middle of the interval. In all of our cases the interval was very small and hence the profile was calculated at the phase corresponding to the middle of the interval. The program can calculate the line profile either way.

Parameter Fitting

Two methods have been used to fit the theoretical line profile to the observed one. The first one is the method of Differential Corrections (DC) and the second is the Simplex method. Each method has its advantages and disadvantages. An advantage of DC over Simplex is that it provides error estimates. The best procedure is to fit the observed line profile by the Simplex method, and then use the DC method as the last step to get error estimates.

Simplex

The Simplex method was introduced by Nedler and Mead and is discussed by Caceci and Cacheris (1984). It requires only function evaluations and no derivatives. One of the advantages of the Simplex method is that divergence is impossible, while a disadvantage is that one cannot get standard error estimates. This method also is slow.

A simplex is "a geometric figure that has one more vertex than the space in which it is defined has dimensions" (Caceci and Cacheris, 1984). For example, a simplex on a plane is a triangle. The basic idea in the Simplex method is to build a simplex in the N+1 dimensional space described by the parameters one wants to fit. Thus if there are two parameters 'a' and 'b' then one can consider them as axes in a plane on which one creates a simplex (a triangle). Each vertex is represented by three values: 'a', 'b', and 'R' where 'R' is the weighted sum of squares of the residuals.

To reach the lowest value of 'R', the simplex is moved "downhill", accelerating and slowing down as needed. At a given stage, the program finds which vertex has the largest R. It rejects that vertex and substitutes another. The program computes the new vertex according to one of these mechanisms: reflection, expansion, contraction,

and shrinkage. Figure 14 illustrates these four mechanisms while Figure 15 shows an example of a simplex moving on 'R's contour plot for a two parameter fit.

Although the Simplex method never diverges, some problems did arise. If the initial guess is very bad or if the increments are very small there will be a failure to converge and the program can end prematurely. For some cases the method was restarted at a point where the program claimed to have found a minimum. In some cases where there was suspicion that there was more than one solution the program was run again with different starting guesses.

B = Vertex
W = worst vertex
R = reflected vertex
E = expanded vertex
C = contracted vertex
S = shrunken vertices
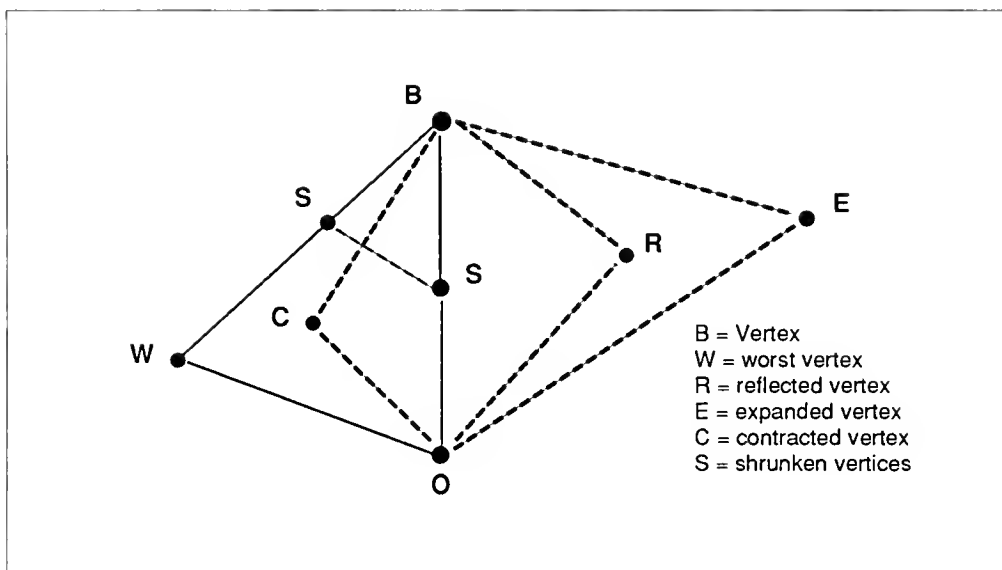
Figure 14: Two dimensional simplex illustrating the four mechanisms of movement. (Caccci and Cachcris, 1984)
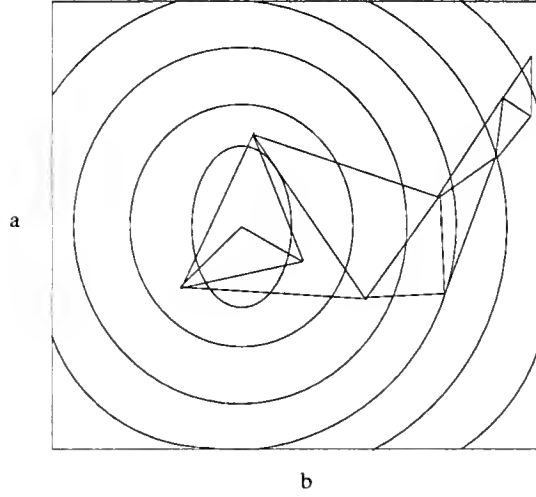
Figure 15: An example of the simplex moving on the
response surface's contour plot (Caceci and Cacheris, 1984)

Differential Corrections

The equation of condition for the least squares method is

$$O - C = \frac{\partial f}{\partial p_1}\Delta p_1 + \frac{\partial f}{\partial p_2}\Delta p_2 + \frac{\partial f}{\partial p_3}\Delta p_3 + \cdots\cdots \tag{5.7}$$

where, for the line profile problem

$O - C$ = observed - computed flux

f = residual flux

p = a parameter

$\frac{\partial f}{\partial p}$ = partial derivatives

Δp = parameter corrections

Thus for each observation one has one such equation. The normal equations can be
written in matrix form as

$$A^T W A X = A^T W d \tag{5.8}$$

where

X = n×1 matrix of computed corrections to our estimates of the parameters

n = number of parameters

d = m×1 matrix of residuals based on the previous estimate of the parameters

m = number of observations

A = m×n matrix of partial derivatives

W = m×m matrix whose diagonal elements consists of the weight assigned to each

observation.

Using matrix methods these equations are solved for the correction terms which will

then be added to the initial guesses for the parameters. The partial derivatives are

obtained numerically from the following equation

$$\frac{\partial f}{\partial p_1} = \frac{f(p_1 + dp_1, p_2, \cdots) - f(p_1, p_2, \cdots)}{dp_1} \tag{5.9}$$

where dp's are the parameter increments.

The weighted least squares iterative differential correction solution is given by the

following equation

$$X = \left(A^T W A\right)^{-1} A^T W d \tag{5.10}$$

The covariance matrix $\left(A^T W A\right)^{-1}$ provides a means of estimating the errors of the

solution vector X. One assumes that the errors in X depend only on d, and that the

errors in d are independent and follow the normal frequency distribution. If ϵ_j is the

error in X caused by the jth component of d then

$$\varepsilon^2 = \sigma^2 \left(A^T . W . A\right)^{-1} \tag{5.11}$$

where σ is the mean error of unit weight. Thus,

$$\sigma^2 = r^T \cdot \frac{r}{m-n} \tag{5.12}$$

where r = residuals. To get probable errors, ϵ_j is multiplied by 0.6745.

CHAPTER 6
RESULTS AND CONCLUSION

General Discussion

Seventeen systems have been analyzed and the rotation rates of the primary stars of these systems have been determined by the Differential Correction method (DC) and the Simplex method. The basic data on these systems are listed in Table 5. The photometric and spectroscopic elements were obtained from the literature. Each system will be discussed individually in the next section. Table 6 lists the spectroscopic elements for all systems while Table 7 lists photometric elements. The basic data and the spectroscopic data were obtained from the Eighth Catalogue of the Orbital Elements of Spectroscopic Binary Systems (Batten, Fletcher and MacCarthy, 1989). In Table 6 some of the systems have no K_2 values, which means that a_2 is not measured spectroscopically. In these cases a is obtained from a_1 and the mass ratio (m_2/m_1) listed in Table 7. Table 8 lists the line profile parameters along with their errors from the Differential Correction method and Table 9 lists the parameters obtained from the Simplex method.

Table 10 lists the equatorial velocities obtained from this work and other work. F_1 values obtained by analysis of the Rossiter effect are averages of those from Twigg (1979) and from Wilson and Twigg (1980). The values in the fifth column, $F_1(sp)$, were taken from Van Hamme and Wilson (1990), who listed values of F_1 obtained from previous line profile work. The seventh column lists the limiting value of F, which tells how fast a binary star component would rotate if it were centrifugally limited and had the same size (as it does with its present rotation). The procedure to calculate

59

F_{cr} is explained by Van Hamme and Wilson (1990). The equatorial velocities listed in column eight were calculated from the values of semi-major axis, side radii (r_1(side)), and the period.

Figures 17 to 33 show the theoretical fit to the observed data. Figures 34 to 50 (see Appendix A) are computer generated pictures of these systems at various phases along with their light curves and photometric elements, while Figures 51 to 67 (see Appendix B) are plots of the observations.

It is important to choose suitable lines for analysis. A number of systems were not analyzed either because the lines were very asymmetrical or seem blended. If the higher excitation lines such as He I and He II are compared with H lines then it is seen that in some cases the He lines are broader than the H lines. Hansen and McNamara (1959) for RZ Sct and Hiltner (1946) for RY Per suggested two reasons for this. One possibility is that the H lines arise from a more slowly rotating disk or envelope structure around the primary, while the He lines arise in the true stellar photosphere. Another is that the normal H lines are severely modified by absorption and/or emission.

Some of the lines seem to be blended. Near the bottom of primary eclipse the light from the secondary star may equal or even exceed that of the primary star. In this case some of the observed line profiles may be blended. This could hamper the determination of the line center. However, for the case of Algol type binaries, light curve solutions show that for most of the partial phases the light from the primary is much greater than that of the secondary. Hence there should not be significant blending of the spectral features of the two stars, except for a few weak lines (Twigg, 1979).

As mentioned earlier, two methods were used to fit the data. The Simplex method

usually required a large amount of computer time but there was no convergence problem. The Differential Correction method found the minimum quickly, but, in some cases, ran into a convergence problem. This is possible if the computation of derivatives and residuals lack precision. It can be overcome by using a fine enough computing grid, which usually increases the computing time. Another reason could be that the derivatives and residuals contain systematic errors, which vary from iteration to iteration (Wilson, 1988). Numerical derivatives will contain systematic errors if they are computed asymmetrically. The Differential Correction method has a provision to compute symmetrical derivatives. However this will double the computing time.

The parameters adjusted in both the DC and Simplex methods are the damping constant (Γ), the number of absorbers along the line of sight (Nf), turbulent velocity (V_{turb}), and the rotation rate of the primary star (F_1). The value of the effective temperature was taken from the photometric solution and was not adjusted. Two other parameters (ϵ and ρ) also were kept fixed. The value of ρ was always 0, which means no continuum scattering. Continuum scattering becomes important for O-type stars. Since all the stars in this sample are late B-type or later, continuum scattering is not important. The other parameter, ϵ, was kept fixed at 1, which means a pure absorption line. ϵ equal to 0 means a pure scattering line. Realistically ϵ should be between 0 and 1. However it is difficult to obtain a theoretical value for ϵ. It also is not well determined by fitting line profiles. Solutions were made by fixing values of ϵ at 0.3 and 0.7, but, the fits were not good, so ϵ was kept fixed at 1.

Table 5: Basic system data

NAME	PERIOD (in days)	SPECTRAL TYPE (Component 1)	SPECTRAL TYPE (Component 2)
S Cnc	9.4845	B9.5 V	G8 III
RZ Cas	1.1952	A3 V	
TV Cas	1.8127	B9 V	
U Cep	2.4930	B7 V	G8 III-IV
SW Cyg	4.5728	A3e	K0
S Equ	3.4361	B8 V	
RY Gem	9.3009	A0 V	K0 IV
RW Mon	1.9061	B9 V	F9 IV
TU Mon	5.0490	B2 V	A5
DM Per	2.7277	B5 V	A5 III
RW Per	13.199	B9.6IIIe	K2 III-IV
RY Per	6.8636	B5 V	F6 IV
β Per	2.8673	B8 V	

Table 5– – (Continued)

NAME	PERIOD (in days)	SPECTRAL TYPE (Component 1)	SPECTRAL TYPE (Component 2)
Y Psc	3.7659	A3 V	K0 IV
U Sge	3.3806	B7.5 V	G4 III-1V
RZ Sct	15.190	B2 II	A0 II-III
Z Vul	2.4549	B4	A3 III

Table 6: Spectroscopic data

NAME	a /(R$_{sun}$)	K$_1$ km sec^{-1}	K$_2$ km sec^{-1}	V$_\gamma$ km sec^{-1}	f(m) /M$_{sun}$
S Cnc	26.27	9.5	126.7	11.0	-
RZ Cas	6.42	70.1	-	-46.6	4.3×10^{-2}
TV Cas	11.2	87.9	-	0.5	1.3×10^{-1}
U Cep	14.7	120	182	-2	-
SW Cyg	13.94	43	-	-1	3.3×10^{-2}
S Equ	14.63	23.4	-	-48.0	4.4×10^{-3}
RY Gem	25.79	27.1	121	11.8	-
RW Mon	9.97	74.4	-	4.3	8.2×10^{-2}
TU Mon	31.43	55	260	20	-
DM Per	16.17	70.5	223.7	-	-
RW Per	34.10	18.5	-	6.5	8.7×10^{-3}
RY Per	32.38	27	-	4.5	1.3×10^{-2}
β Per	13.99	44.0	201	-	-

Table 6– – (Continued)

NAME	a /(R$_{sun}$)	K$_1$ km sec^{-1}	K$_2$ km sec^{-1}	V$_\gamma$ km sec^{-1}	f(m) /M$_{sun}$
Y Psc	13.80	37	-	6	1.9×10^{-2}
U Sge	18.49	69.7	209	-6.5	-
RZ Sct	49.5	36.5	-	-14.5	7.7×10^{-2}
Z Vul	15.02	89.8	219.7	-21.8	-

Table 7: Photometric elements

STAR	F_1	i	T_1 (K)	T_2 (K)	Ω_1	Ω_2	m_2/m_1	r_1(side)
S Cnc	13.0	84°.84	10500	4836	12.252	1.912	0.085	0.086
RZ Cas	-	82°.71	9700	5226	4.753	2.574	0.35	0.228
TV Cas	-	80°.3	10800	5100	3.846	2.678	0.40	0.294
U Cep	5.0	82°.13	13600	4896	6.996	3.148	0.646	0.174
SW Cyg	11.66	82°.70	9070	3813	8.937	2.609	0.366	0.167
S Equ	-	87°.4	11400	5690	5.266	2.019	0.12	0.195
RY Gem	14.4	83°.10	9400	4043	11.768	2.187	0.182	0.096
RW Mon	5.0	87°.96	10650	5055	6.001	2.619	0.371	0.203

Table 7- - (Continued)

STAR	F_1	i	T_1 (K)	T_2 (K)	Ω_1	Ω_2	m_2/m_1	r_1(side)
TU Mon	-	89°.1	15520	7280	5.662	2.257	0.21	0.184
DM Per	-	78°.7	15900	8224	4.426	2.510	0.32	0.245
RW Per	16.21	80°.03	9700	3973	14.090	2.103	0.15	0.077
RY Per	10.8	81°.65	20700	6017	9.176	2.474	0.304	0.133
β Per	-	82°.31	12000	4888	5.151	2.299	0.227	0.204
Y Psc	-	87°.1	9300	4860	5.285	2.329	0.24	0.199
U Sge	1.44	88°.26	12000	4700	5.088	2.681	0.401	0.216
RZ Sct	6.77	83°.10	22700	7500	6.066	2.416	0.277	0.241
Z Vul	-	88°.9	19840	9410	3.715	2.739	0.43	0.309

Table 8: Line profile parameters (Differential Corrections method) with their probable errors

STAR	F_1	$\Gamma[10^8]$	$Nf[10^4]$	$V_{Iurb.}$(km sec^{-1})
S Cnc	13.15 ± 0.23	1.23 ± 0.26	2.66 ± 0.58	2.66 ± 0.20
RZ Cas	1.38 ± 0.02	11.0 ± 0.26	0.67 ± 0.03	2.98 ± 0.01
TV Cas	0.89 ± 0.01	0.43 ± 0.10	0.41 ± 0.13	8.84± 0.11
U Cep	6.59 ± 0.07	2.62 ± 0.29	4.33 ± 0.43	3.36 ± 0.13
SW Cyg	8.06 ± 0.11	1.83 ± 0.14	6.89 ± 0.52	2.75 ± 0.15
S Equ	1.17 ± 0.04	1.01 ± 0.43	0.16 ± 0.05	8.33 ± 0.47
RY Gem	8.80 ± 0.10	5.12 ± 0.23	3.48 ± 0.21	2.51 ± 0.22
RW Mon	1.30 ± 0.03	2.11 ± 0.23	3.31 ± 0.34	1.26 ± 0.08
TU Mon	4.87 ± 0.05	3.12 ± 0.12	9.10 ± 0.28	2.77 ± 0.08
DM Per	2.64 ± 0.04	2.74 ± 0.13	5.60 ± 0.18	2.72 ± 0.42
RW Per	16.21 ± 0.24	2.55 ± 0.43	2.18 ± 0.35	6.27 ± 0.36
RY Per	9.63 ± 0.16	6.02 ± 0.82	3.04 ± 0.47	2.32 ± 0.30
β Per	1.14 ± 0.01	6.18 ± 0.49	0.19 ± 0.01	6.86 ± 0.05
Y Psc	1.01 ± 0.04	2.80 ± 0.42	1.05 ± 0.17	7.14 ± 0.26

Table 8– – (Continued)

STAR	F_1	$\Gamma[10^8]$	$Nf[10^4]$	$V_{turb.}(km\ sec^{-1})$
U Sge	1.34 ± 0.05	27.3 ± 1.46	0.05 ± 0.01	4.83 ± 0.02
RZ Sct	4.49 ± 0.31	2.97 ± 0.92	3.55 ± 0.99	2.20 ± 0.17
Z Vul	1.41 ± 0.01	3.18 ± 0.04	3.12 ± 0.07	4.48 ± 0.15

Table 9: Line profile parameters (Simplex method)

STAR	F_1	$\Gamma [10^8]$	Nf $[10^4]$	V_{turb}(km sec^{-1})
S Cnc	13.01	1.23	2.68	2.65
RZ Cas	1.38	11.38	0.66	2.93
TV Cas	0.88	0.42	0.40	8.60
U Cep	6.62	2.68	4.34	3.38
SW Cyg	-	-	-	-
S Equ	1.15	1.12	0.15	8.41
RY Gem	8.99	5.14	3.48	2.53
RW Mon	1.29	2.17	3.25	1.24
TU Mon	4.89	3.12	9.10	2.76
DM Per	2.64	2.75	5.56	2.73
RW Per	16.11	2.53	1.99	6.58
RY Per	9.60	6.03	3.03	2.33
β Per	1.13	6.18	0.19	6.86

Table 9– – (Continued)

STAR	F_1	Γ [10^8]	Nf [10^4]	V_{turb}(km sec^{-1})
Y Psc	1.02	2.80	1.06	7.15
U Sge	1.34	27.29	0.05	4.83
RZ Sct	4.34	2.98	3.56	2.21
Z Vul	1.41	3.44	2.97	4.51

Discussion on Individual Systems

S Cnc

The photometric and spectroscopic elements were taken from Van Hamme (private communication). The primary star's rotation is asynchronous. However, there are no signs of circumstellar matter in the form of emission lines, although the line profiles are asymmetrical. Etzel and Olson's (1985) photometric and spectroscopic results show that there might be an extended atmosphere surrounding the Roche lobe filling component. Usually it is the primary of an Algol type binary which shows anomalous photometric and spectroscopic behavior. Etzel and Olson (1985) mention that S Cnc represents an unusual case among longer period Algol type systems, in that there is no apparent disk about the hotter component despite the fact that it rotates much faster than synchronously. Popper and Tomkin's (1984) spectroscopic observations and Etzel and Olson's (1985) photometric and spectroscopic observations give a very small mass for the Roche lobe filling component (0.18 solar masses). According to Popper and Tomkin (1984) the Roche lobe-filling subgiant of S Cnc has the smallest known stellar mass established directly from spectrographic observations. Absence of an accretion disk and the small mass for the secondary may be indicative of the end of normal mass transfer.

Van Hamme (private communication) found an F_1 of 13.0 from his photometric analysis. This work gives a value of 13.15 from Differential Corrections and 13.01 from the Simplex method. The critical value for F_1 is 28.5. Since the small mass of the secondary is indicative of the end of normal mass transfer, the system is at a stage in which the primary's rotation, which probably was very fast during the normal mass transfer stage, has slowed down due to tidal braking.

RZ Cas

The photometric elements by Chambliss (1976) were used for the analysis. The primary's temperature was obtained from the spectral type (A2 V). The light curves show no gas streaming effects. However a period study by Hall (1976) shows sudden period decreases. Other studies also have shown an overall period decrease. Conservative mass transfer from the less massive component in a binary results in a period increase. Since the period of RZ Cas is decreasing one can infer that the mass transfer is non-conservative: some angular momentum must either be lost from the system or stored temporarily as rotation. According to the Biermann and Hall (1973) period change model a dynamical instability causes a sudden outflow of mass from the cooler star. Sudden outflow of mass results in period decrease because angular momentum is taken from the orbit and stored temporarily as rotation in or around the hotter star. This mass transfer spins up the primary which means that F_1 must be a little greater than 1.

The spectroscopic elements were taken from Duerbeck and Hanel (1979). They obtained orbital solutions from a least squares fit of the hydrogen lines and metallic lines. However the solutions differed in the γ–velocities and in the shape of the curve. The adopted solution was one from the metallic lines. The deviations of the hydrogen lines from the adopted curve show that outside eclipses the disturbances are strongest around phases 0.2–0.3 and 0.8–0.9. Duerbeck and Hanel (1979) suggest that this result is similar to the one described by Plavec (1967) where he mentions the presence of red displaced absorption lines around phase 0.3 and 0.8 in Algol systems S Equ, U Cep, U Sge and RW Tau, and ascribes them to the absorptional effects of circumstellar matter.

Previous line profile work gives a value of 1.16 for F_1. Twigg (1979) finds a value

of 1.6 through an analysis of the Rossiter effect. Line profile analysis gives 1.38 from both the DC and the Simplex methods. Probably the secondary is in the slow phase of mass transfer and sudden bursts of mass exchange spin up the primary, with subsequent tidal drag.

TV Cas

The photometric elements are from Wlodarczyk (1983). The primary temperature was obtained from the spectral type (B9 V). The spectroscopic elements were taken from the DAO catalog (Batten, Fletcher and MacCarthy, 1989). Period studies show some interesting results. Tremko and Bakos (1976) show that the period is decreasing. TV Cas is presumably semi-detached with its secondary filling its Roche lobe. Hence there should be some mass transfer from the secondary to the primary. Because of this mass transfer the orbital period should increase. If the period is decreasing, as in this case, mass transfer could perhaps be taking place in the opposite direction. Tremko and Bakos (1976) state that such mass transfer could be caused by a gentle stellar wind from the primary component. This seems to be a very unlikely explanation. Another explanation (Frieboes-Conde and Herczeg, 1973) could be the light-time effect of a third body.

Previous line profile work gives a value of F_1 as 0.73. (Van Hamme and Wilson, 1990). This work gives 0.88 for F_1. Here we have a close binary system where one of the stars seems to be rotating slower than synchronously, which is difficult to believe. Van Hamme and Wilson (1990) suggested that one explanation could be the mixing of a slowly rotating inner envelope with the observable surface layers. Twigg (1979) found a value of 2.1 for F_1 from the Rossiter effect.

U Cep

The photometric elements are from Terrell (private communication). The primary temperature was taken from the spectral type. The spectroscopic solution is from Tomkin (1981). The primary velocity curve has large scatter. This is because all the lines of the primary have irregular, asymmetric and broad profiles. The primary line profiles are distorted by the gas stream from the secondary to the primary.

Light curves of U Cep show many disturbances. Olson (1978) noticed large, rapid changes in the light curves outside eclipse. The ultraviolet light curve showed a broad, deep dip near orbital phase 0.6. Olson attributed this to a cool spot on the primary star about 2500 K cooler than the normal photosphere. Compared with other classical Algol-type eclipsing binaries, U Cep has unusually high circumstellar activity. Some eclipsing binaries exhibit very strong emission lines of N V, C IV, Si IV, Fe III, and other species in the far ultraviolet region (Plavec and Koch, 1978). Plavec (1980) called this group of binaries W Serpentis stars. Observations during the primary eclipse by Plavec (1983) in 1981 August and December showed a spectrum rich in emission lines similar to those observed in the W Serpentis stars. According to Plavec (1983) the ionization energy for these emissions comes from the accretion process since all the binaries in this group show large scale mass transfer. The energy cannot be supplied by the component stars, and it has been shown (Plavec et al., 1982) that it does not originate in the chromospheres of the late type components.

It is reasonable to assume that all W Serpentis systems are in double contact (see section 4 in chapter 1). Thus one might suspect U Cep to be a double contact system. However light curve solutions give a value of 5 for F_1, whereas F_1 should be 7.44

for double contact. Published spectroscopic results give F_1 as 5.24 (Van Hamme and Wilson, 1990). This work finds F_1 to be about 6.8. However Twigg (1979) found a value of 8 by fitting the Rossiter effect. If the absorption line comes from the circumstellar matter, then an anomalously low F_1 may result from the line profile analysis.

SW Cyg

The photometric solution by Wilson and Mukherjee (1988) was used for this analysis. The spectroscopic parameters were taken from Struve (1946b). The photometric solution corresponds to a double contact configuration. The rotation was found to be 11.66 times the synchronous rate. This corresponds to an equatorial velocity of about 300 km/sec. It is possible that, at such a velocity, all photospheric lines are broadened beyond observability. Yet Struve (1946b) saw lines of Ca II, Mg II, and Fe II. Thus either the lines are circumstellar or the photometric F_1 is wrong. Published spectroscopic velocities (Olson, 1984) give a value of 5.6 for F_1. Thus it is possible that the F_1 determination from light curves is wrong. However it is worthwhile to see the effects of circumstellar gas on F_{ptm} and F_{sp} over a period of time.

This system is in a state of active mass transfer as shown by the frequent period changes, emission lines, fast rotation, and distorted light and velocity curves. According to Wilson and Mukherjee (1988), the presence of equatorial gas could make the primary star to look like a fast rotator, photometrically. This is because the fitting procedure makes use of the shape and surface-brightness distribution of the primary star. For line profile determinations, equatorial darkening diminishes the influence of the fastest rotating regions, and thus should lower the measured rotation rate. In the case of SW

Cyg that is the sense of the discrepancy, but, the difference is large. This makes the photometric F_1 value doubtful.

A semi-detached configuration was assumed for the line profile analysis and the size of the primary star was kept fixed. This was done by changing Ω_1 every time F_1 was changed in the DC method, so that r_1(side) was constant. This gave F_1 as 8.06. Again one is not sure whether the line used for the analysis was circumstellar or photospheric. One way to get around this problem is to analyze more lines. Unfortunately there were not many "clean" lines to analyze. It would be worthwhile to make more observations through many spectral windows. The available data is limited to the spectral range of 4400 A to 4500 A. Due to the nature of this analysis (having a fixed size for the primary star) the Simplex method was not used. Because Ω_1 has to be changed after every iteration if F_1 changes, the Simplex program is not applicable in its present version.

S Equ

The photometric parameters are from Cester et. al. (1979). Plavec's (1966) spectroscopic parameters were used. When Plavec arranged the radial velocities according to photometric phase he found that they showed very little variation except before primary eclipse, where the velocity increased suddenly. At that phase he found that the hydrogen lines from H_β to H_ϵ were all strongly asymmetrical, with the cores shifted toward long wavelengths. This was the case with the MgII line and the K line. When he tried to measure the line centers he found a systematic shift toward positive radial velocities. All this suggests the presence of gaseous streams. Another important result was that the hydrogen lines displayed the same rotational disturbance as the other lines.

According to Plavec (1966), this was the first binary with gaseous stream where this fact was demonstrated.

The light curve of S Equ shows a slight brightening or weak emission just after primary minimum, probably caused by the gas stream projected onto the sky (Piotrowski, et al., 1974). Due to these gas streams the primary's rotation rate should be at least somewhat above synchronous. In fact line profile analysis obtains a value of 1.17 for F_1 from the DC method and 1.15 from Simplex.

RY Gem

The photometric solution was taken from Van Hamme and Wilson (1990) who analyzed the B,V light curves by Hall et al. (1982). In their analysis Hall, et al. adopted a model with circumstellar rings around the primary. Van Hamme and Wilson (1990) included the rotation effects, which Hall et al. did not take into account, but did not include the disk effects. The results from both work are similar except for the F_1 value, which was taken to be 1 by Hall et al. Spectroscopic parameters also were taken from the simultaneous solution by Van Hamme and Wilson (1990) from radial velocity curves by McKellar (1949) and Popper (1989).

Line profile analysis gives a value of 8.80 for F_1 from the DC method and 8.99 from Simplex, while the photometric value is 14.1. Fig. 23 shows the fit to the observed line profile which is asymmetric. Blending of lines could explain the asymmetry in the observed line. Thus our value may not be accurate. Twigg (1979) gets a value of 4.5 from the Rossiter effect. It seems that one gets different values depending on the type of observations. There are no references in the literature on this binary regarding equatorial velocities obtained from line profiles. One explanation for the different values

could be that the analyzed line is not photospheric. Popper's (1989) radial velocity work contains no observations during primary eclipse, so the Rossiter spike does not show. McKellar's (1949) observations for the primary star show much scatter. However his observations show the Rossiter effect. The Rossiter spike may be affected by both the rotation of the primary and the circumstellar ring, and Twigg's value may not represent the true rotation of the primary star .

RW Mon

The photometric and spectroscopic solution is from Van Hamme and Wilson (1990). RW Mon is suspected to be a fast rotator because of the emission lines seen in totality by Kaitchuck, Honeycutt, and Schlegel (1985). Presence of emission lines during totality means that circumstellar gas is present around the primary, indicating mass transfer and the possible spin-up of the primary star. Unfortunately no good radial velocity work has been published for RW Mon. The only radial velocity work is by Heard and Newton (1969), whose observations were published by Van Hamme and Wilson (1990).

Van Hamme and Wilson (1990) get a value of 4.99 for F_1 both photometrically and spectroscopically. There is no other published evidence of fast rotation for RW Mon. Line profile analysis gives an F_1 of 1.30 from the DC method and 1.29 from Simplex. So the question of whether the line is photospheric or circumstellar arises again.

TU Mon

TU Mon is an ordinary semi-detached close binary system consisting of a bright B5V primary and an A5 subgiant which fills its Roche lobe. The photometric elements are from Cester et. al. (1977). The spectroscopic elements are from Deutsch (1945) and Popper (1967). Both the DC and the Simplex method yield a value of 4.9 for F_1.

The analysis of the light curve assumed synchronous rotation. Fig. 25 shows the fit to the observed line profile. The line is asymmetric and is probably a blended line and hence the value for F_1 may not be correct.

DM Per

DM Per is an Algol type eclipsing binary consisting of a B5V primary and an A5III secondary. It is a part of a triple system with the third component having a mass of 3.6 solar masses (Hilditch et al., 1986). DM Per is an early type semi detached system and, although it has a large total mass and a small difference in the spectral types, it can be classified as a classical Algol system The first detailed photoelectric study of this system was made by Colacevich (1950). He noticed that at the end of the primary minimum the brightness of the system remained nearly constant during the phase interval 0.08 to 0.1 and then gradually reached a maximum value. He explained this as due to an obscuring gas stream which leaves the secondary component and flows toward the primary component, turns around the star, and comes partly or entirely back to the secondary component.

The photometric and spectroscopic elements are from Hilditch et al. (1986). The primary's rotation is asynchronous. Line profile analysis gives a value of 2.64 for F_1 from both the DC and Simplex methods. However the fit to the observed profile is not good. The line seems to be blended and asymmetric which accounts for the poor fit.

RW Per

RW Per is a long period Algol type eclipsing binary system with a B9 primary and a K2 secondary. The orbital period is 13.199 days. The photometric solution is from Wilson and Plavec (1988) while the spectroscopic solution is from Struve (1945).

According to Wilson and Plavec (1988) the primary of RW Per is in rapid rotation. From their light curve analysis they find that the primary is rotating about 28 times faster than synchronous. Olson et. al. (1992) gets about the same F_1 from independent observations. Wilson and Plavec (1988) also find the primary to be nearly filling it's rotational lobe. If it filled up its rotational lobe, the system would be a double contact binary. Such fast rotation implies considerable mass transfer. Hence one can expect an accretion disk around the primary. However neither spectroscopic nor photometric results do not show any concrete evidence of an accretion disk.

Hall (1969) studied several old light curves and two new photoelectric light curves. He found that there was a steady decrease in the duration of totality of the primary eclipse and the eclipse was partial in 1967. He suggested that the primary star of RW Per has more than doubled its size since 1900. Later Hall and Stuhlinger (1978) suggested a growing disk around the primary to account for the changes. Young and Snyder (1982) also tried to explain the change of eclipse from total to partial by an accretion disk whose radius was increasing due to an increase in mass transfer. Olson et al. (1992) suggested that the variations in the duration of totality are due to the slowly changing polar radius of the primary star.

Wilson and Plavec (1988) looked at a number of light curves and came to the conclusion that "there is no substantial basis for a long-term secular decrease in the duration of totality." In fact, they analyzed light curves with two models, one having a disk and the other none. However they did not find any evidence for a disk. If there were a disk there should be the expected 'W-Ser type' emission lines. But Dobias and Plavec (1987) did not find such lines (UV emission lines of Si IV, C IV etc.).

The present line profile analysis gives a value of about 16.1 for F_1. Since the photometric solution corresponded to a value of 28 for F_1 one had to re-analyze the light curves using the F_1 value obtained from a prelimnary line profile analysis, and the new photometric solution was then used for the profile analysis. This procedure was continued till the DC method gave a very small correction for the F_1 parameter.

Light curve analysis gives a value of 28 for the rotation parameter. If there is no disk, the rotation parameter can be found directly as suggested by Wilson and Plavec (1988). If there is a disk, then the photometric value for F_1 may be incorrect. A possible explanation (Van Hamme and Wilson, 1992) for the differences in F_1 (photometric vs. spectroscopic) is that most of the matter from the mass losing star is falling on a small zone on the equator of the mass gaining star thus spinning up that region. The higher levels may or may not be spun up. Photometrically, if the equator is spun up, there will be polar flattening and one will get a high value for F_1. Spectroscopically it is possible that a fast rotating equatorial zone is so narrow that the absorption line from the zone makes little contribution to the overall profile (Van Hamme and Wilson, 1990). Also the rotation could have changed between the photometric and spectroscopic observations.

RY Per

Van Hamme and Wilson's (1986b) photometric and spectroscopic solution was used for this analysis. The primary star is classified as a Rapidly Rotating Algol (RRA). RRA's are binaries whose primary stars are rotating faster than synchronously (Wilson et al., 1985). The spectral type of the primary is B3V, which corresponds to a temperature of 18,800 K. Van Hamme and Wilson (1986b) assumed a mean surface temperature of 20,700 K since a rapidly rotating star seen equator on will appear cooler

than its true average temperature. The scaling procedure has been described by Van Hamme and Wilson (1986a). The scaled up temperature of the primary was used for the line profile analysis.

RY Per has been investigated spectrographically by Hiltner (1946) and Popper (1982). Hiltner (1946) observed both stars' radial velocity curves. However, for the primary star, the velocity curves for hydrogen and helium are not the same. The most significant difference is in the rotational effect, with helium showing twice the rotational velocity of hydrogen. The velocity curves for the two elements are different in amplitude and there is a large difference in the γ velocities. Hiltner (1946) explained this discrepancy by suggesting that a stream of hydrogen flows from the secondary to the primary star. This explanation was further strengthened when spectrograms taken just before first contact showed that hydrogen lines had a second component displaced to the red presumably coming from the flow of material from the secondary to the primary.

The photometric F_1 is 10.82. Previous line broadening work reviewed by Van Hamme and Wilson (Van Hamme and Wilson, 1986b) gives a value of 9.11 for F_1. Twigg (1979) found a value of 10.0 from the Rossiter effect. Line profile analysis produces a value of 9.63, which is very close to that of previous line broadening work.

β Per

The photometric elements are from Kim (1989) while the spectroscopic elements are from Tomkin and Lambert (1978). Algol is a triple star system in which the brightest member (Algol A) is eclipsed every 2.8673 days by the subgiant secondary star, Algol B. Algol C orbits Algol A and B in 1.862 years. The secondary star (Algol B) fills its Roche lobe. The primary star is in or close to synchronous rotation.

Algol is in the slow mass transfer stage, which is believed to follow the W Serpentis stage. One theory (Wilson, 1989b) suggests that a W Ser star is in the rapid phase of mass transfer. After that stage has ended, one has a Rapidly Rotating Algol (RRA). After tidal braking has acted for a sufficient interval of time, an RRA will become a system like Algol. This system does not show much evidence of mass transfer. However, there has been observational evidence of mass ejection from the primary. This was suggested by Kondo et al. (1977) to explain the shortward shift of the entire set of Mg II lines in the UV spectrum of Algol. Even after Kondo et al. (1977) took into account the primary star's orbital velocity, there still was a shortward shift. They claimed that the Mg II lines originated from an optically thick expanding shell.

Light curve analysis of Algol (Kim, 1989) assumes synchronous rotation. The present line profile analysis gives a value of 1.14 for F_1. Previous spectroscopic work found a value of 1.04. Rucinski (1979) has developed a line profile synthesis method from which he finds that the rotation of the primary is very well synchronized with the orbital motion. An unusual result from his model was the very high value for microturbulent velocity (35 km/sec) compared to our value of 7.5 km/sec. He also found that the primary's angular rotation is not very far from uniform.

Y Psc

The members of Y Psc are of spectral types A3 V and K0 IV . Spectroscopic data by Struve (1946b) shows that the radial velocity curve is distorted by a gas stream. A $H\beta$ violet-shifted emission feature seen during egress from primary eclipse reveals the presence of the gas stream. The photometric solution was taken from Mezzetti et al. (1980). Both the DC and the Simplex method give a value of about 1.01 for F_1. Twigg

(1980) obtained a value of 1.65 by fitting the amplitude of the Rossiter effect.

U Sge

The components of U Sge are of spectral types B7.5 V and G IV . The photometric and spectroscopic solutions are from Van Hamme and Wilson (1986). Their simultaneous (photometric and radial velocity) solution was used for the line profile analysis. U Sge seems to be a slightly asynchronous rotator. The light curves are not very erratic, suggesting a small mass transfer rate. Dobias and Plavec (1985) have compared U Sge with U Cep by means of IUE spectral scans. They mention the fact that although the systems have similar characteristics, U Cep is more active than U Sge. Van Hamme and Wilson (1986b) suggested that the difference is because of the very rapid rotation of U Cep brought on by active recent mass transfer. Due to the rapid rotation the primary may be unable to accept the transferred material.

Even though mass transfer occurs in this system, emission in the optical spectrum was seen only by McNamara (1951). Dobias and Plavec (1985) state that UV emission lines were present during some total eclipses. McNamara (1951) finds that the hydrogen lines are strongly asymmetrical. The hydrogen lines give velocities which are different from other line measures, especially between phases 0.14 and 0.3 and from 0.76 to 0.92. This can be explained partly by absorption in gaseous streams. Also the H lines do not show the rotational disturbances displayed by other lines. As explained before for S Equ, this either could mean that the H lines are circumstellar or that there is a severe blending problem in the cores of the H lines during eclipse. Plavec (1983) suggested that all gainers in Algol-type systems are surrounded by a hot, turbulent region. All of these effects suggest mass transfer and non-synchronous rotation.

Van Hamme and Wilson (1986b) list a table of published rotation rates for U Sge. Most of the values are from the line broadening method. However the values are mostly inconsistent. One interesting fact arises from the table. Olson (1984) gives two values of F_1 separated by 12 years. His 1970 observations yield a value of 1.12, while his 1982 observations give 1.65. This suggests that over this interval the primary (the mass gaining star) may have spun up due to mass transfer. However this analysis gives a value of 1.34. This could mean that the star's rotation has slowed down over 9 years, probably due to tidal braking. Van Hamme and Wilson (1986b) adopted a value of 1.44 for F_1 for their light curve analysis of observations made by McNamara and Feltz (1976) in 1976. The theoretical line profile does not fit at all at the shoulders, possibly due to a blending problem.

RZ Sct

The photometric and spectrometric elements are from Wilson et al. (1985). RZ Sct may be a double contact binary in which both components fill their limiting lobes. A fit to the light curve (Wilson et al., 1985) yields $F_1 = 6.66$. However a Differential Corrections solution of the Hansen and McNamara (1959) single lined radial velocity curve (including the Rossiter spikes) yielded $F_1 = 9$. This is about 35% larger than the photometric value. A fit of the light curve with a fixed value of $F_1(9.0)$ produced poor results. Also, rotational spikes obtained by keeping F_1 fixed at 6.66 did not match the observed ones. Hence, insofar as the primary rotation is concerned, the light and radial velocity curves do not agree. Wilson et al. (1985) suggest that the orbital semi-major axis is larger than previously estimated by about 35%. This not only brings into agreement the photometric and spectroscopic rotation rate, but also improves the

agreement between the observed and expected absolute masses for both components.

From line profile analysis, F_1 is equal to 4.49 and 4.34 from the DC and Simplex methods respectively. These are smaller than the photometric value. Previous spectroscopic work gives F_1 as 5.8.

Z Vul

Z Vul is a seventh magnitude B-type eclipsing binary, period being about 2.4549 days. The stars are nearly the same size although the primary is about 10 times more luminous than the secondary. The photometric solution is from Cester (1977) while the spectroscopic solution is from Popper (1957). The photometric solution assumed synchronous rotation. Line profile analysis gives a value of 1.41 from both the DC and Simplex methods. Previous line broadening work yielded a value of 1.42. Thus it seems that, for this system, one gets consistent values for F_1.

Rotation Statistics

One of the most important and interesting aspects of binary star evolution is the relation between W Serpentis stars and Algols. As explained earlier in Chapter 1, W Serpentis stars are a class of close binaries defined at present mainly from an observational point of view. According to Wilson (1989a) most of the W Serpentis stars are in the rapid phase of mass transfer (RPMT) and have disks of gas, transferred from the mass losing secondary, around the now more massive primary star. Unfortunately the primary star is concealed by the disk and thus cannot be seen. It is highly probable that these primary stars have reached their centrifugal rotation limit. These stars will only be 'seen' when the disk has cleared away. The residual object may be an Algol type binary in which the mass transfer is in the slow phase (Wilson, 1989a). Since the

mass transfer rate is an important factor in determining the rotation rate, there should be a few stars between the W Serpentis and Algol stages, in which the mass transfer rate is just sufficient to maintain centrifugally limited rotation. Rotational statistics of W Serpentis stars and Algols will help in understanding the above problems, though it is difficult to obtain rotation statistics for W Serpentis stars. Some Algol systems are very erratic in their behavior and may partly be understood by means of rotational statistics. Finally rotational statistics can help determine how many stars are in double contact, which should help in understanding binary star evolution.

Table 10 lists the rotation values of the Algols analyzed in this work, while Table 11 lists the rotation rates of other Algols taken from Table VI of Van Hamme and Wilson (1990). In both the tables the rotation parameter R is used instead of F. $R = (F-1) / (F_{cr} - 1)$ was introduced by Wilson (1989a) to transform F values onto a 0–1 scale, where zero indicates synchronous rotation and unity indicates centrifugally limited rotation. There are two efficient mechanisms for changing rotation (Wilson, 1990). One is tidal braking for slowing rotation and the other is the accretion process which increases rotation. Thus, depending on the mass transfer rate, the rotation of an Algol primary should flip between two extremes – synchronous rotation and centrifugally limited rotation. Hence a frequency plot of the rotation parameter R should show a large spike at R = 0 and a smaller spike at R = 1, with a few systems in between. Figure 16 shows such a frequency plot. The shaded bars represent Algol primaries whose rotations were obtained from line broadening while the unshaded ones represent those whose rotations were obtained from light curve analysis. The reason that the low-R end is dominated by line broadening cases and the high-R end by light curve cases is that rotation is

well determined from light curve analysis only for fast rotators and not for slow and intermediate rotation speeds. If this figure is compared with Figure 3 in Wilson (1989a) an increase in systems with intermediate R is seen. Improved statistics are needed to test the reliability of such a frequency plot.
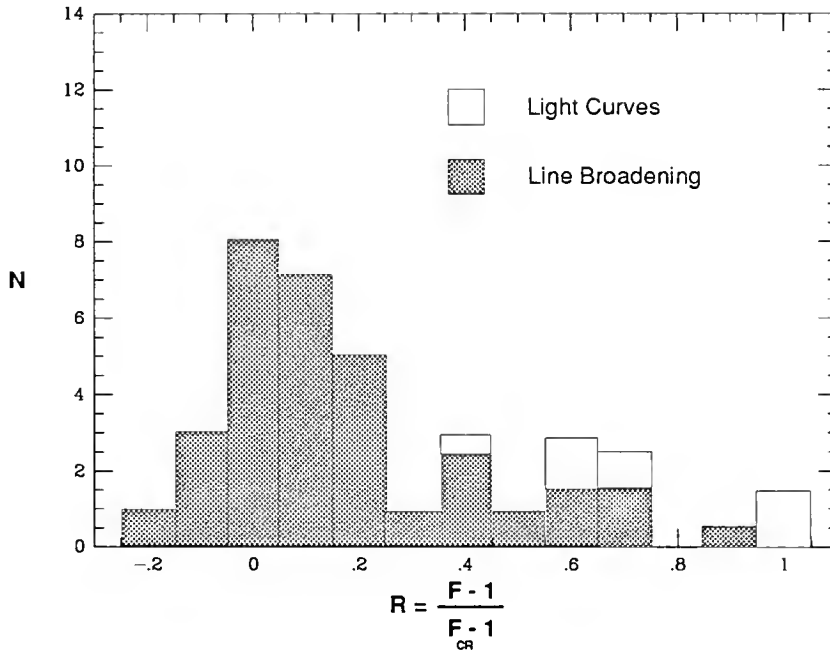

Figure 16: Histogram made from rotation measures in Table 10 and 11 showing the numbers, N, of Algol primary stars with various rotation rates. Stars with both kinds of determinations are represented by half an open box and half a shaded box, so as to conserve the total number of stars.

Observational selection effects (Van Hamme and Wilson, 1990) undoubtedly affect such a plot. Fast rotators are sometimes ignored by observers and theorists because they have erratic light and velocity curves. Photometric rotation rates usually are not well determined for slow rotators because light curves are only slightly affected by small departures from synchronism. There are few determinations of rotation rates of

fast rotators from line profile analysis. This could be due to the absorption lines being so shallow, due to strong rotational broadening, that they discourage observers. Also, some of the absorption lines have blending problems caused by emission lines from circumstellar gas.

Conclusions

Table 10 gives F_1 values obtained by several methods. The differences between the values obtained from this work (F_1 (DC) or F_1(Simplex)) and previous line profile analysis (F_1 (sp.)) can at least partly be attributed to the fact that this work has taken into account many kinds of broadening effects such as tidal and rotational distortion, gravity and limb darkening, etc., and intrinsic effects such as micro-turbulent velocity and damping. It may not be good to compare F values from the Rossiter effect with those obtained here. Measurement of the rotational eclipse disturbance in velocity curves requires many spectra, and the velocity shifts in which one is interested suffer from subjective effects.

The differences in the values obtained from this thesis and the photometric values may perhaps be explained as follows (Van Hamme and Wilson, 1990). Most of the matter from the mass losing star should fall onto a small equatorial region of the mass gaining star. Thus the equatorial band should rotate faster than the rest of the photosphere. Hence one has strong differential rotation in latitude. The fast rotation of the equatorial band will produce the equatorial extension (or polar flattening) characteristic of a fast rotating star. It also will produce strong equatorial gravity darkening. Thus, photometrically, one will find a high value of F_1. The absorption line

does not come only from the small equatorial band but from the entire star. Hence the rotation rate obtained from line profiles should be smaller. There is also the possibility that the line does not originate from the photosphere but from circumstellar gas. This may be the case with RW Mon, where photometrically $F_1=5.0$ while this work gives 1.27.

Another reason for the differences could be that only the outer envelope of the mass receiving star is spun up by mass transfer. This envelope could then spin down very fast, perhaps over a few years. RW Per has a photometric F_1 of 28 but a line profile value of 16.1. The light curve analysis was done on observations taken in 1978 while the line profiles were observed in 1990. It may be that the star (envelope) spun down over these 12 years to account for the difference in values.

Among all the binaries in this sample, two of them were not known to be asynchronous rotators. They are DM Per, with F equal to 2.64 and TU Mon, with F equal to 4.89. S Cnc was suspected to be a fast rotator and was verified by this work and Van Hamme and Wilson's (private communication) light curve analysis. Previous line profile work showed the primary of TV Cas to be rotating slower than synchronous and this again was verified from this work.

With regards to other line broadening parameters, one is not sure of the accuracy of the numbers since there is no way of matching the numbers with previous work. There has been curve of growth analysis on one of the stars (RY Gem) which provides us with a value for the number of absorbers and micro-turbulent velocity (Karetnikov and Mecheneva, 1987). They obtain a value of 9.5 km/sec for the micro-turbulent velocity while this work gives 2.5. They also get a value of 3.83 for logN, N being

the number of absorbers, as opposed to 4.54 from this work. Analysis of other lines may provide a handle on the accuracy of the other parameters, namely micro-turbulent velocity, damping constant and the number of absorbers along the line of sight.

Future Work

Most of the binaries should be observed spectroscopically through at least several spectral windows. It may be possible to use a stellar atmosphere program to predict the behavior of absorption lines in various wavelength ranges, so that an observer will know which spectral window to use. Some of the binaries should be observed photometrically again since it is possible that mass transfer might have spun up the mass receiving star or that it has been spun down via tidal braking. It might also be possible to modify the model to take into account differential rotation.

Table 10: Rotation values from various methods

STAR	F_1(dc)	F_1 (simplex)	F_1(ptm)	F_1(sp) (previous)	F_1 (Rossiter)	F_{cr}	$V_{eq.}\sin i$ (km sec^{-1})	$V_{syn}\sin i$ (km sec^{-1})	$R=(F-1)/(F_{cr}-1)$
S Cnc	13.15	13.01	13.0	-	-	28.52	157.9	12.0	0.44 (sp) 0.44 (ptm)
RZ Cas	1.38	1.38	-	1.16	1.60	5.65	84.9	61.5	0.08
TV Cas	0.89	0.88	-	0.73	2.10	3.57	80.7	90.7	- 0.04
U Cep	6.59	6.62	5.0	5.24	9.00	7.44	339.1	51.5	0.87 (sp) 0.62 (ptm)
SW Cyg	8.06	-	11.66	5.6	5.00	11.66	206.1	25.6	0.66 (sp) 1.0 (ptm)
S Equ	1.17	1.15	-	1.41	-	8.00	49.1	42.0	0.02

Table 10– – (Continued)

STAR	F_1(dc)	F_1 (simplex)	F_1(ptm)	F_1(sp) (previous)	F_1 (Rossiter)	F_{cr}	$V_{eq.} \sin i$ (km sec^{-1})	$V_{syn} \sin i$ (km sec^{-1})	$R=(F-1)/(F_{cr}-1)$
RY Gem	8.80	8.99	14.4	-	4.50	24.24	117.8	13.4	0.34 (sp) 0.58 (ptm)
RW Mon	1.30	1.29	5.0	-	-	7.22	69.8	53.7	0.05 (sp) 0.64 (ptm)
TU Mon	4.87	4.89	-	-	-	8.37	282.4	58.0	0.53
DM Per	2.64	2.64	-	-	-	5.06	190.4	72.1	0.40
RW Per	16.21	16.11	28.8	-	-	29.65	159.8	9.9	0.53 (sp) 0.97 (ptm)
RY Per	9.63	9.60	10.8	9.11	9.5	14.50	302.7	31.4	0.64 (sp) 0.73 (ptm)
β Per	1.14	1.13	-	1.04	-	7.09	56.9	49.9	0.02
Y Psc	1.01	1.02	-	1.01	1.65	7.28	37.3	36.9	0.00

Table 10– – (Continued)

STAR	F_1(dc)	F_1 (simplex)	F_1(ptm)	F_1(sp) (previous)	F_1 (Rossiter)	F_{cr}	$V_{eq.}\ sin\ i$ (km sec^{-1})	$V_{syn}\ sin\ i$ (km sec^{-1})	$R=(F-1)\ /\ (F_{cr}-1)$
U Sge	1.34	1.34	-	1.31	4.5	5.93	80.1	59.8	0.07 (sp)
RZ Sct	4.49	4.34	6.7	5.8	12.5	6.7	177.2	39.5	0.62 (sp) 1.0 (ptm)
Z Vul	1.41	1.41	-	1.42	-	3.30	134.9	95.7	0.18

Table 11: Rotation statistics of Algols from the literature

Star	Spectral Type	Period (days)	F_1(sp)	F_{cr}	$V_{eq}\sin i$ (km sec^{-1})	$V_{syn}\sin i$ (km sec^{-1})	R
IM Aur	B7	1.25	1.27	2.34	135	106	0.20
R CMa	F1	1.14	1.45	3.49	98	68	0.18
XX Cep	A8	2.34	1.04	6.60	47	45	0.01
U CrB	B6	3.45	1.35	9.32	60	44	0.04
W Del	B9.5	4.81	1.36	14.04	30	22	0.03
TW Dra	A5	2.80	1.28	6.21	50	39	0.05
AI Dra	A1	1.19	0.86	3.32	85	99	-0.06
AS Eri	A3	2.66	1.51	11.02	45	30	0.05
TT Hya	B9.5	6.95	11.5	24.85	168	15	0.44
δ Lib	A0	2.33	0.77	3.49	68	88	-0.09
AW Peg	A4	10.6	14.8	53.68	101	7	0.26(sp) 0.66(ptm)
RT Per	F2	0.85	0.58	4.01	50	86	-0.09
IZ Per	B8	3.69	2.94	3.72	185	63	0.71

Table 11– – (Continued)

Star	Spectral Type	Period (days)	$F_1(sp)$	F_{cr}	$V_{eq}\sin i$ (km sec^{-1})	$V_{syn}\sin i$ (km sec^{-1})	R
V505 Sgr	A2	1.18	0.89	3.26	101	114	-0.05
RW Tau	B8	2.77	2.3	8.00	94	41	0.18
λ Tau	B2	3.96	1.11	3.73	88	79	0.05
X Tri	A3	0.97	0.56	3.80	50	89	-0.16
TX UMa	B8	3.07	1.81	10.12	67	37	0.09
DL Vir	A3	1.32	1.77	4.85	121	68	0.20
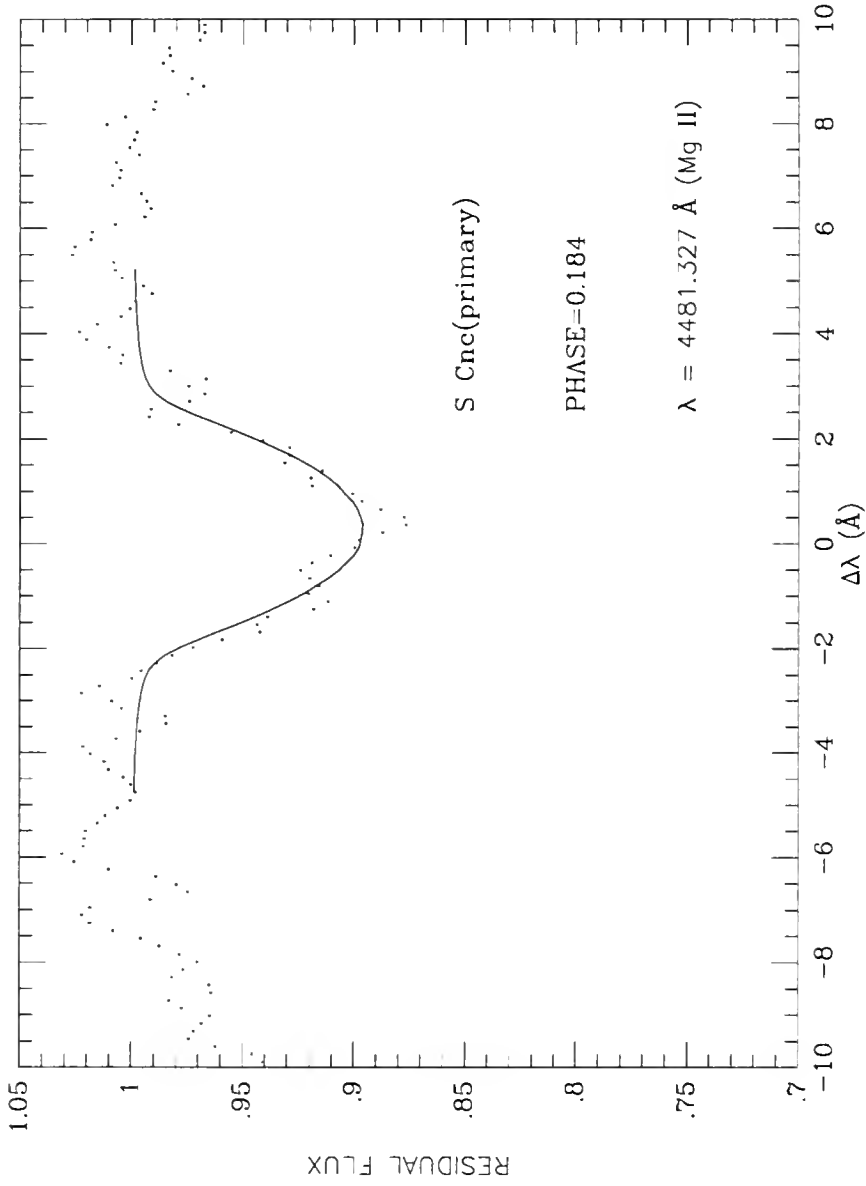
Figure 17: Fit to the observed line profile (dots) for S Cnc
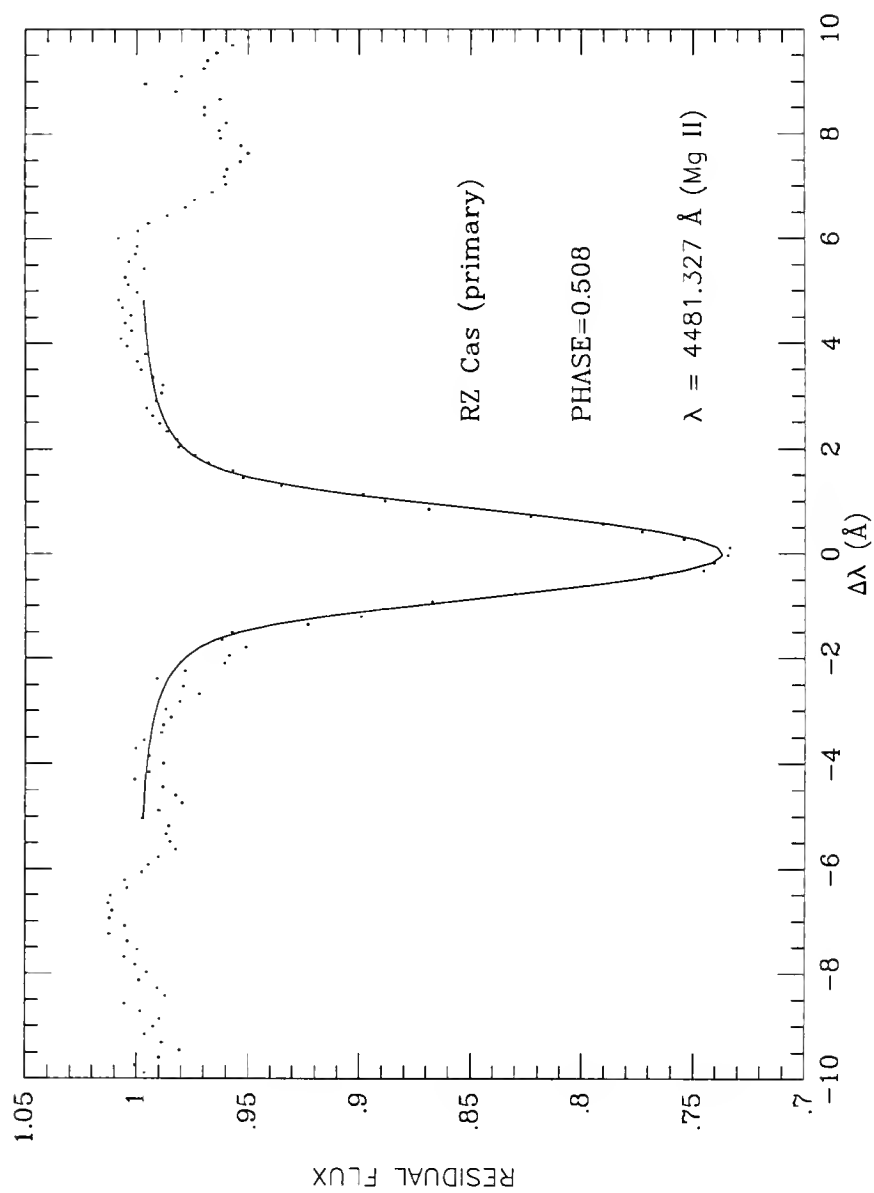
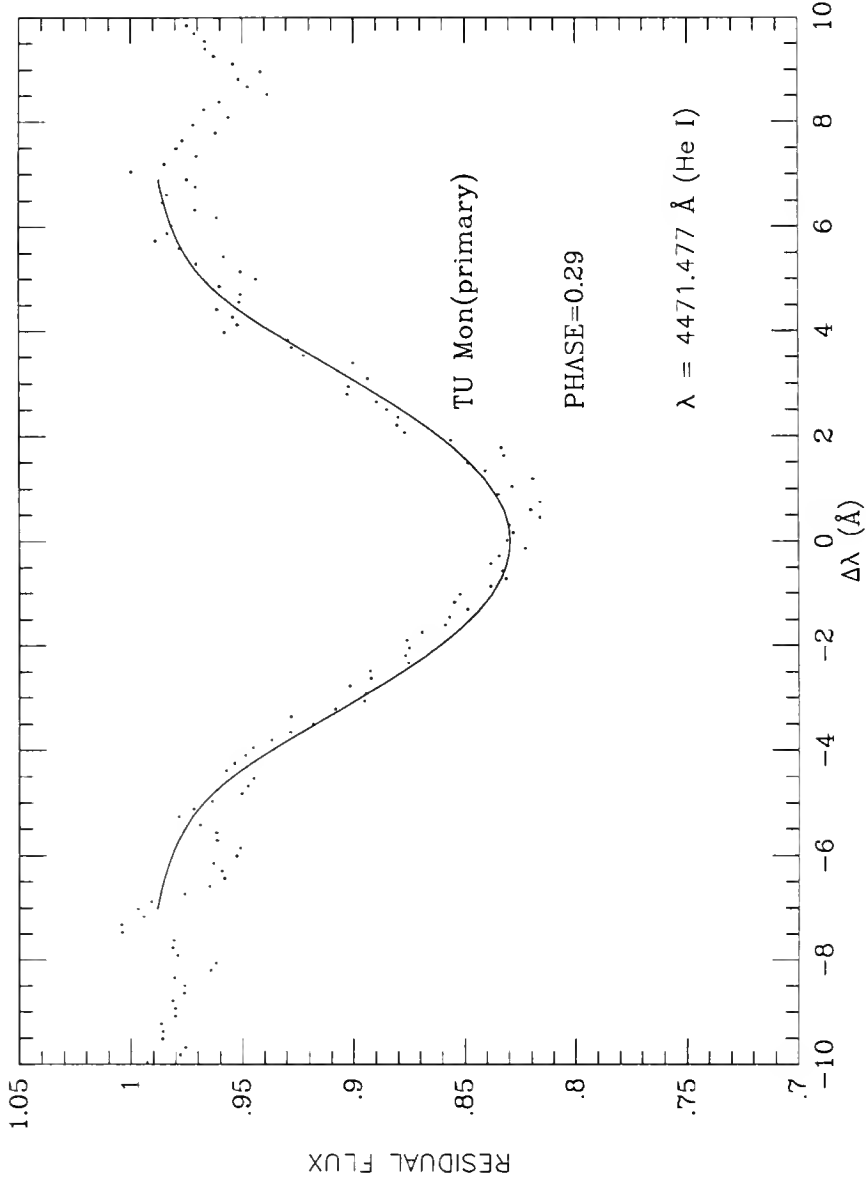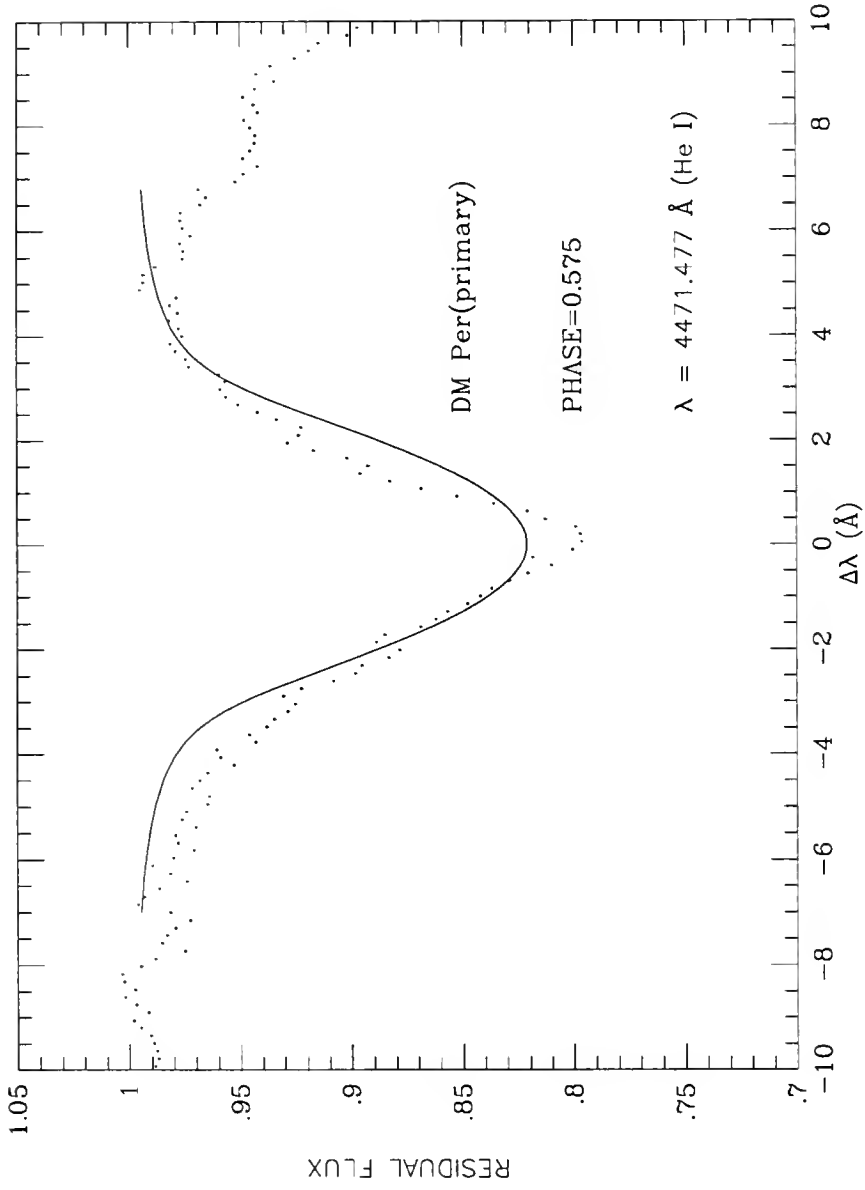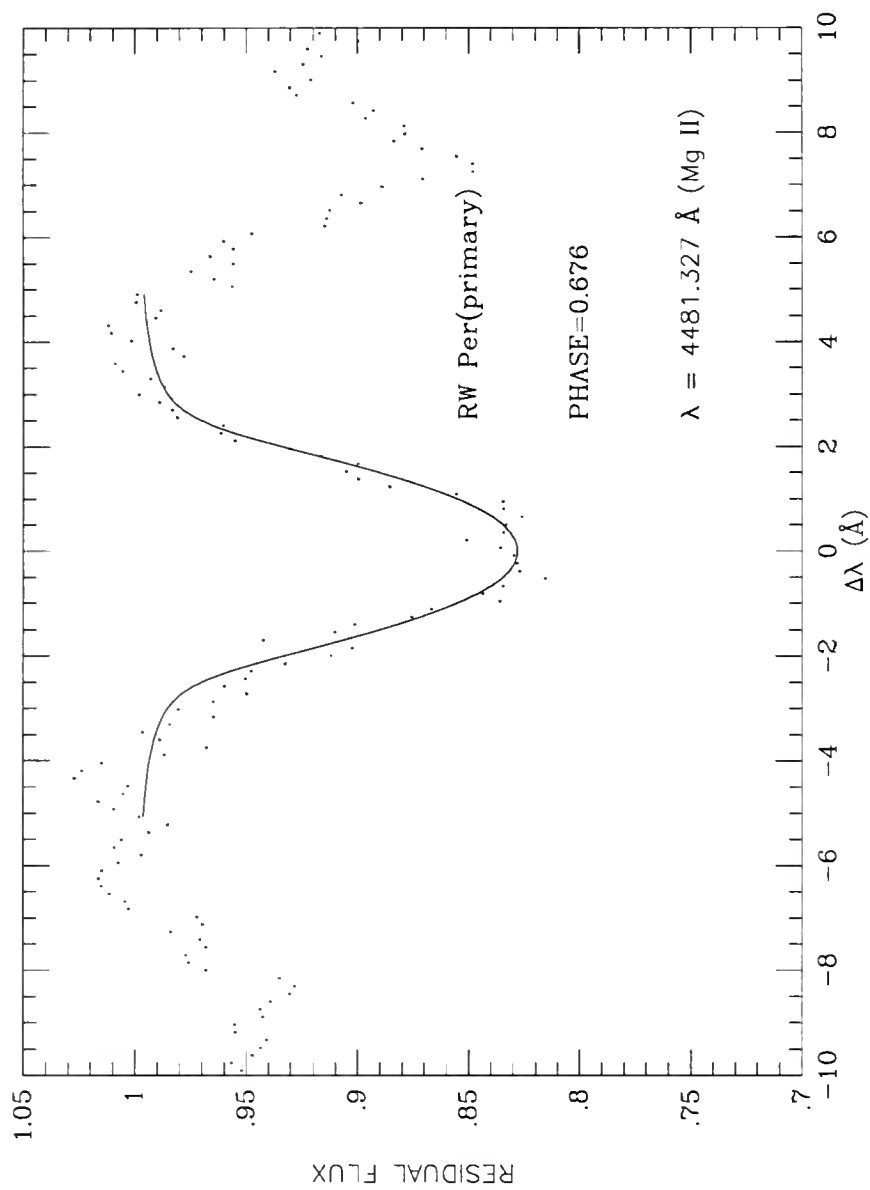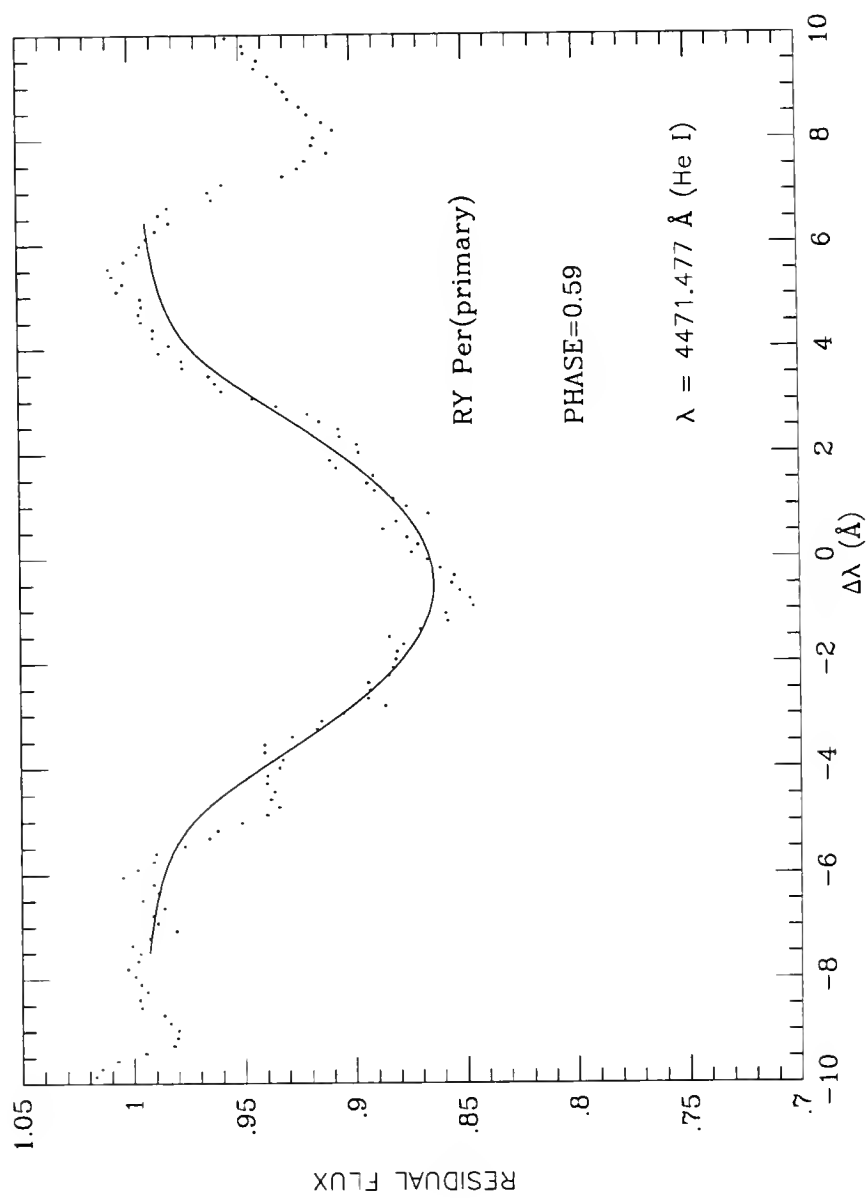Figure 18: Fit to the observed line profile (dots) for RZ Cas
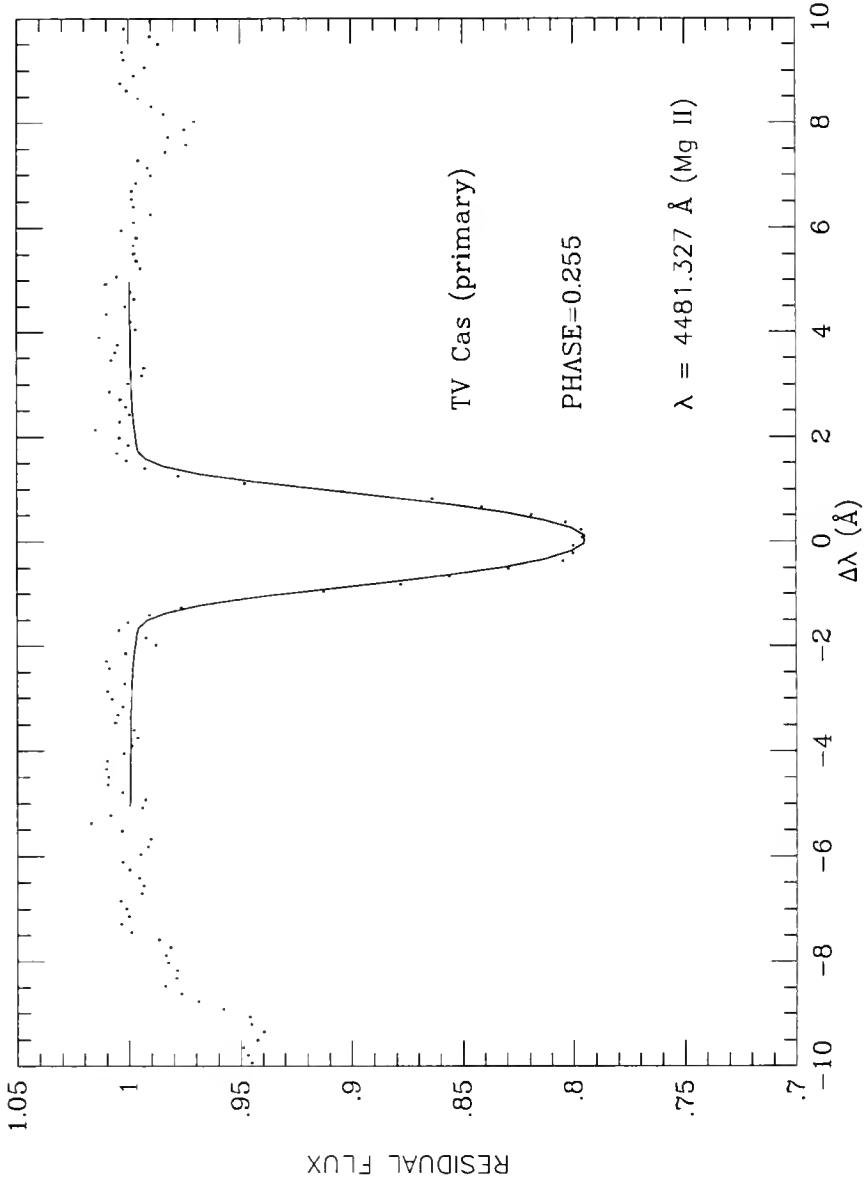
Figure 19: Fit to the observed line profile (dots) for TV Cas
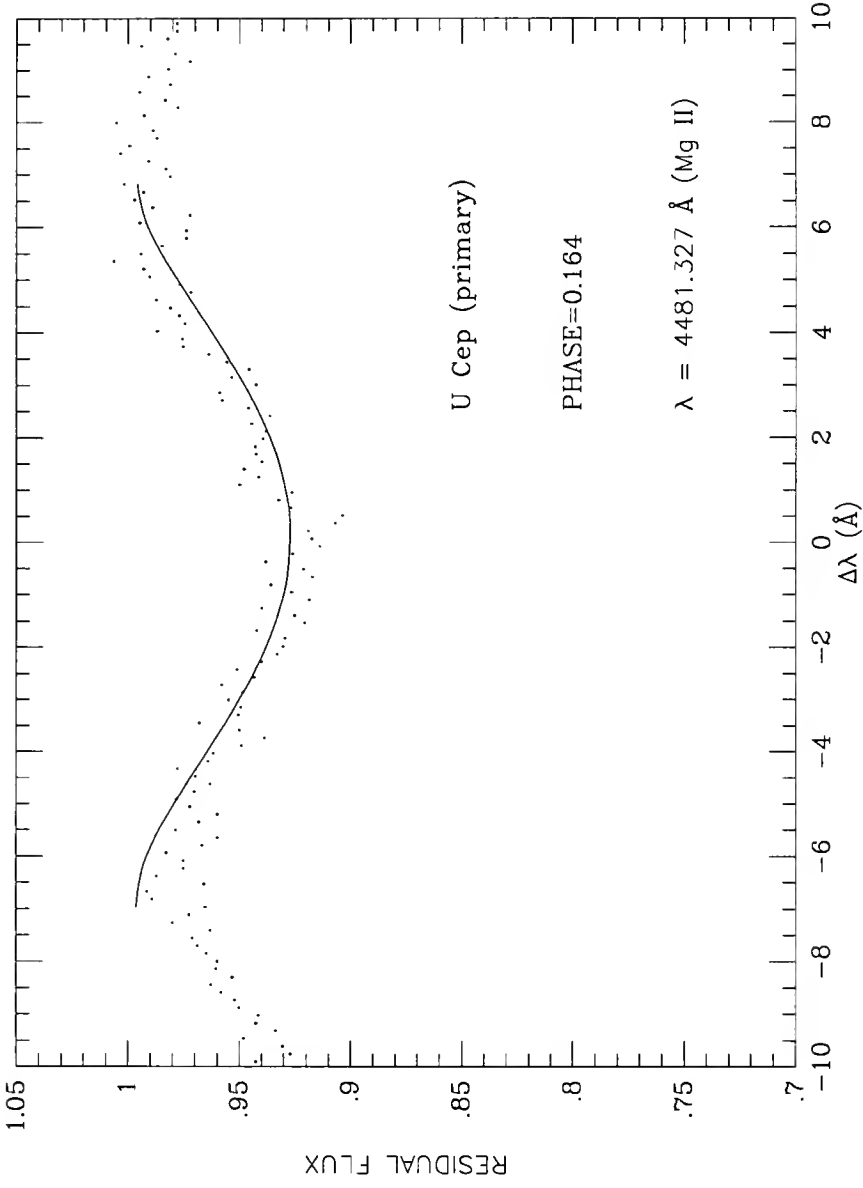
Figure 20: Fit to the observed line profile (dots) for U Cep
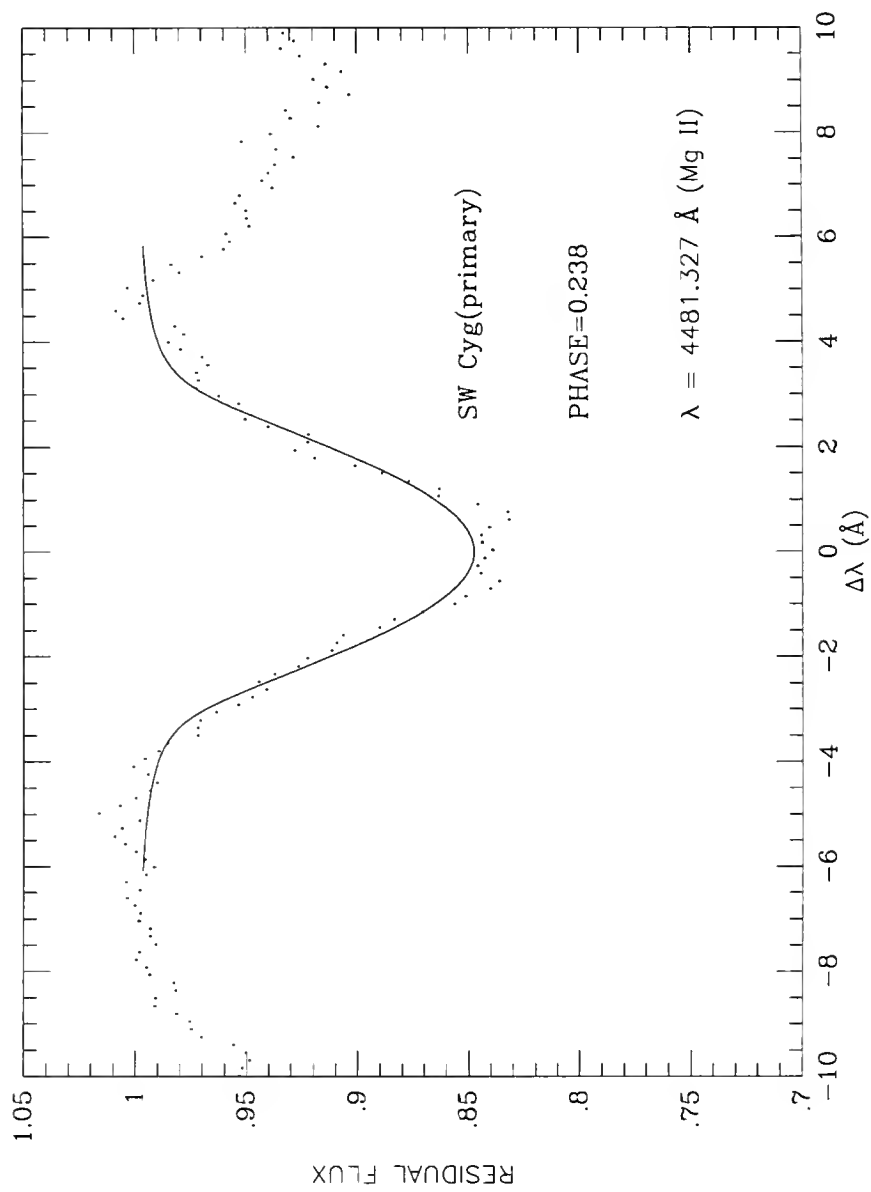
Figure 21: Fit to the observed line profile (dots) for SW Cyg

S Equ (primary)

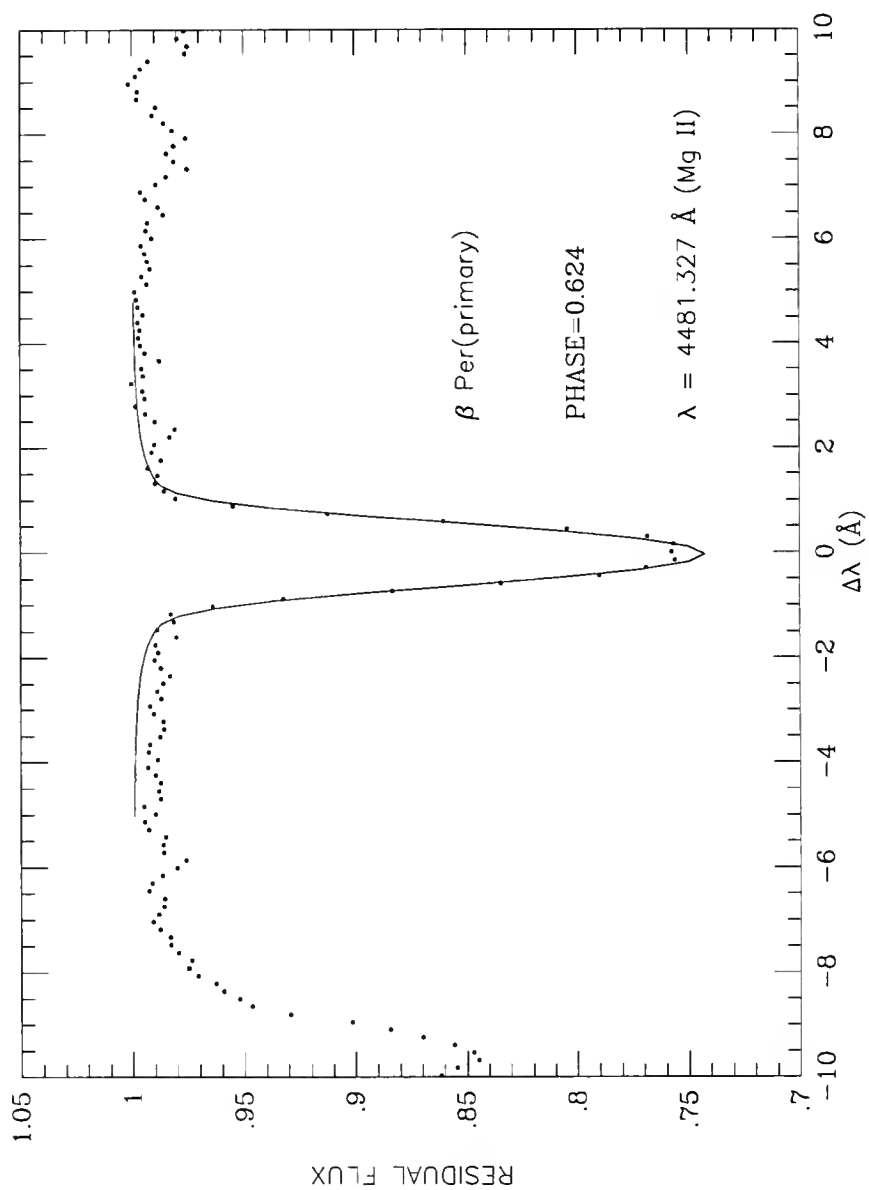PHASE=0.242

λ = 4481.327 Å (Mg II)
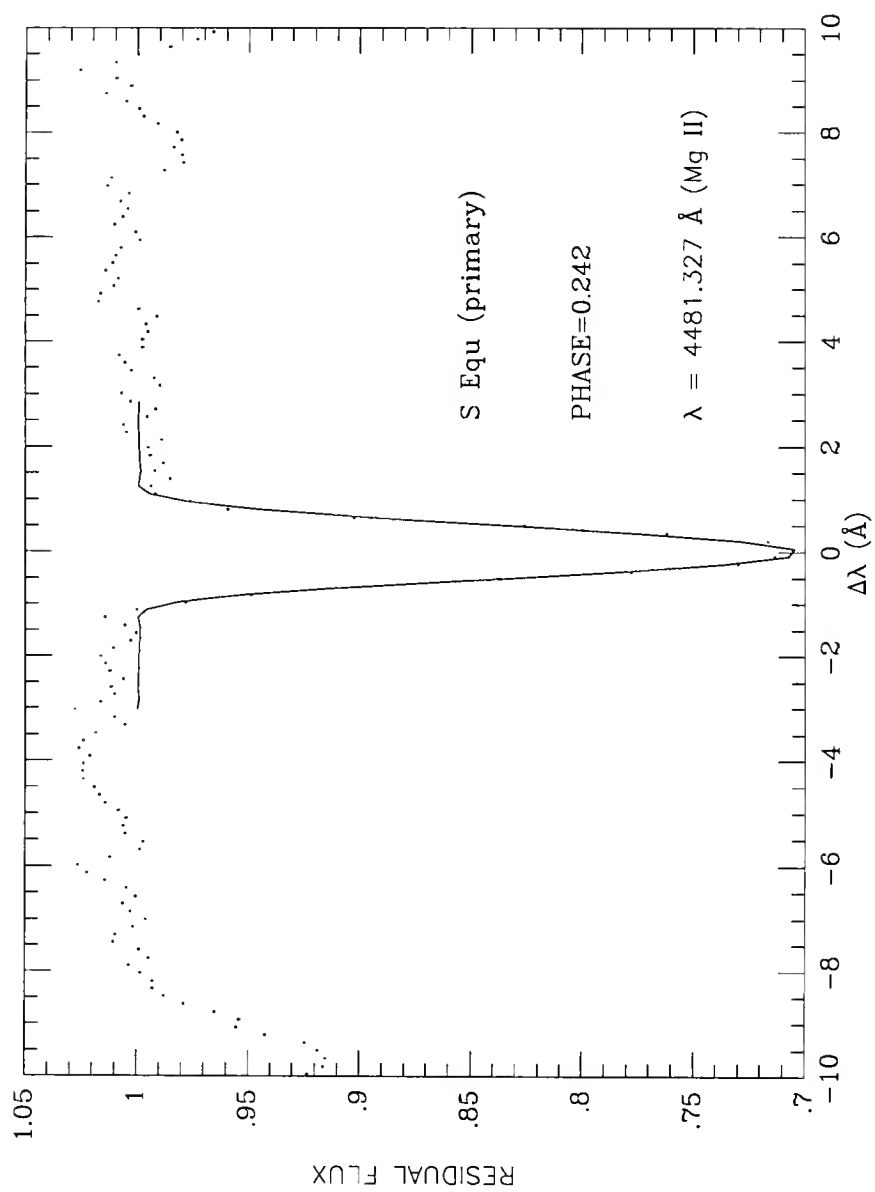
Figure 22: Fit to the observed line profile (dots) for S Equ
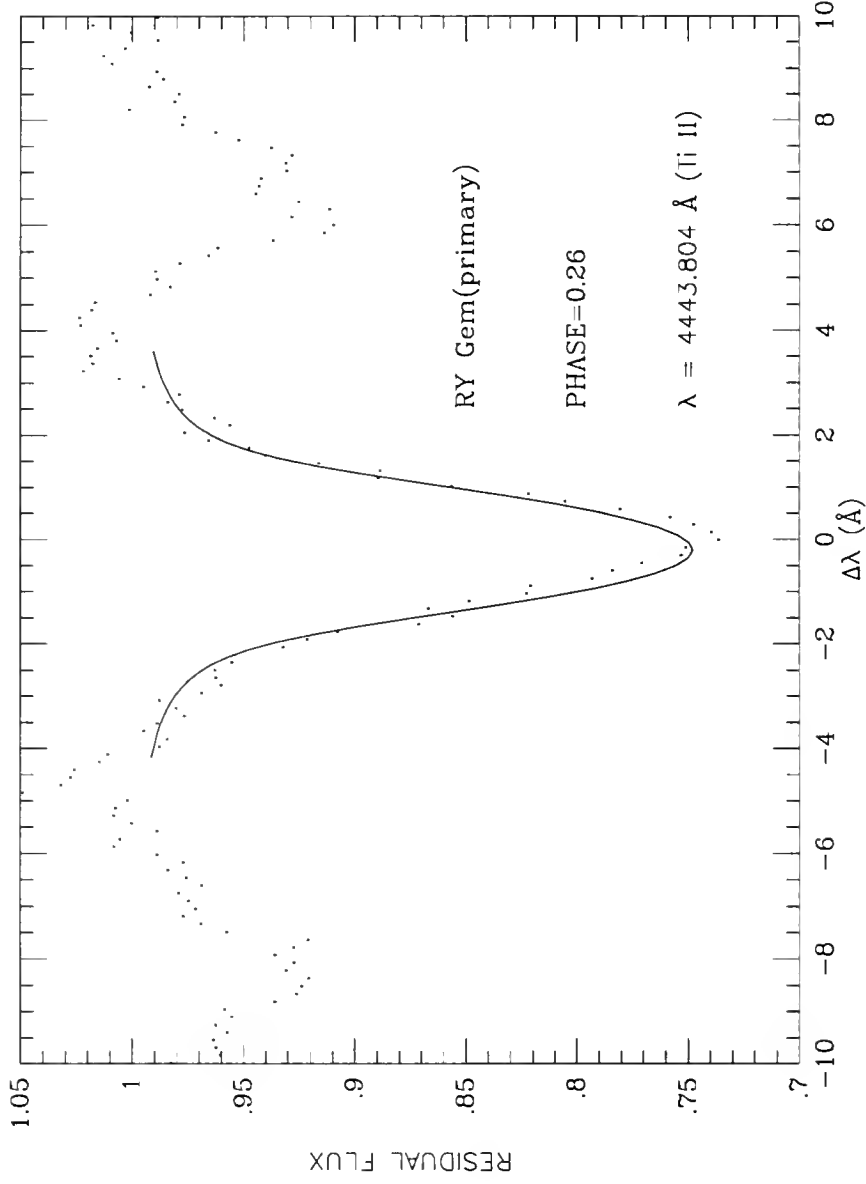
Figure 23: Fit to the observed line profile (dots) for RY Gem
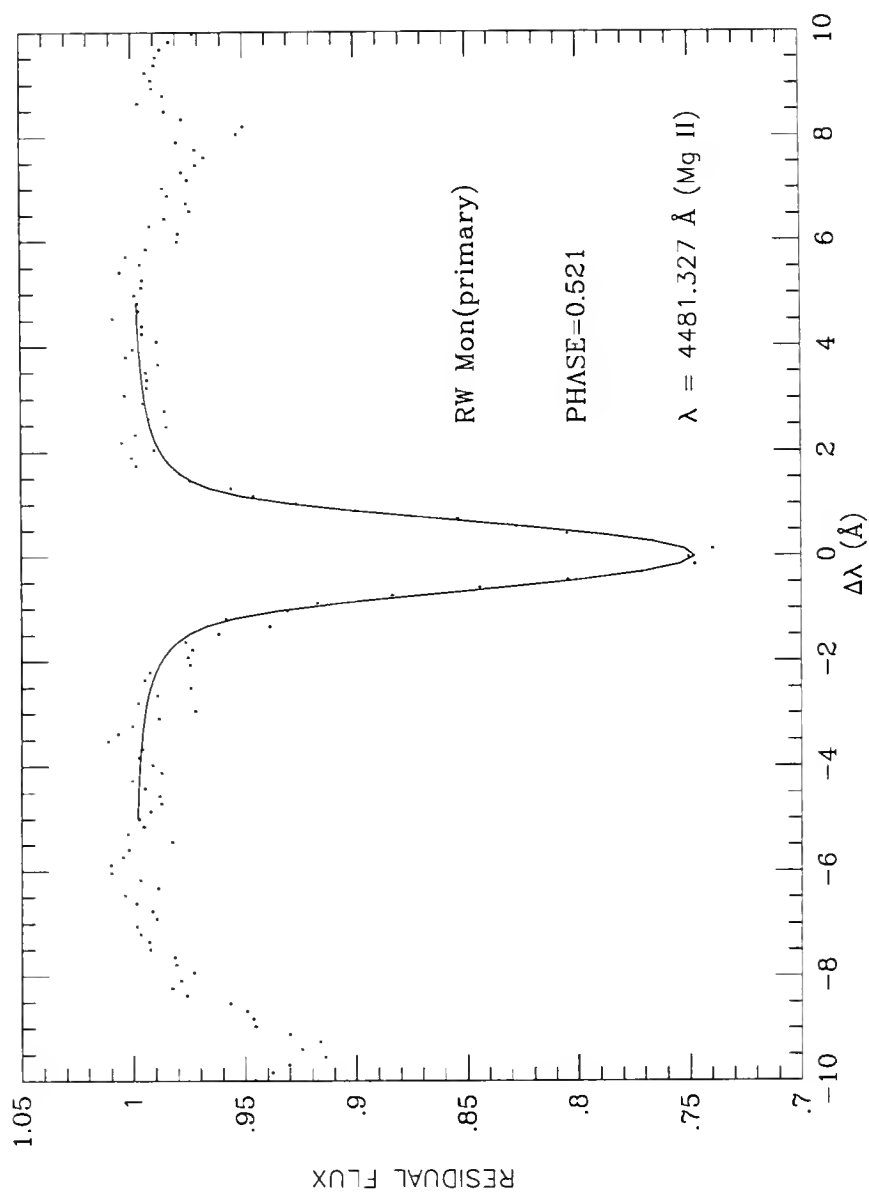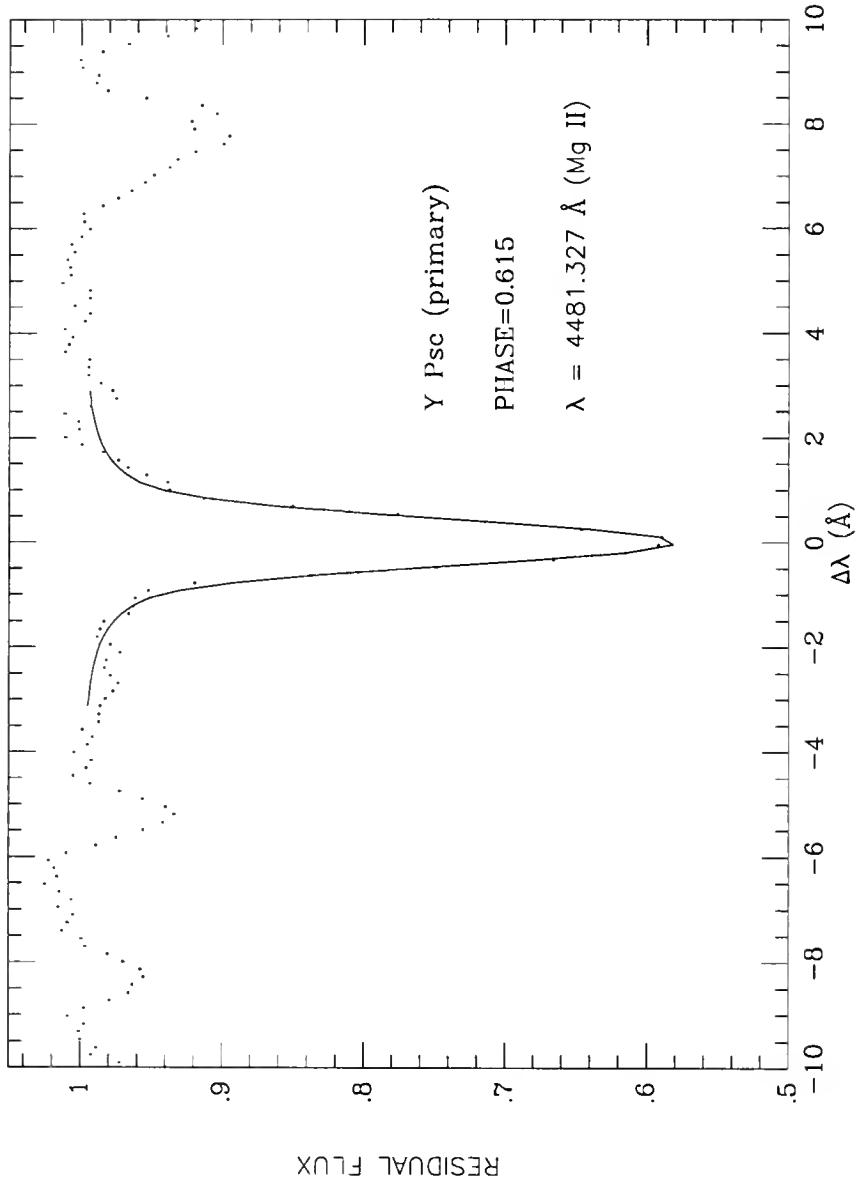
Figure 24: Fit to the observed line profile (dots) for RW Mon

TU Mon(primary)

PHASE=0.29

λ = 4471.477 Å (He I)

Figure 25: Fit to the observed line profile (dots) for TU Mon

Figure 26: Fit to the observed line profile (dots) for DM Per

Figure 27: Fit to the observed line profile (dots) for RW Per

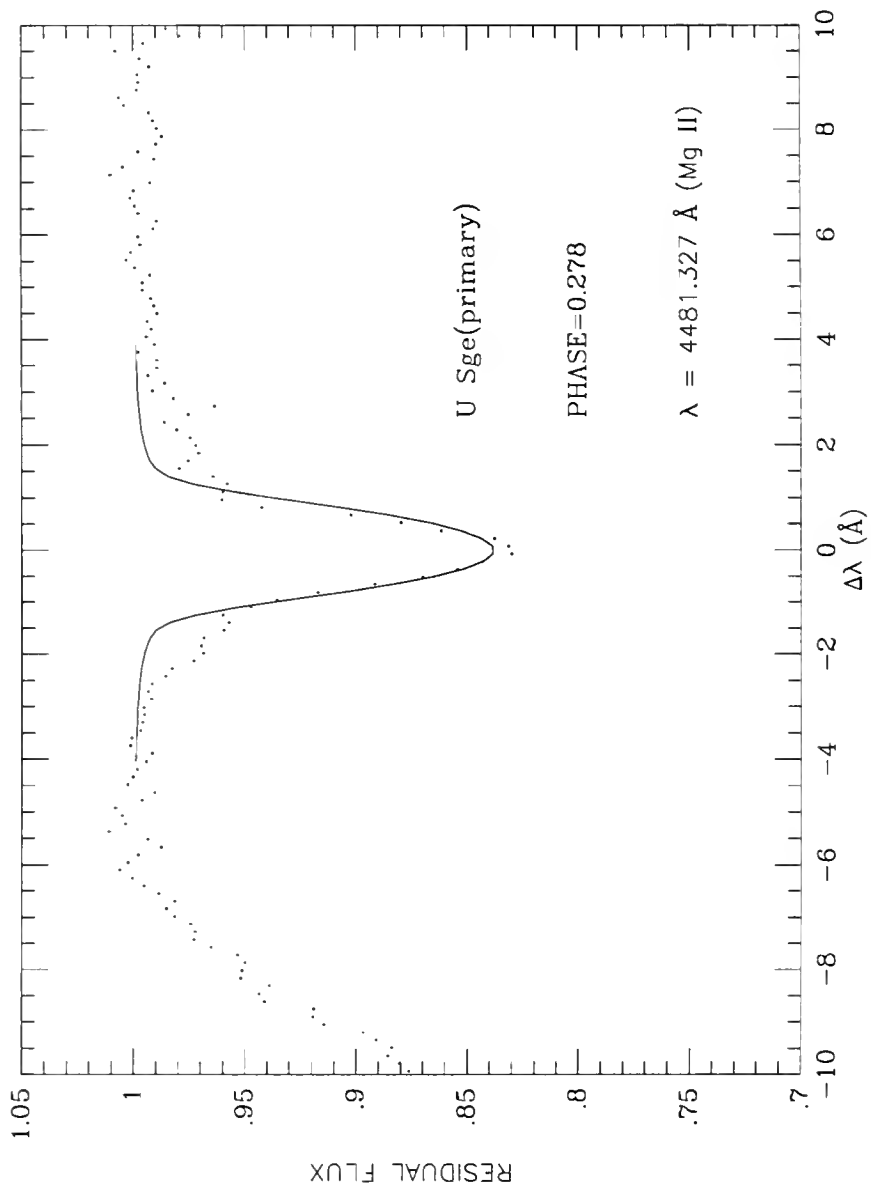Figure 28: Fit to the observed line profile (dots) for RY Per

β Per(primary)

PHASE=0.624

λ = 4481.327 Å (Mg II)

Figure 29: Fit to the observed line profile (dots) for β Per

Figure 30: Fit to the observed line profile (dots) for Y Psc

U Sge(primary)

PHASE=0.278

λ = 4481.327 Å (Mg II)

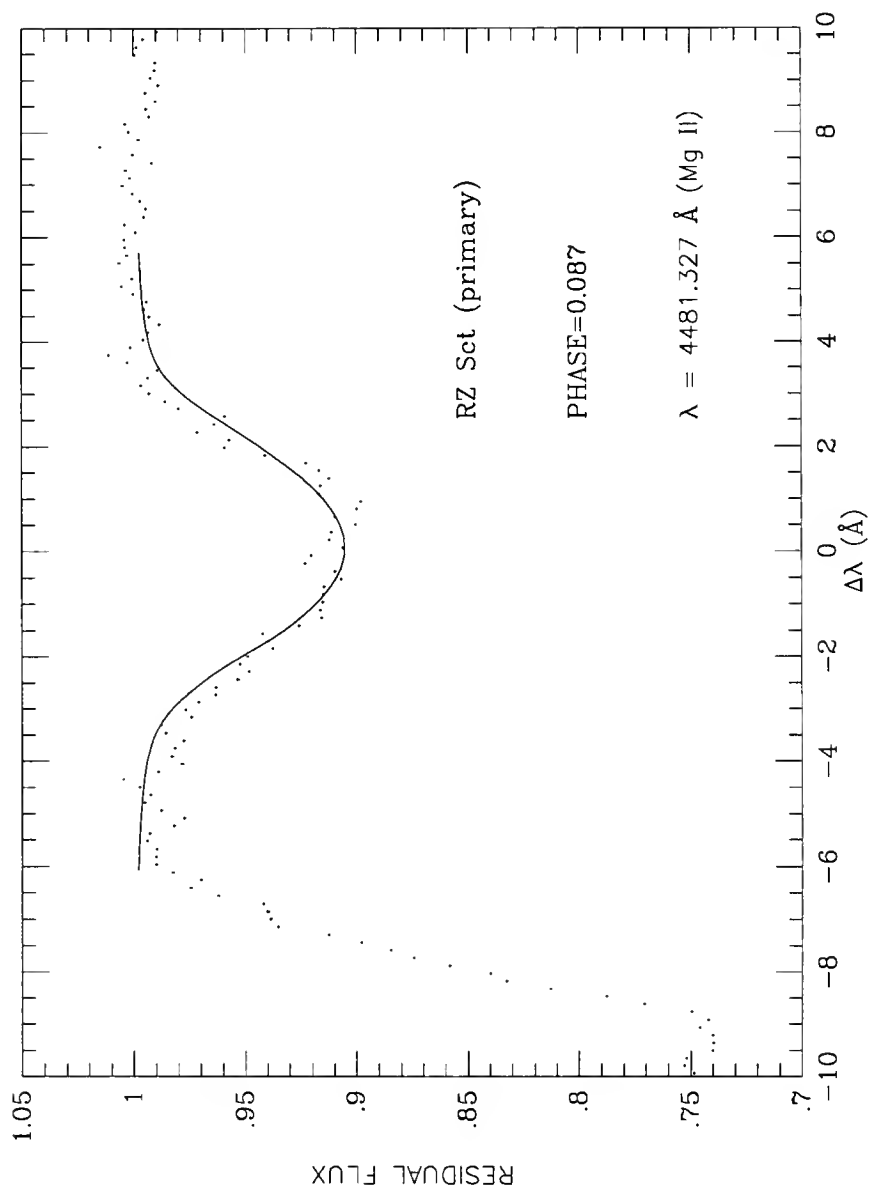Figure 31: Fit to the observed line profile (dots) for U Sge

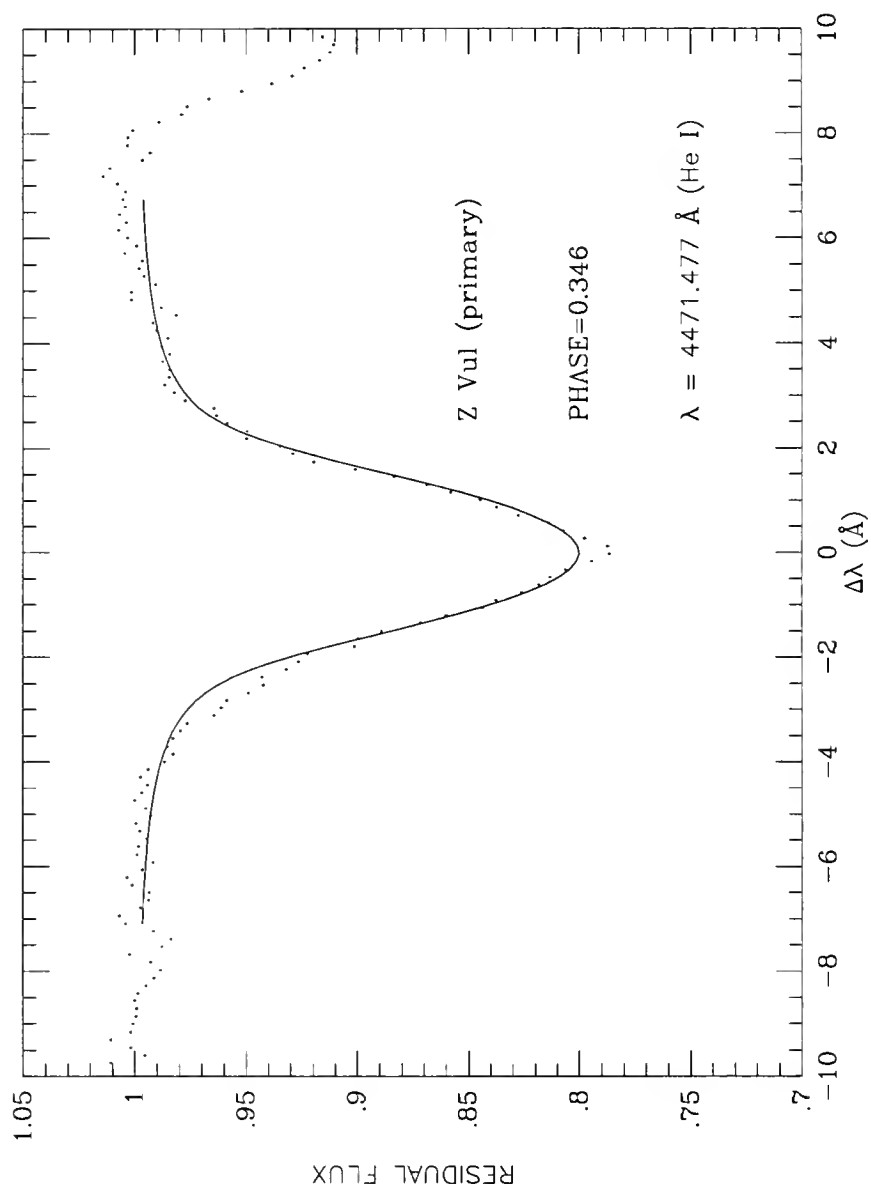Figure 32: Fit to the observed line profile (dots) for RZ Sct

Figure 33: Fit to the observed line profile (dots) for Z Vul

APPENDIX A
LIGHT CURVES

Appendix A contains figures showing the system at different orbital phases along with their light curves and photometric and spectroscopic parameters (Terrell et al., 1992). The light curves shown are U, V, and I from top to bottom. The two vertical lines above the light curves represent the 0 and 0.5 phases respectively. The three horizontal lines on either sides of the light curves represent half the light of the system for each light curve. For the light curves the abscissa is the orbital phase from 0 to 1, while the ordinate represents normalized light. The top part of each figure represents the system at different orbital phases starting from phase 0 to phase 0.5. The small circle at the right shows the Sun to scale.
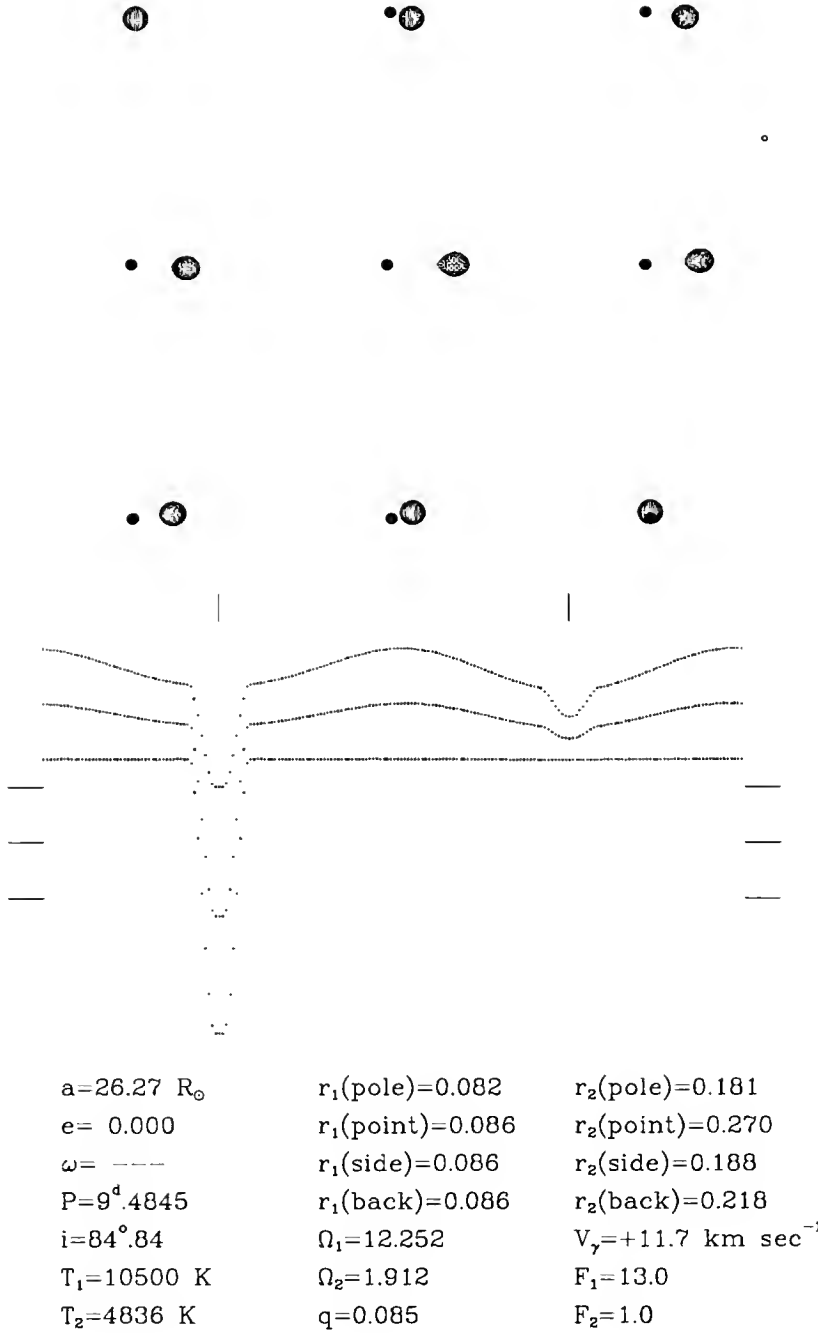
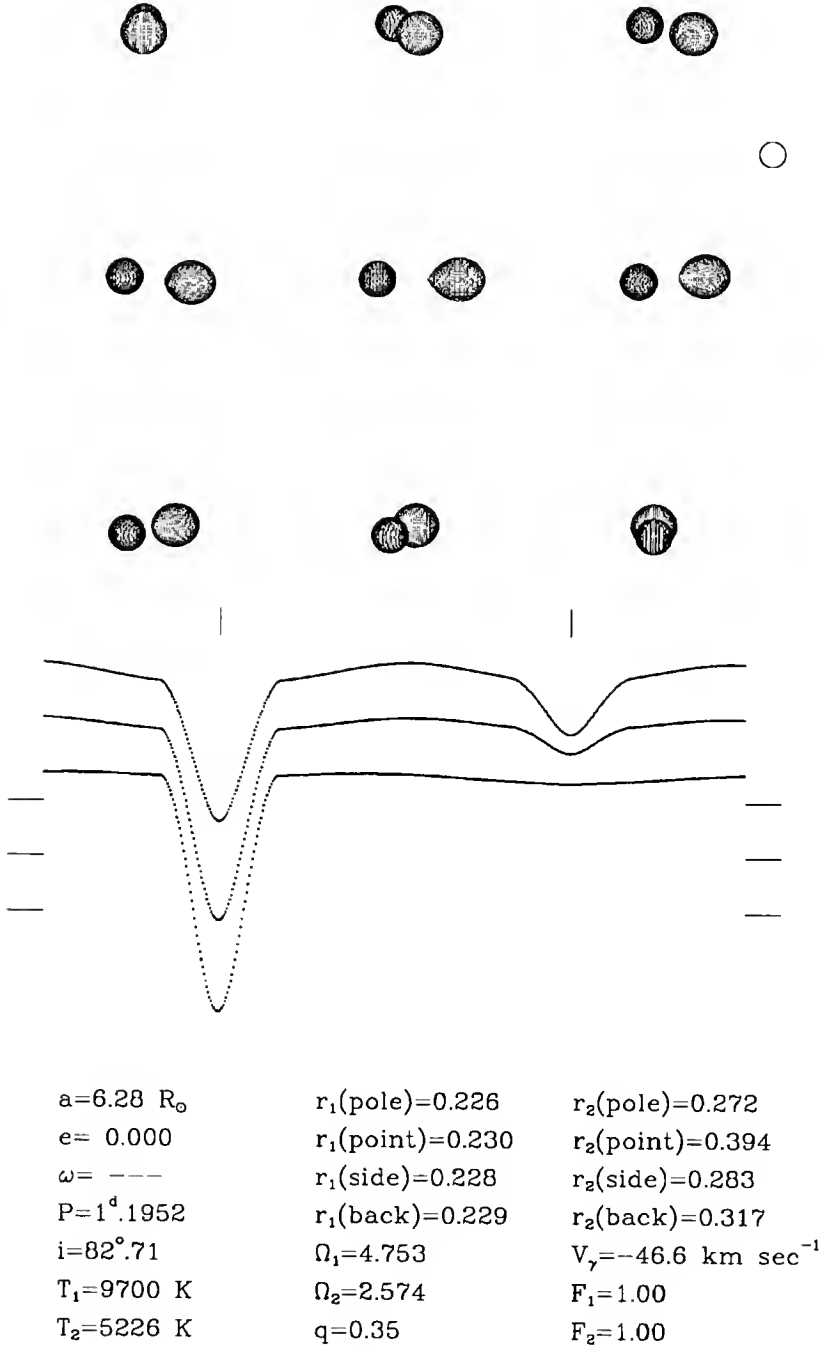| a=26.27 $R_\odot$	r_1(pole)=0.082	r_2(pole)=0.181
e= 0.000	r_1(point)=0.086	r_2(point)=0.270
$\omega=$ ---	r_1(side)=0.086	r_2(side)=0.188
P=9^d.4845	r_1(back)=0.086	r_2(back)=0.218
i=84°.84	Ω_1=12.252	V_γ=+11.7 km sec^{-1}
T_1=10500 K	Ω_2=1.912	F_1=13.0
T_2=4836 K	q=0.085	F_2=1.0

Figure 34: The system S Cnc at different orbital phases along with its light curves and photometric elements

$a=6.28 \ R_\odot$ $r_1(pole)=0.226$ $r_2(pole)=0.272$

$e=0.000$ $r_1(point)=0.230$ $r_2(point)=0.394$

$\omega= \ ---$ $r_1(side)=0.228$ $r_2(side)=0.283$

$P=1^d.1952$ $r_1(back)=0.229$ $r_2(back)=0.317$

$i=82^\circ.71$ $\Omega_1=4.753$ $V_\gamma=-46.6 \ km \ sec^{-1}$

$T_1=9700 \ K$ $\Omega_2=2.574$ $F_1=1.00$

$T_2=5226 \ K$ $q=0.35$ $F_2=1.00$

Figure 35: The system RZ Cas at different orbital phases along with its light curves and photometric elements
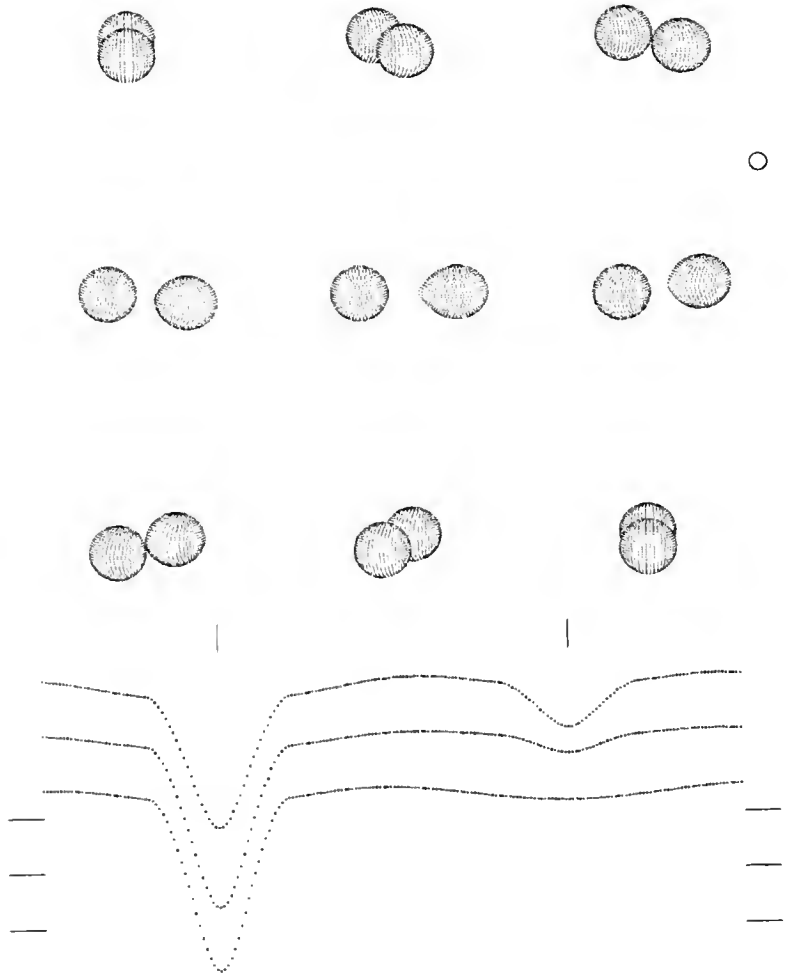
a=11.2 $R_\odot$	r_1(pole)=0.289	r_2(pole)=0.283
e= 0.000	r_1(point)=0.300	r_2(point)=0.404
ω= ---	r_1(side)=0.294	r_2(side)=0.295
P=1^d.8127	r_1(back)=0.298	r_2(back)=0.327
i=80°.3	Ω_1=3.846	V_γ=+0.5 km sec^{-1}
T_1=10800 K	Ω_2=2.678	F_1=1.00
T_2=5100 K	q=0.40	F_2=1.00

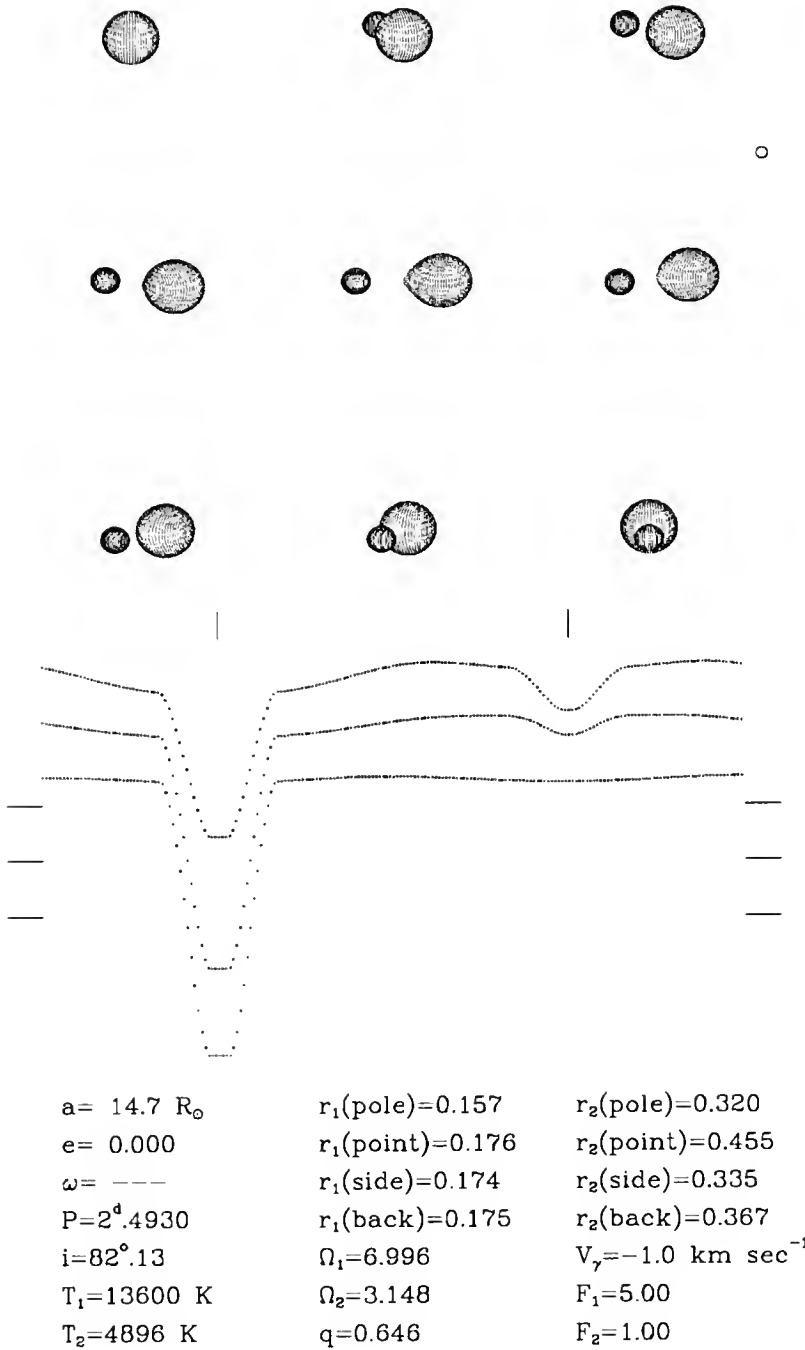Figure 36: The system TV Cas at different orbital phases along with its light curves and photometric elements

$$
\begin{array}{lll}
a= 14.7\ R_\odot & r_1(\text{pole})=0.157 & r_2(\text{pole})=0.320 \\
e= 0.000 & r_1(\text{point})=0.176 & r_2(\text{point})=0.455 \\
\omega= \ \text{---} & r_1(\text{side})=0.174 & r_2(\text{side})=0.335 \\
P=2^d.4930 & r_1(\text{back})=0.175 & r_2(\text{back})=0.367 \\
i=82^\circ.13 & \Omega_1=6.996 & V_\gamma=-1.0\ \text{km sec}^{-1} \\
T_1=13600\ \text{K} & \Omega_2=3.148 & F_1=5.00 \\
T_2=4896\ \text{K} & q=0.646 & F_2=1.00
\end{array}
$$

Figure 37: The system U Cep at different orbital phases along with the light curves and photometric elements

$$
\begin{array}{lll}
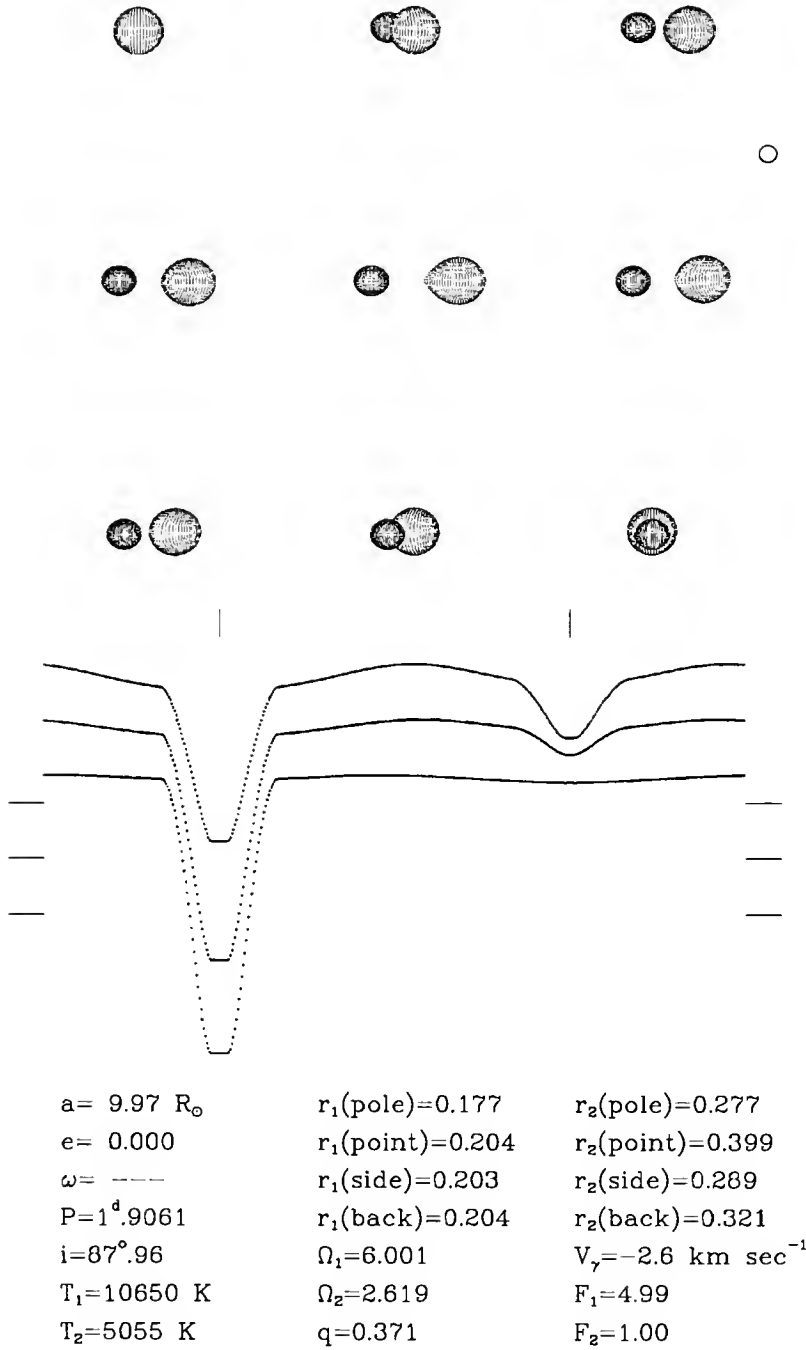a= \ 13.94 \ R_{\odot} & r_1(\text{pole})=0.117 & r_2(\text{pole})=0.276 \\
e= \ 0.000 & r_1(\text{point})=0.175 & r_2(\text{point})=0.398 \\
\omega= \ --- & r_1(\text{side})=0.167 & r_2(\text{side})=0.288 \\
P=4^d.573 & r_1(\text{back})=0.171 & r_2(\text{back})=0.320 \\
i=82°.70 & \Omega_1=8.937 & V_\gamma=-1.0 \ \text{km sec}^{-1} \\
T_1=9070 \ K & \Omega_2=2.609 & F_1=11.66 \\
T_2=3813 \ K & q=0.3664 & F_2=1.00 \\
\end{array}
$$
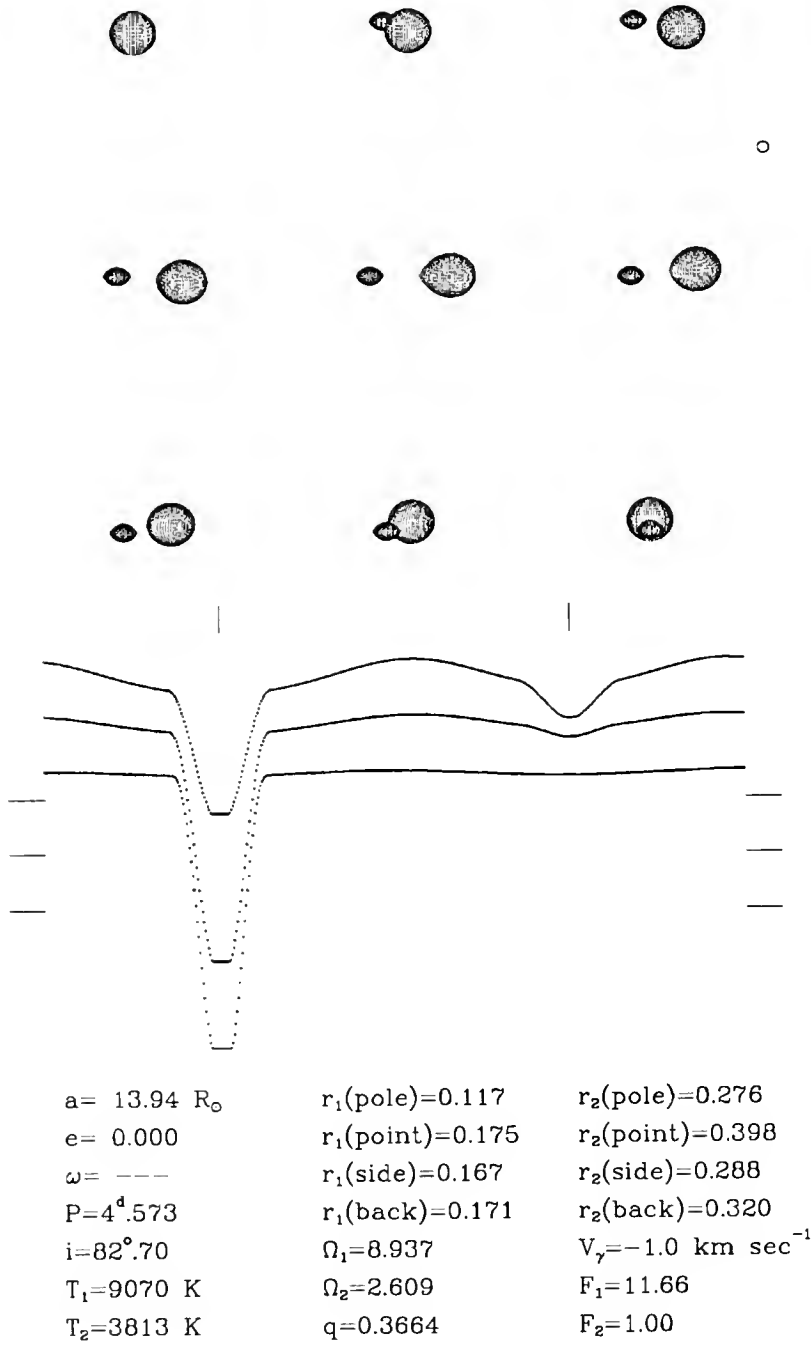
Figure 38: The system SW Cyg at different orbital phases along with its light curves and photometric elements

|		
a= 14.63 $R_\odot$	r_1(pole)=0.194	r_2(pole)=0.200
e= 0.000	r_1(point)=0.195	r_2(point)=0.297
ω= ---	r_1(side)=0.195	r_2(side)=0.208
P=3^d.4361	r_1(back)=0.195	r_2(back)=0.240
i=87°.4	Ω_1=5.266	V_γ=−48.0 km sec^{-1}
T_1=11400 K	Ω_2=2.019	F_1=1.00
T_2=5690 K	q=0.12	F_2=1.00
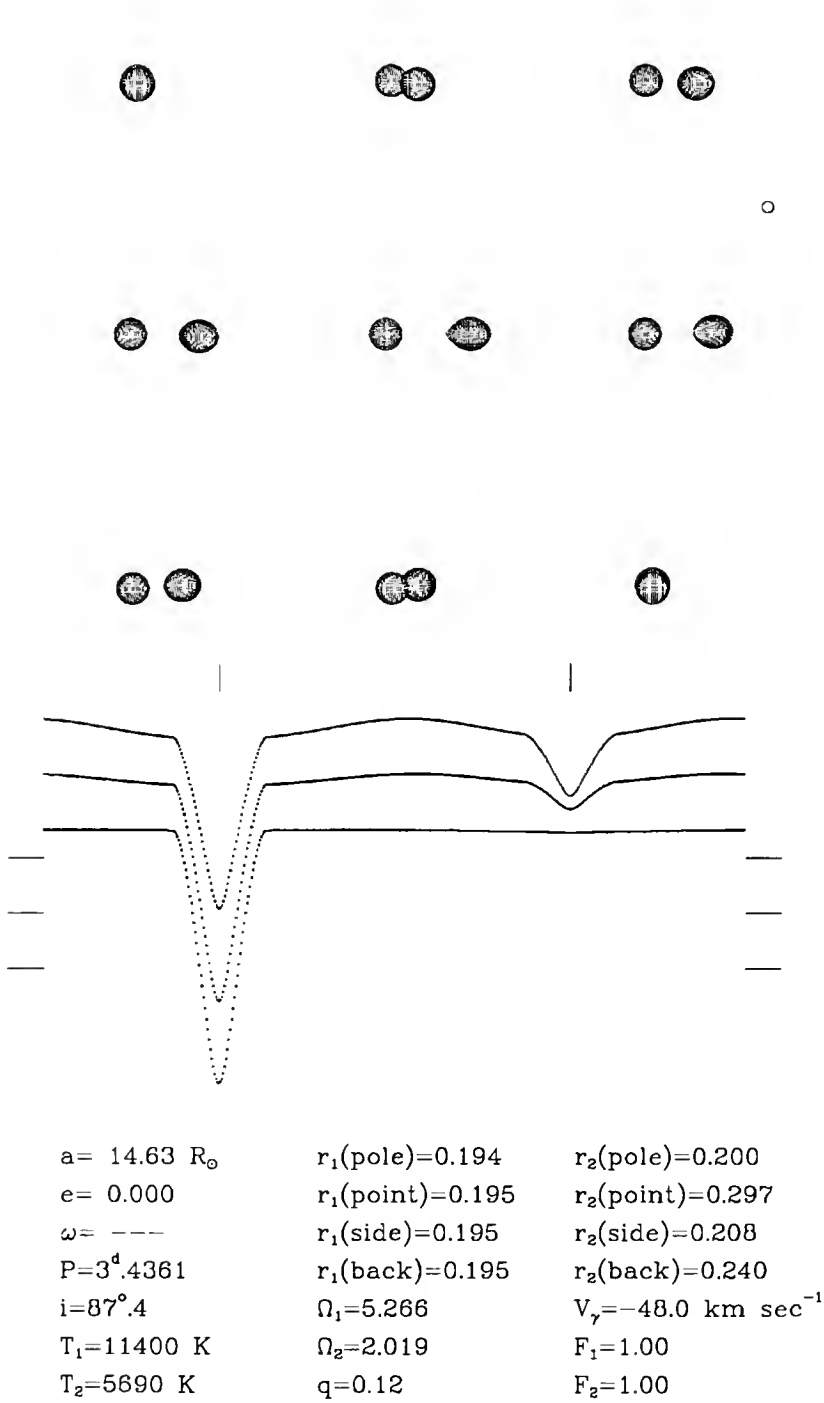
Figure 39: The system S Equ at different orbital phases along with its light curves and photometric elements

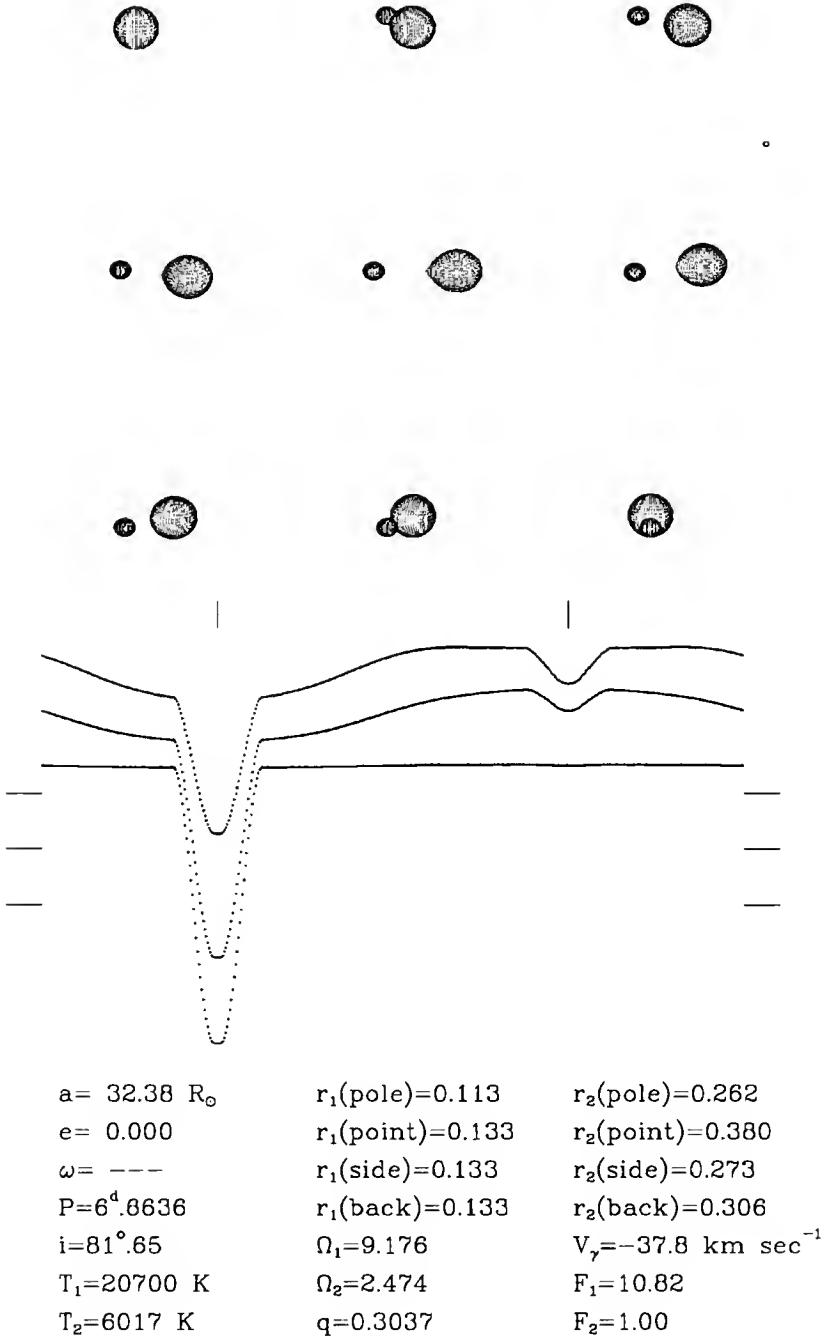|		
a= 25.79 $R_\odot$	r_1(pole)=0.086	r_2(pole)=0.227
e= 0.000	r_1(point)=0.096	r_2(point)=0.333
ω= ---	r_1(side)=0.096	r_2(side)=0.236
P=9^d.3005	r_1(back)=0.096	r_2(back)=0.268
i=$83°$.10	Ω_1=11.768	V_γ=+15.1 km sec^{-1}
T_1=9400 K	Ω_2=2.187	F_1=14.42
T_2=4043 K	q=0.1819	F_2=1.00
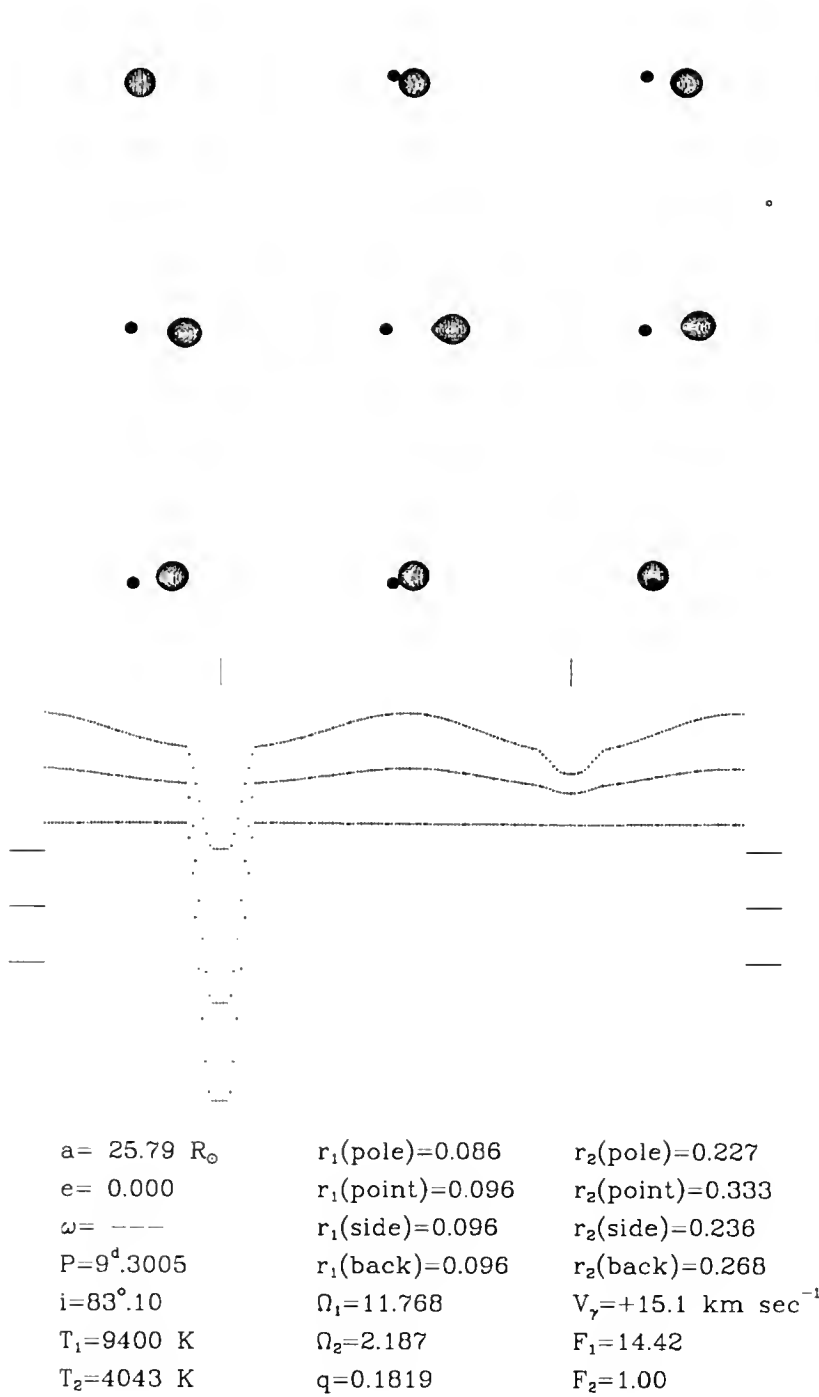
Figure 40: The system RY Gem at different orbital phases
along with its light curves and photometric elements

$$a= 9.97\ R_\odot \qquad r_1(\text{pole})=0.177 \qquad r_2(\text{pole})=0.277$$
$$e= 0.000 \qquad r_1(\text{point})=0.204 \qquad r_2(\text{point})=0.399$$
$$\omega= \ --- \qquad r_1(\text{side})=0.203 \qquad r_2(\text{side})=0.289$$
$$P=1^d.9061 \qquad r_1(\text{back})=0.204 \qquad r_2(\text{back})=0.321$$
$$i=87°.96 \qquad \Omega_1=6.001 \qquad V_\gamma=-2.6\ \text{km sec}^{-1}$$
$$T_1=10650\ K \qquad \Omega_2=2.619 \qquad F_1=4.99$$
$$T_2=5055\ K \qquad q=0.371 \qquad F_2=1.00$$

Figure 41: The system RW Mon at different orbital phases along with its light curves and photometric elements

a=31.43 $R_\odot$	r_1(pole)=0.183	r_2(pole)=0.236
e= 0.000	r_1(point)=0.184	r_2(point)=0.346
ω= ---	r_1(side)=0.184	r_2(side)=0.246
P=5^d.049	r_1(back)=0.184	r_2(back)=0.278
i=89°.1	Ω_1=5.662	V_γ=+20.0 km sec^{-1}
T_1=15520 K	Ω_2=2.257	F_1=1.00
T_2=7280 K	q=0.21	F_2=1.00
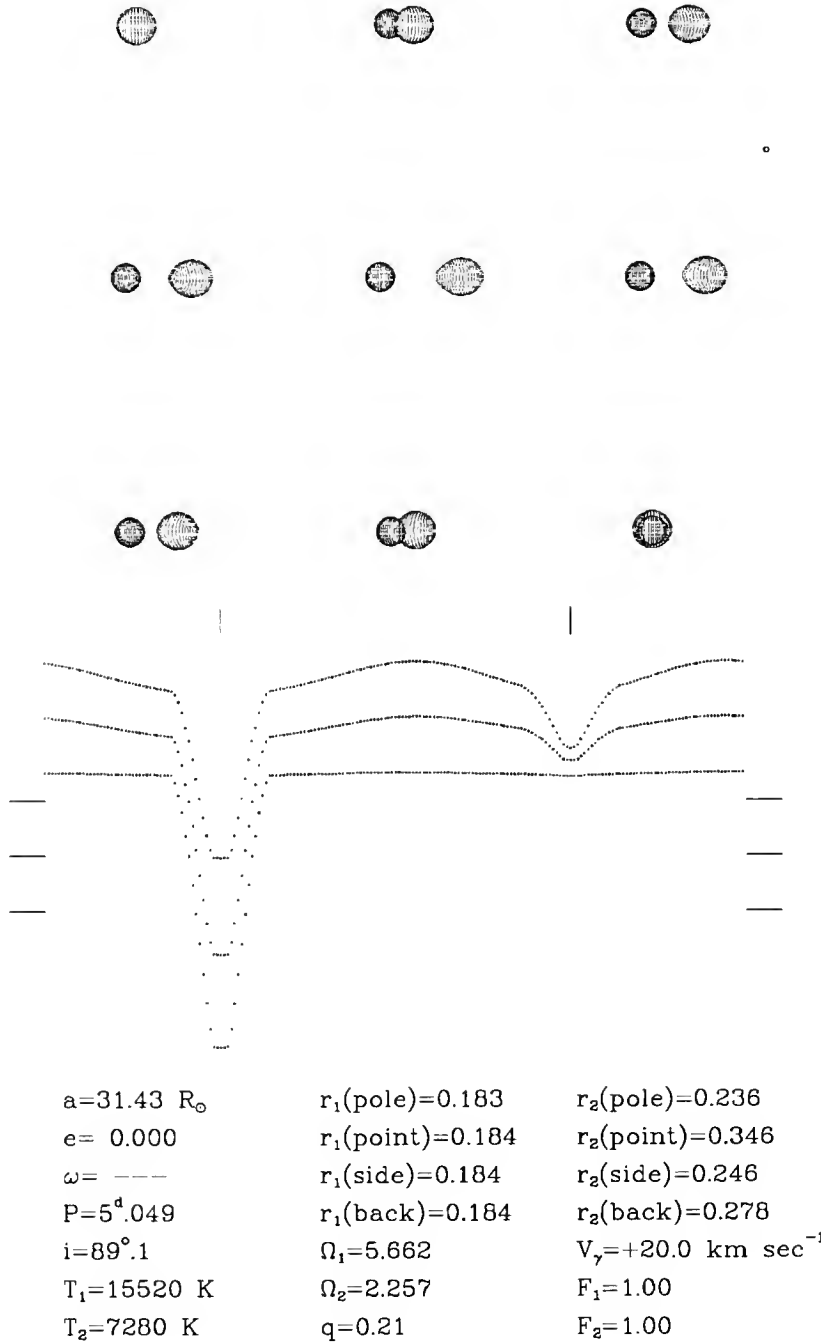
Figure 42: The system TU Mon at different orbital phases along with its light curves and photometric elements
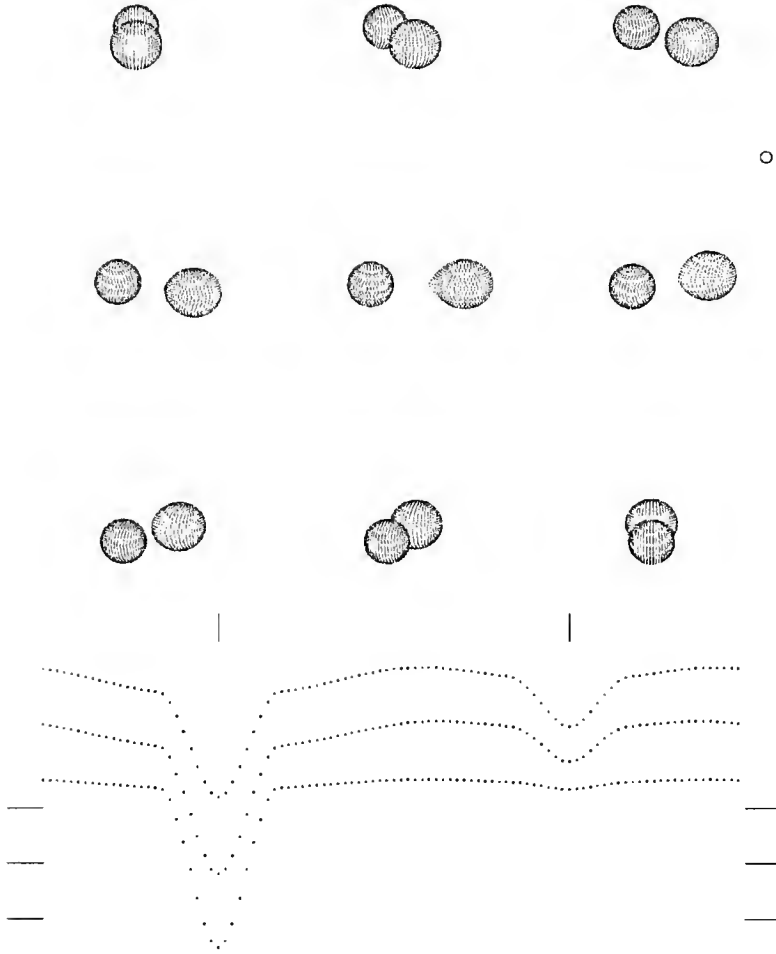
a=16.17 $R_\odot$	r_1(pole)=0.243	r_2(pole)=0.266
e= 0.000	r_1(point)=0.248	r_2(point)=0.385
ω= ---	r_1(side)=0.245	r_2(side)=0.277
P=2^d.7277	r_1(back)=0.247	r_2(back)=0.310
i=78°.7	Ω_1=4.426	V_γ=−13.2 kms sec^{-1}
T_1=15900 K	Ω_2=2.510	F_1=1.00
T_2=8224 K	q=0.32	F_2=1.00

Figure 43: The system DM Per at different orbital phases
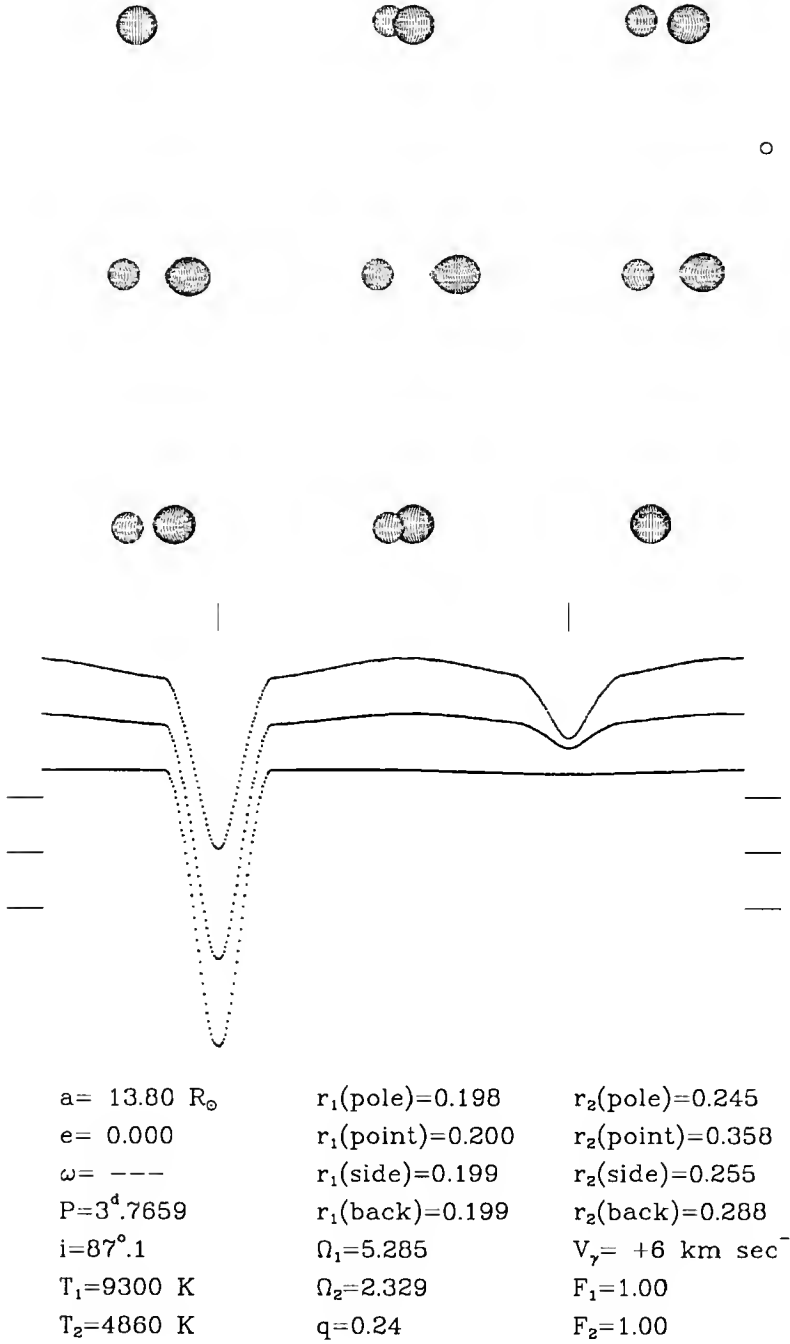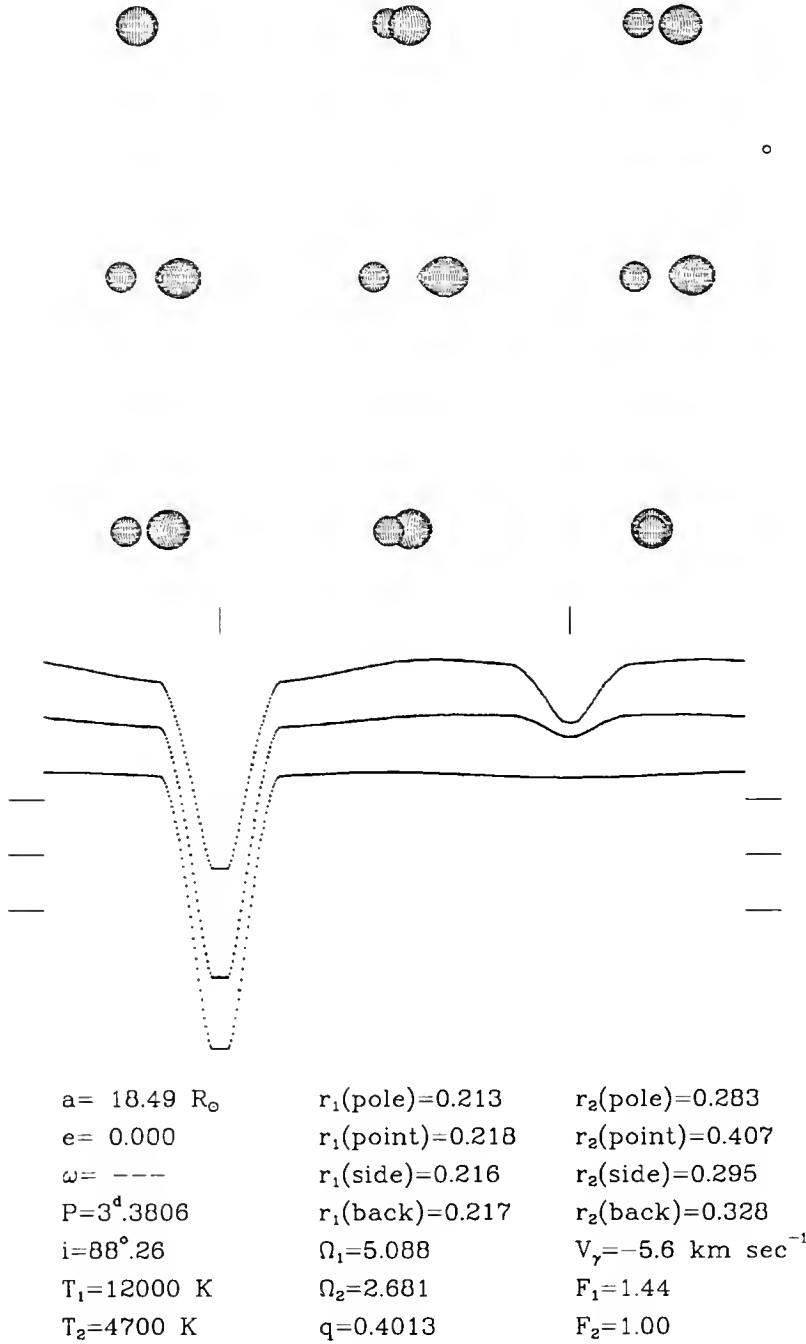along with its light curves and photometric elements
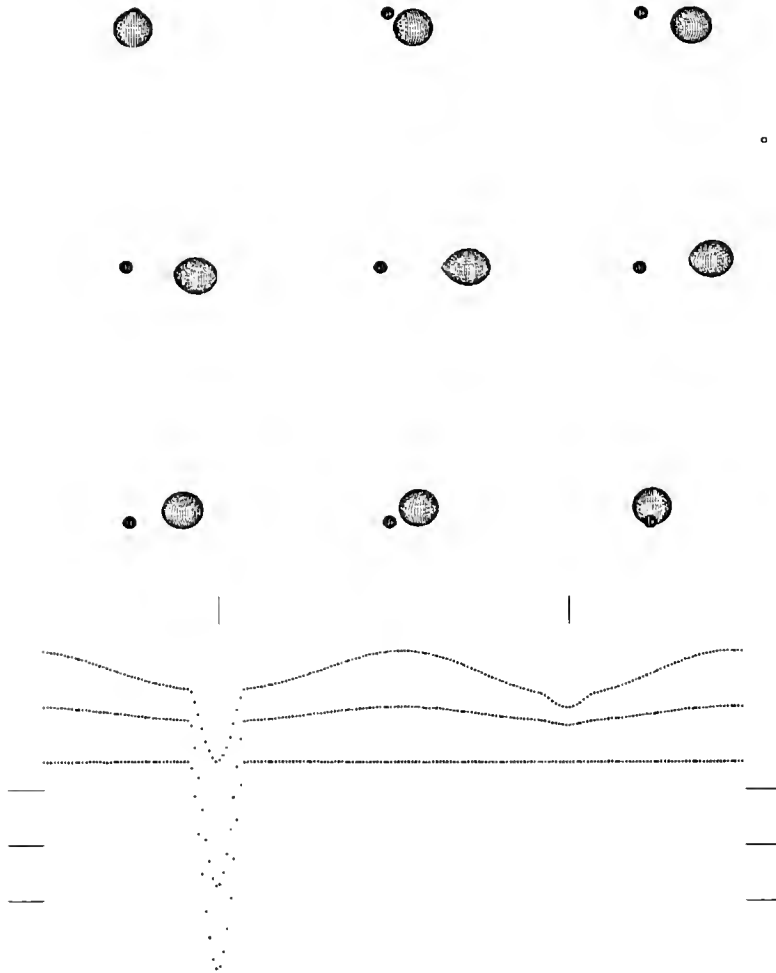
a=34.10 R$_\odot$	r$_1$(pole)=0.072	r$_2$(pole)=0.214
e= 0.000	r$_1$(point)=0.077	r$_2$(point)=0.316
ω= ---	r$_1$(side)=0.077	r$_2$(side)=0.223
P=13^d.1989	r$_1$(back)=0.077	r$_2$(back)=0.255
i=80°.03	Ω_1=14.090	V$_\gamma$=+6.5 km sec^{-1}
T$_1$=9700 K	Ω_2=2.104	F$_1$=16.21
T$_2$=3973 K	q=0.15	F$_2$=1.00

Figure 44: The system RW Per at different orbital phases
along with its light curves and photometric elements

a= 32.38 R$_\odot$	r$_1$(pole)=0.113	r$_2$(pole)=0.262
e= 0.000	r$_1$(point)=0.133	r$_2$(point)=0.380
ω= ---	r$_1$(side)=0.133	r$_2$(side)=0.273
P=6^d.6636	r$_1$(back)=0.133	r$_2$(back)=0.306
i=81°.65	Ω_1=9.176	V$_\gamma$=−37.8 km sec^{-1}
T$_1$=20700 K	Ω_2=2.474	F$_1$=10.82
T$_2$=6017 K	q=0.3037	F$_2$=1.00

Figure 45: The system RY Per at different orbital phases
along with its light curves and photometric elements
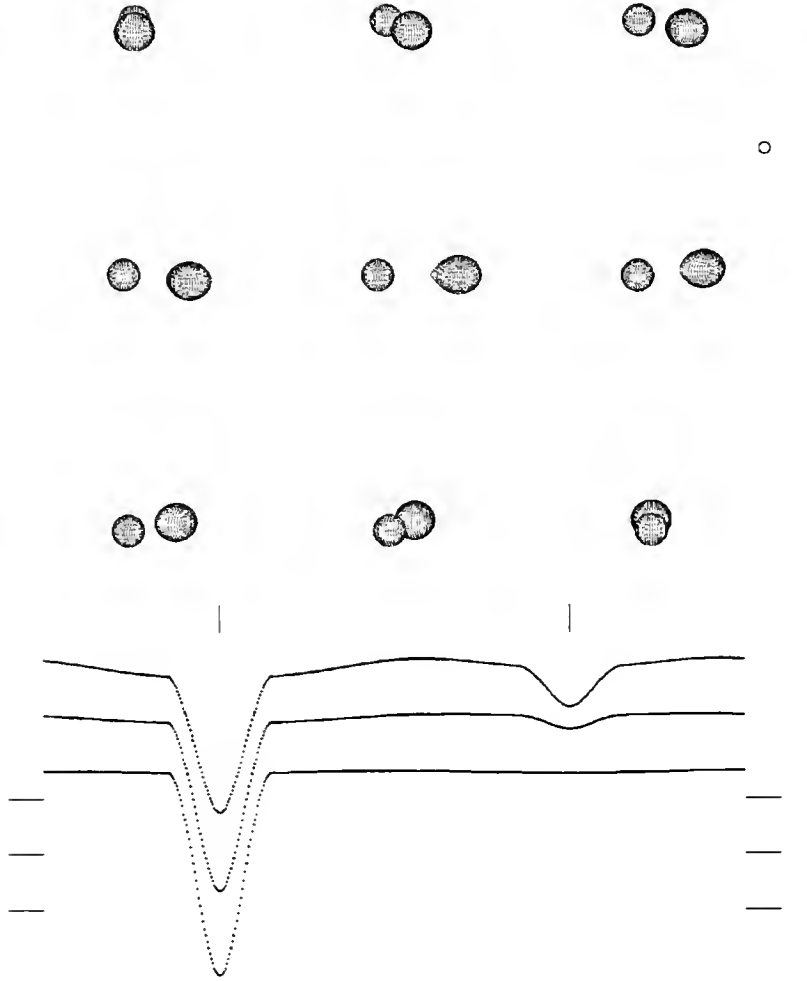
a= 13.99 $R_\odot$	r_1(pole)=0.2029	r_2(pole)=0.2415
e= 0.000	r_1(point)=0.2047	r_2(point)=0.3529
ω= ---	r_1(side)=0.2039	r_2(side)=0.2512
P=2^d.8673	r_1(back)=0.2045	r_2(back)=0.2838
i=82°.31	Ω_1=5.1507	V_γ=−9.0 km sec^{-1}
T_1=12000 K	Ω_2=2.2986	F_1=1.00
T_2=4888 K	q=0.227	F_2=1.00

Figure 46: The system β Per at different orbital phases along with its light curves and photometric elements

a= 13.80 R$_\odot$	r$_1$(pole)=0.198	r$_2$(pole)=0.245
e= 0.000	r$_1$(point)=0.200	r$_2$(point)=0.358
ω= ---	r$_1$(side)=0.199	r$_2$(side)=0.255
P=3^d.7659	r$_1$(back)=0.199	r$_2$(back)=0.288
i=87°.1	Ω_1=5.285	V$_\gamma$= +6 km sec^{-1}
T$_1$=9300 K	Ω_2=2.329	F$_1$=1.00
T$_2$=4860 K	q=0.24	F$_2$=1.00

Figure 47: The system Y Psc at different orbital phases along with its light curves and photometric elements

a= 18.49 R_o	r_1(pole)=0.213	r_2(pole)=0.283
e= 0.000	r_1(point)=0.218	r_2(point)=0.407
ω= ---	r_1(side)=0.216	r_2(side)=0.295
P=3^d.3806	r_1(back)=0.217	r_2(back)=0.328
i=$88°$.26	Ω_1=5.088	V_γ=-5.6 km sec^{-1}
T_1=12000 K	Ω_2=2.681	F_1=1.44
T_2=4700 K	q=0.4013	F_2=1.00

Figure 48: The system U Sge at different orbital phases along with its light curves and photometric elements
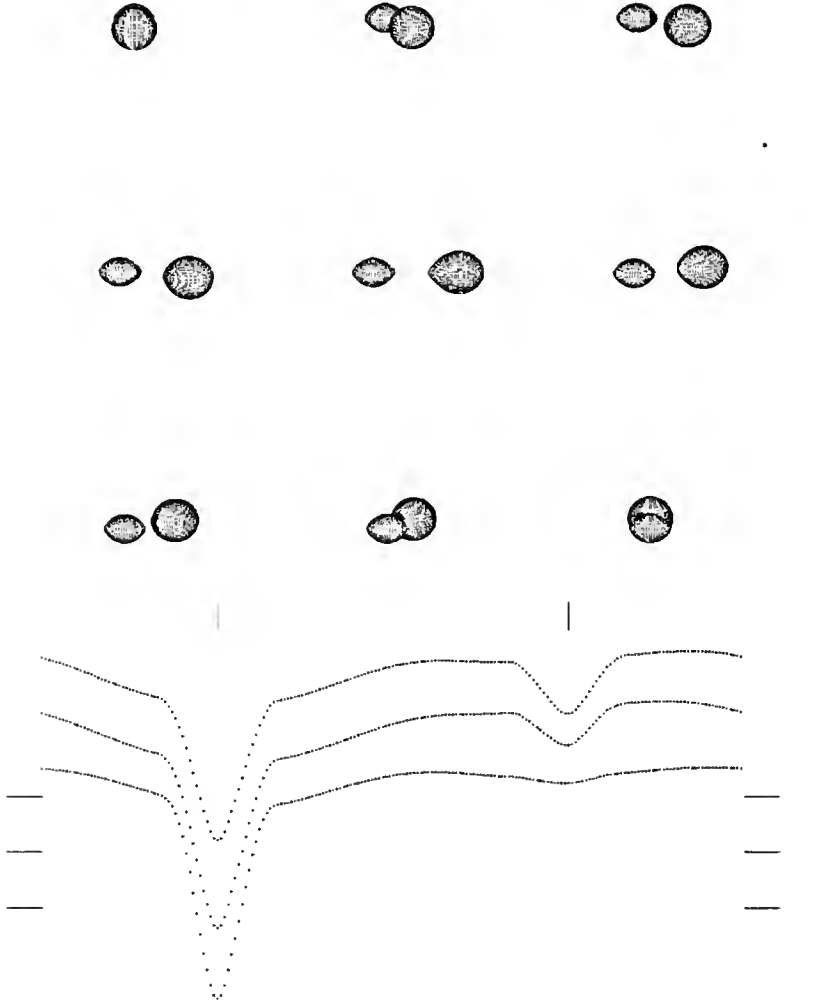
a= 49.5 R$_\odot$	r$_1$(pole)=0.173	r$_2$(pole)=0.256
e= 0.000	r$_1$(point)=0.259	r$_2$(point)=0.372
ω= ---	r$_1$(side)=0.241	r$_2$(side)=0.266
P=15^d.1907	r$_1$(back)=0.249	r$_2$(back)=0.299
i=83°.10	Ω_1=6.066	V$_\gamma$=−13.4 km sec^{-1}
T$_1$=22700 K	Ω_2=2.416	F$_1$=6.66
T$_2$=7500 K	q=0.277	F$_2$=1.0

Figure 49: The system RZ Sct at different orbital phases
along with its light curves and photometric elements

a= 15.02 $R_\odot$	r_1(pole)=0.303	r_2(pole)=0.288
e= 0.000	r_1(point)=0.317	r_2(point)=0.414
ω= ---	r_1(side)=0.309	r_2(side)=0.300
P=2^d.4549	r_1(back)=0.314	r_2(back)=0.333
i=$88°$.9	Ω_1=3.715	V_γ=-21.8 km sec^{-1}
T_1=19840 K	Ω_2=2.739	F_1=1.00
T_2=9410 K	q=0.43	F_2=1.00
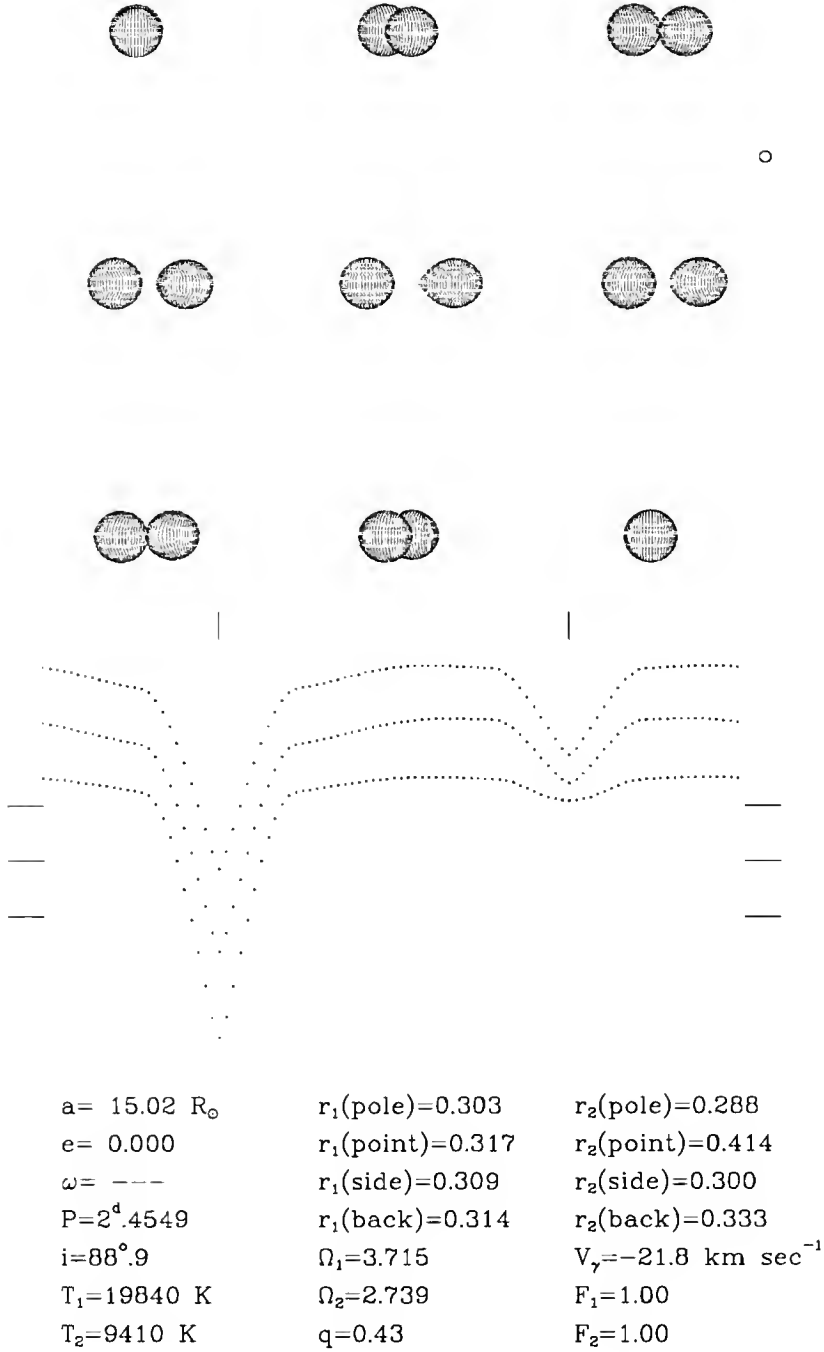
Figure 50: The system Z Vul at different orbital phases
along with its light curves and photometric elements

APPENDIX B
LINE PROFILES

Appendix B contains figures which show the line profiles over the entire observed spectral range (4420 to 4530 Angstrom Units). The figures show the profiles before any corrections (earth's orbital motion and rotation, primary star's orbital motion etc.) were made.
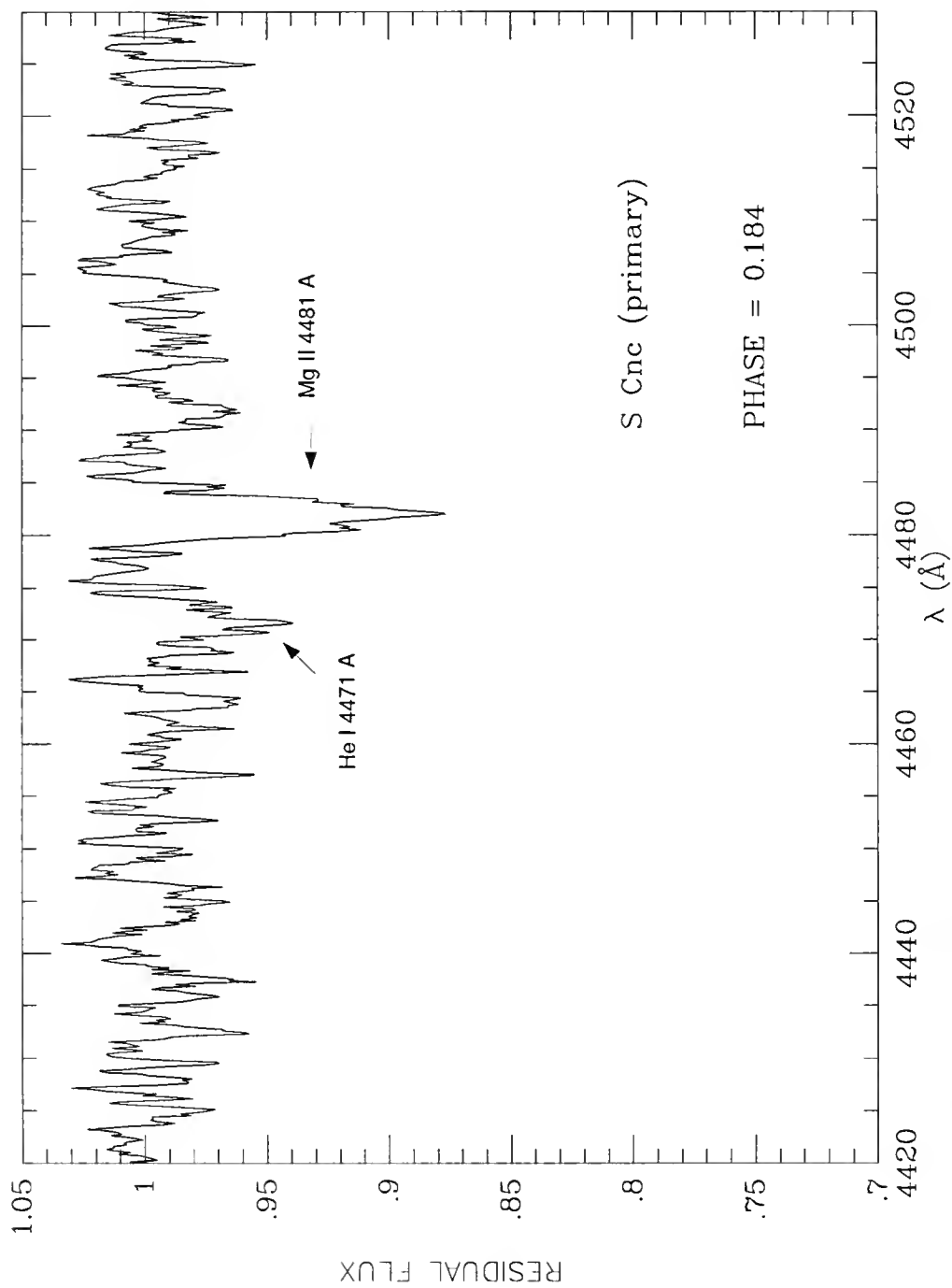
Figure 51: Spectrometry of S Cnc over the wavelength range 4420 – 4530 Angstrom Units
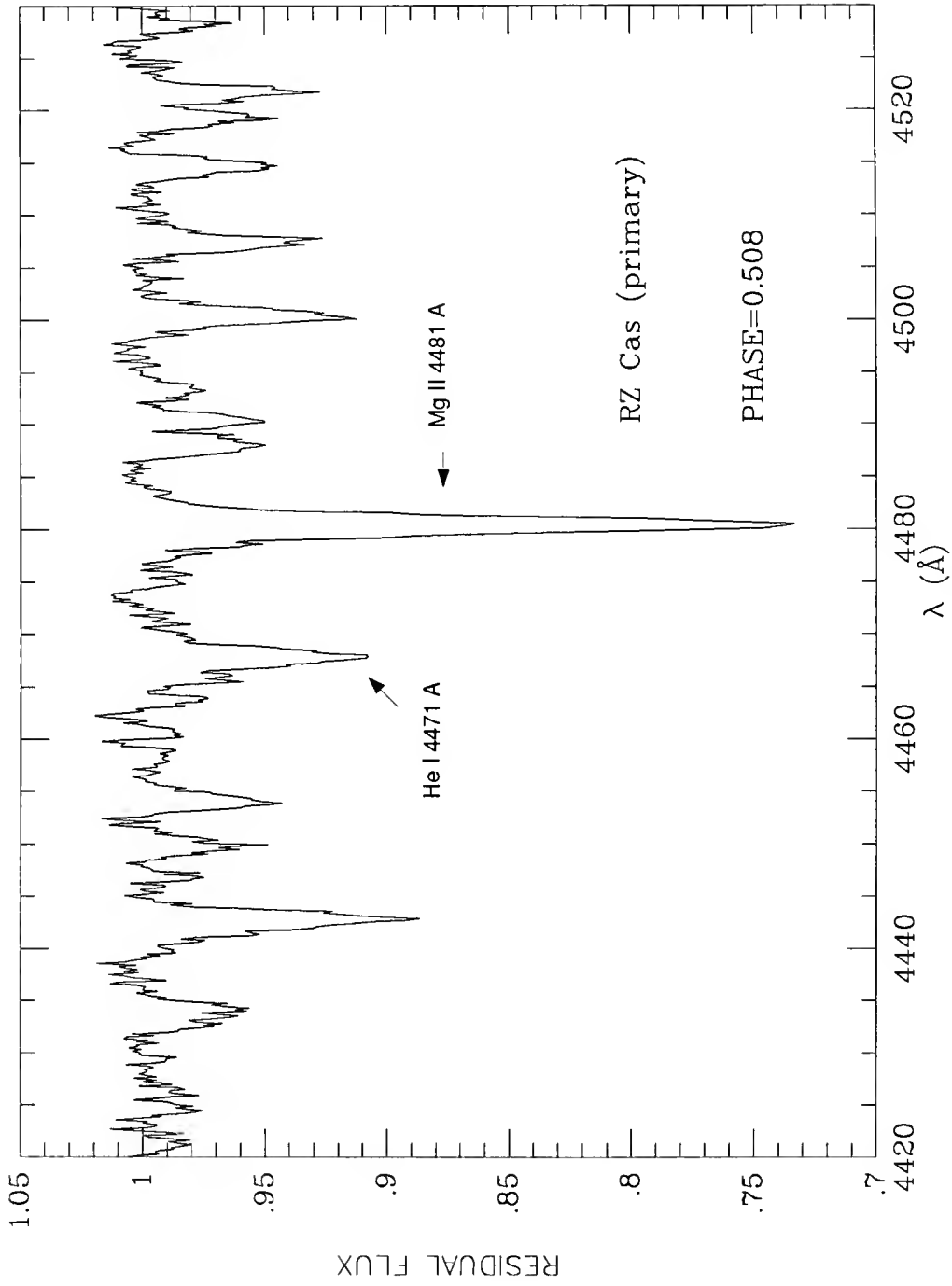
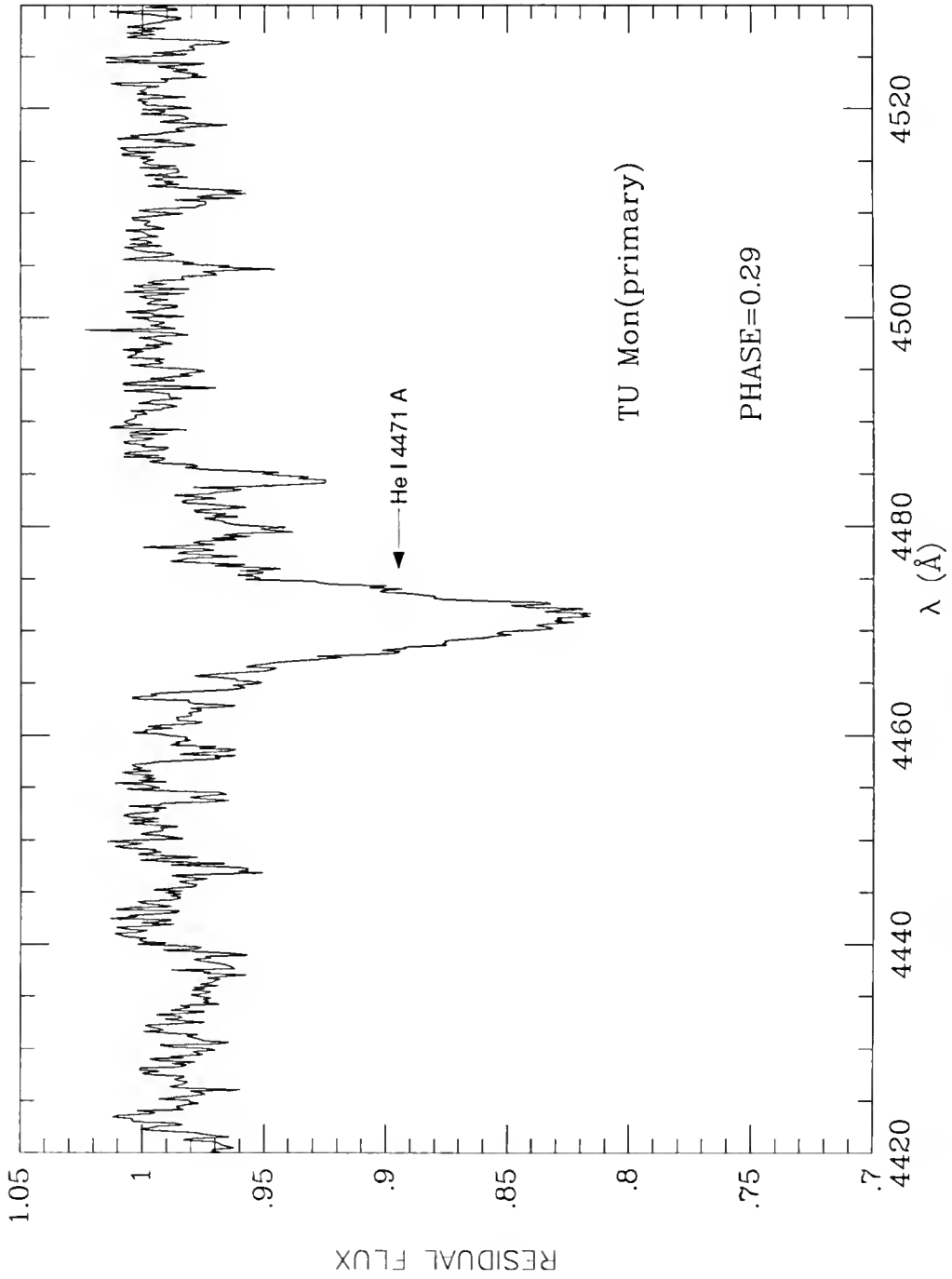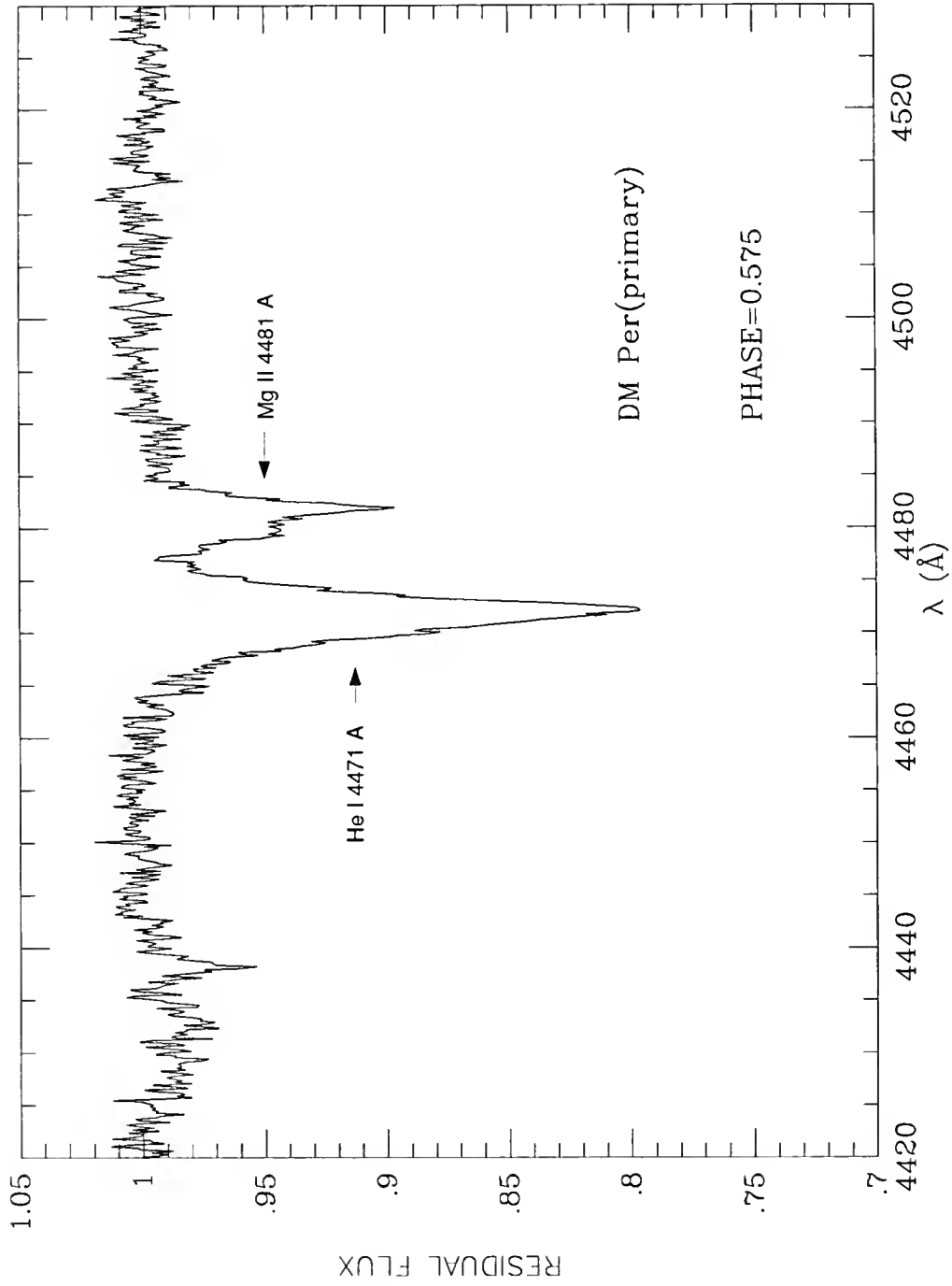Figure 52: Spectrometry of RZ Cas over the wavelength range 4420 – 4530 Angstrom Units
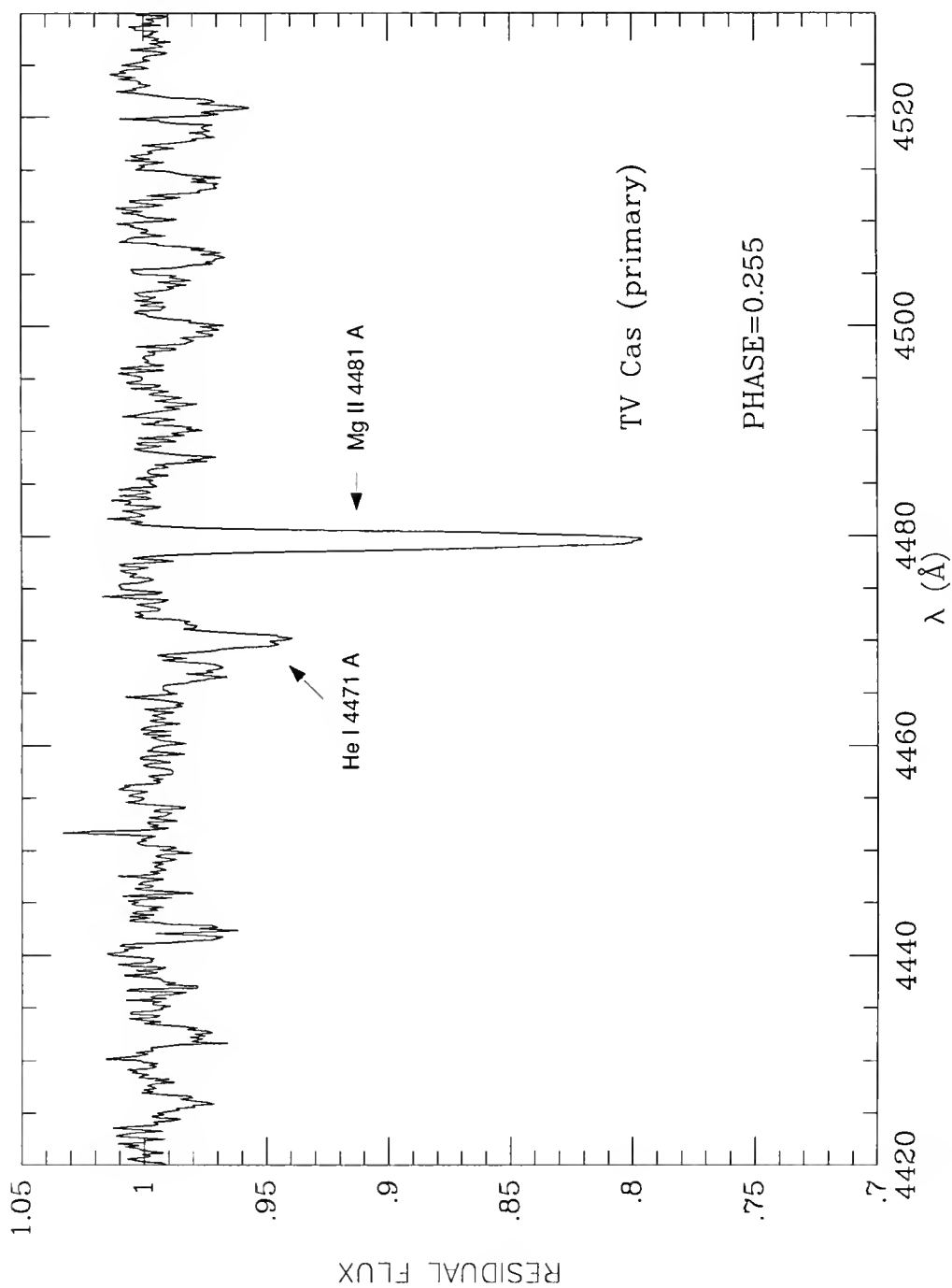
Figure 53: Spectrometry of TV Cas over the wavelength range 4420 – 4530 Angstrom Units
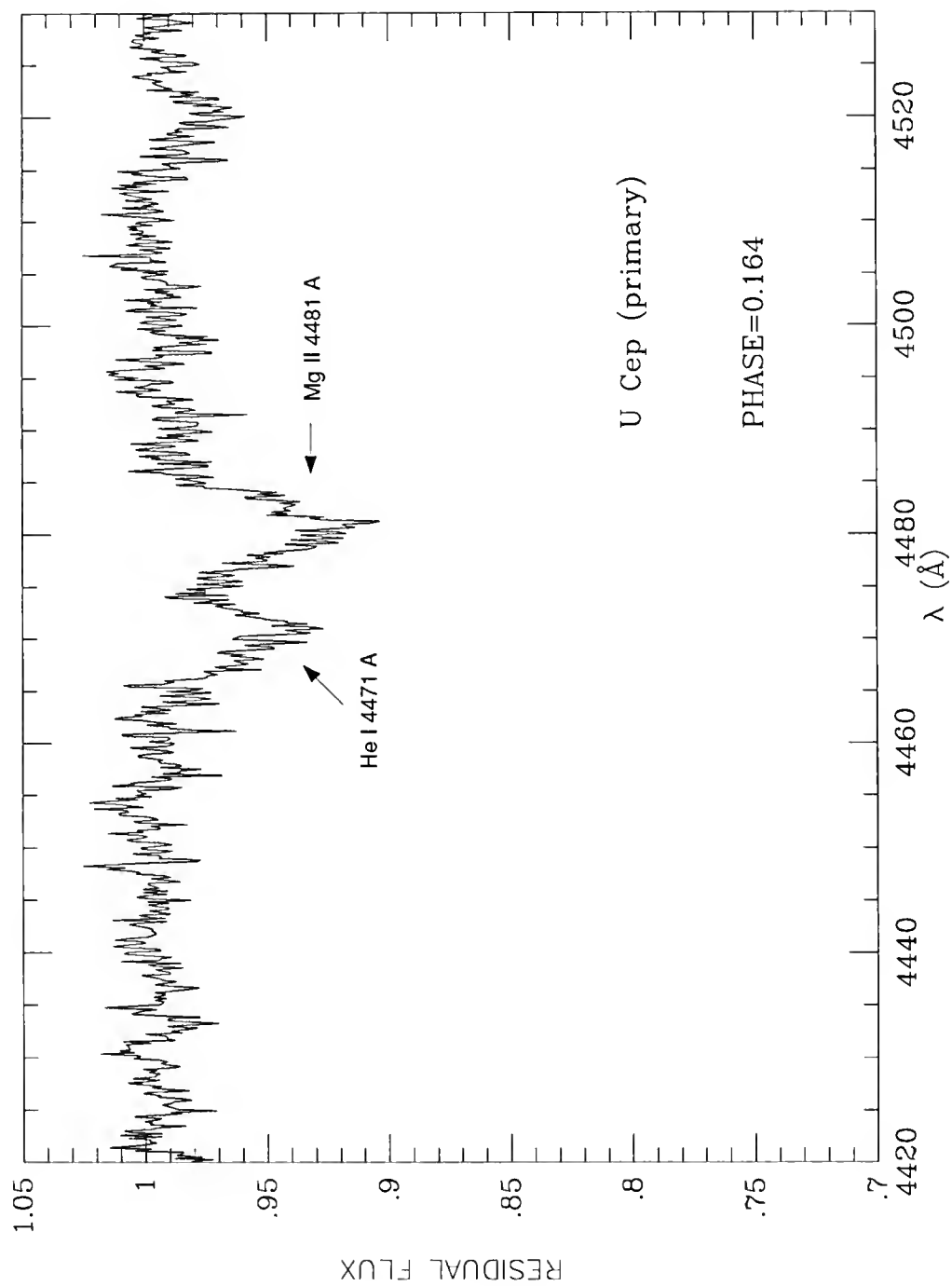
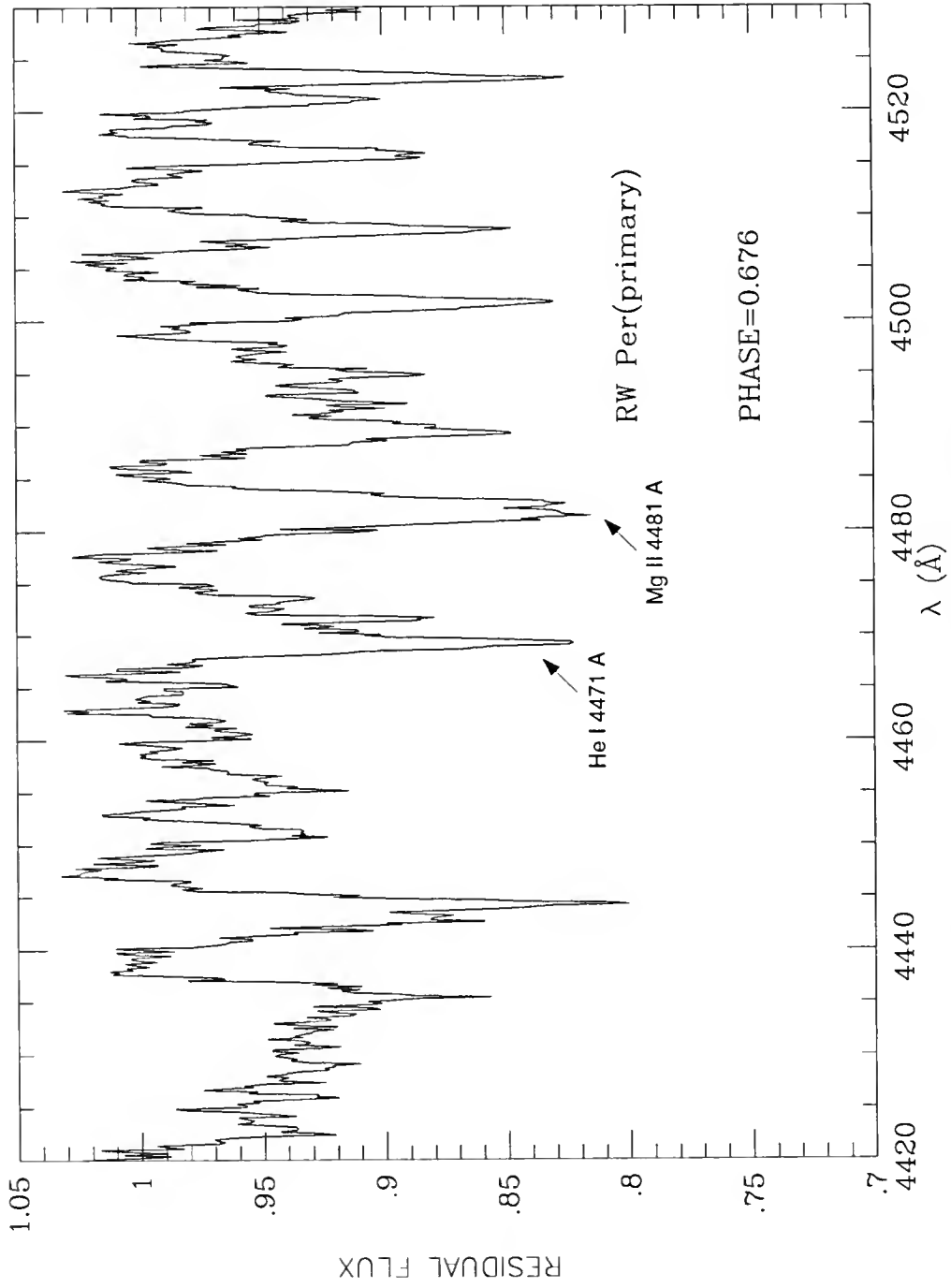Figure 54: Spectrometry of U Cep over the wavelength range 4420 – 4530 Angstrom Units
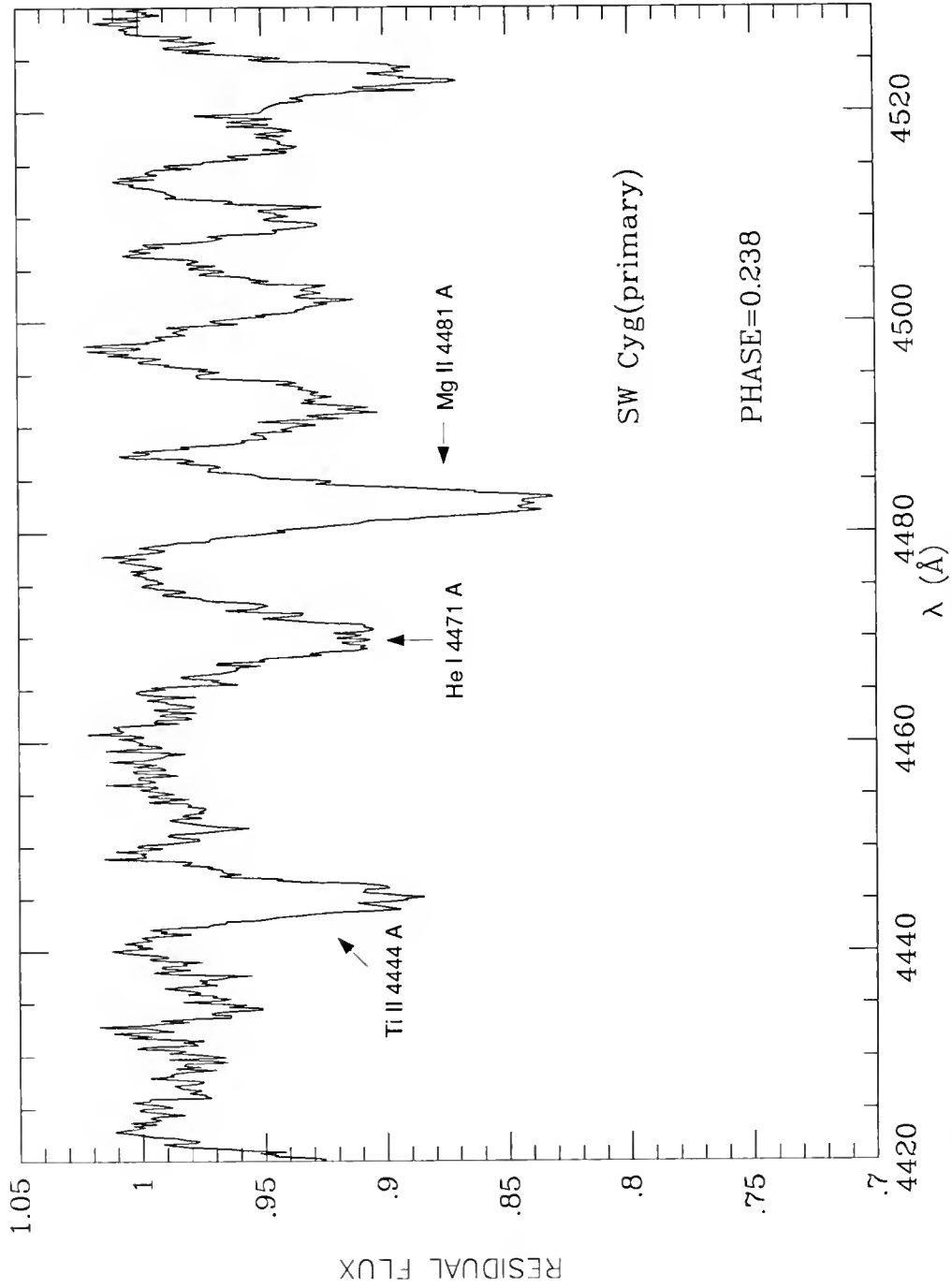
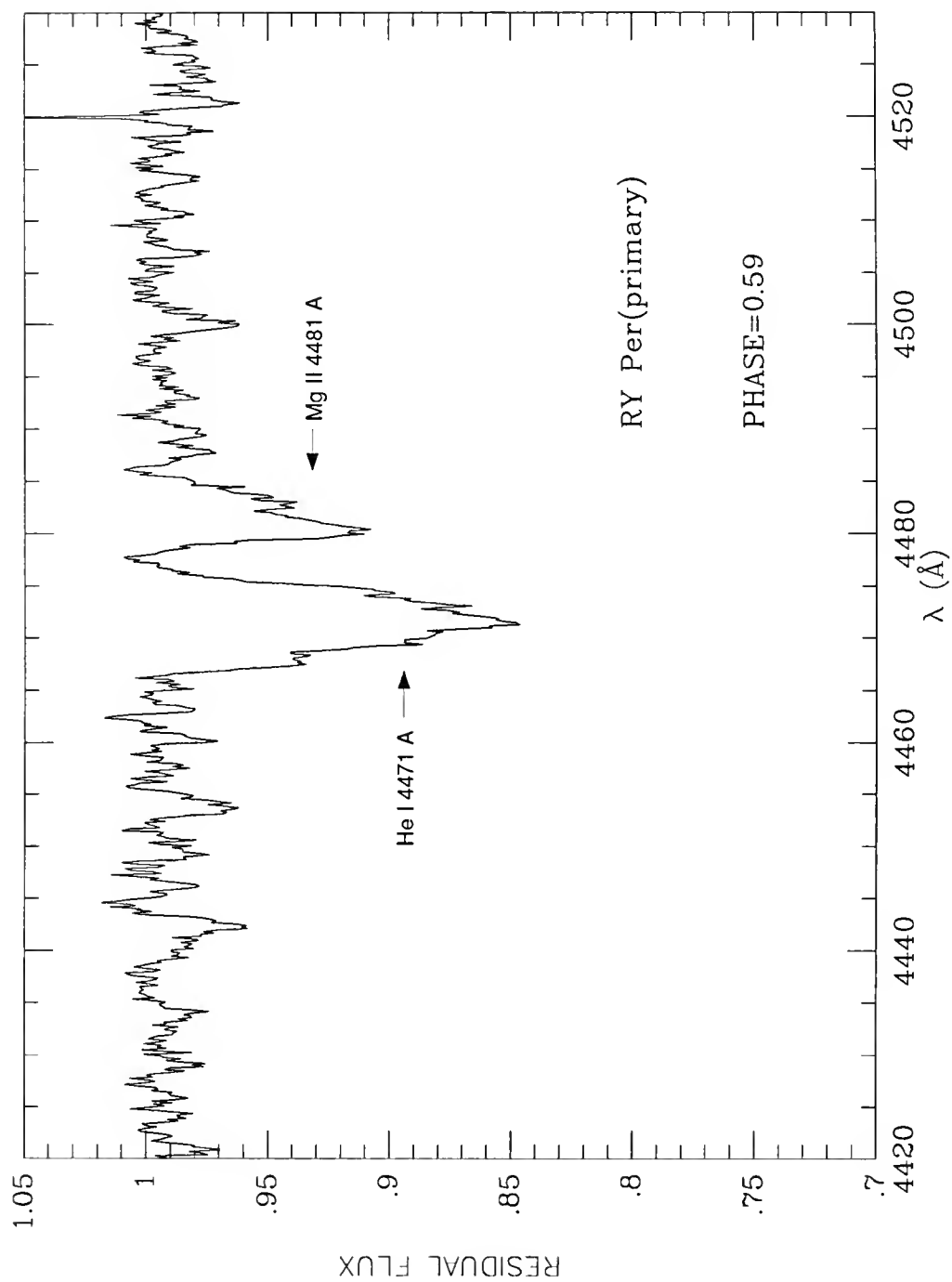Figure 55: Spectrometry of SW Cyg over the wavelength range 4420 – 4530 Angstrom Units
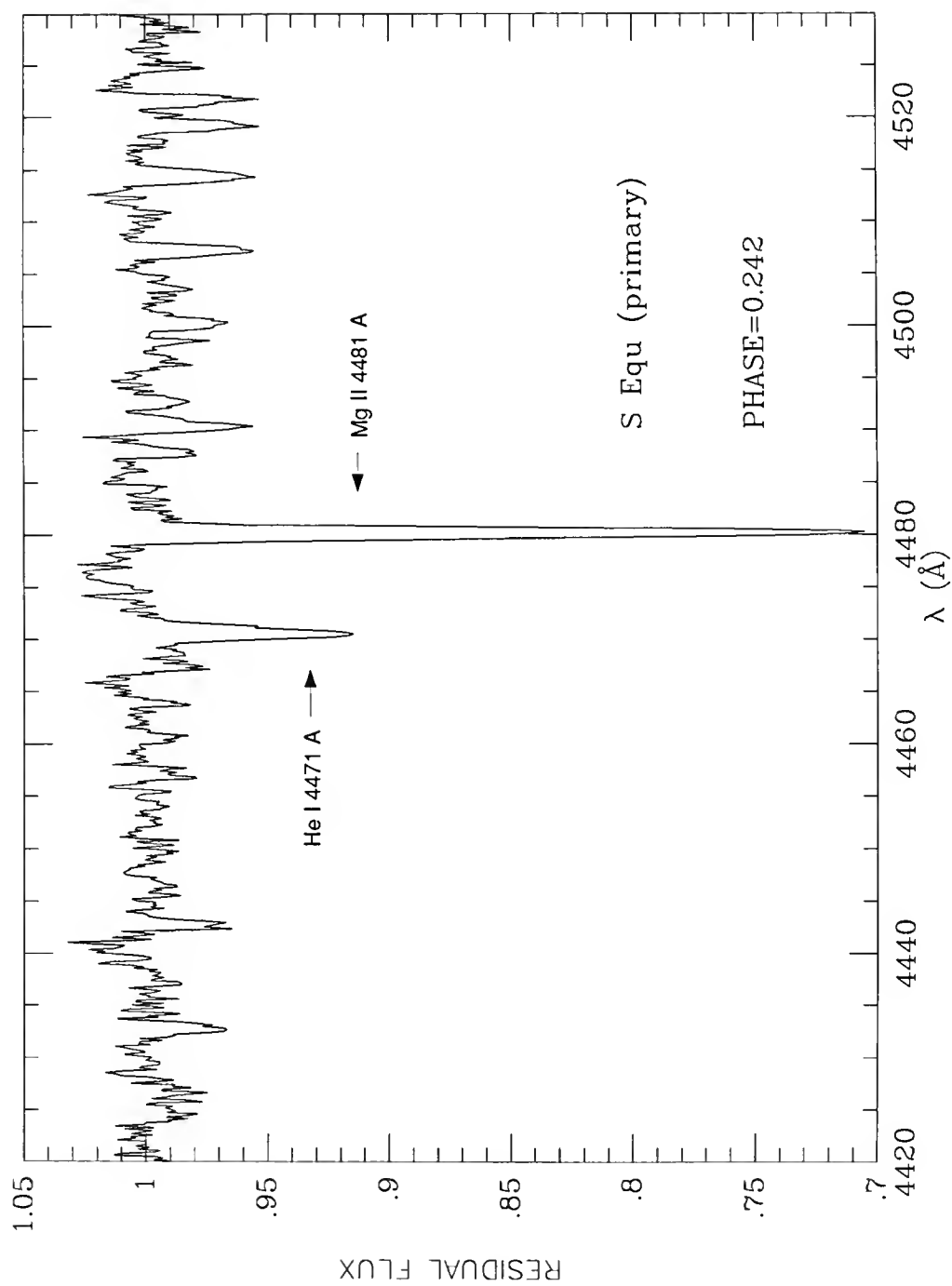
Figure 56: Spectrometry of S Equ over the wavelength range 4420 – 4530 Angstrom Units
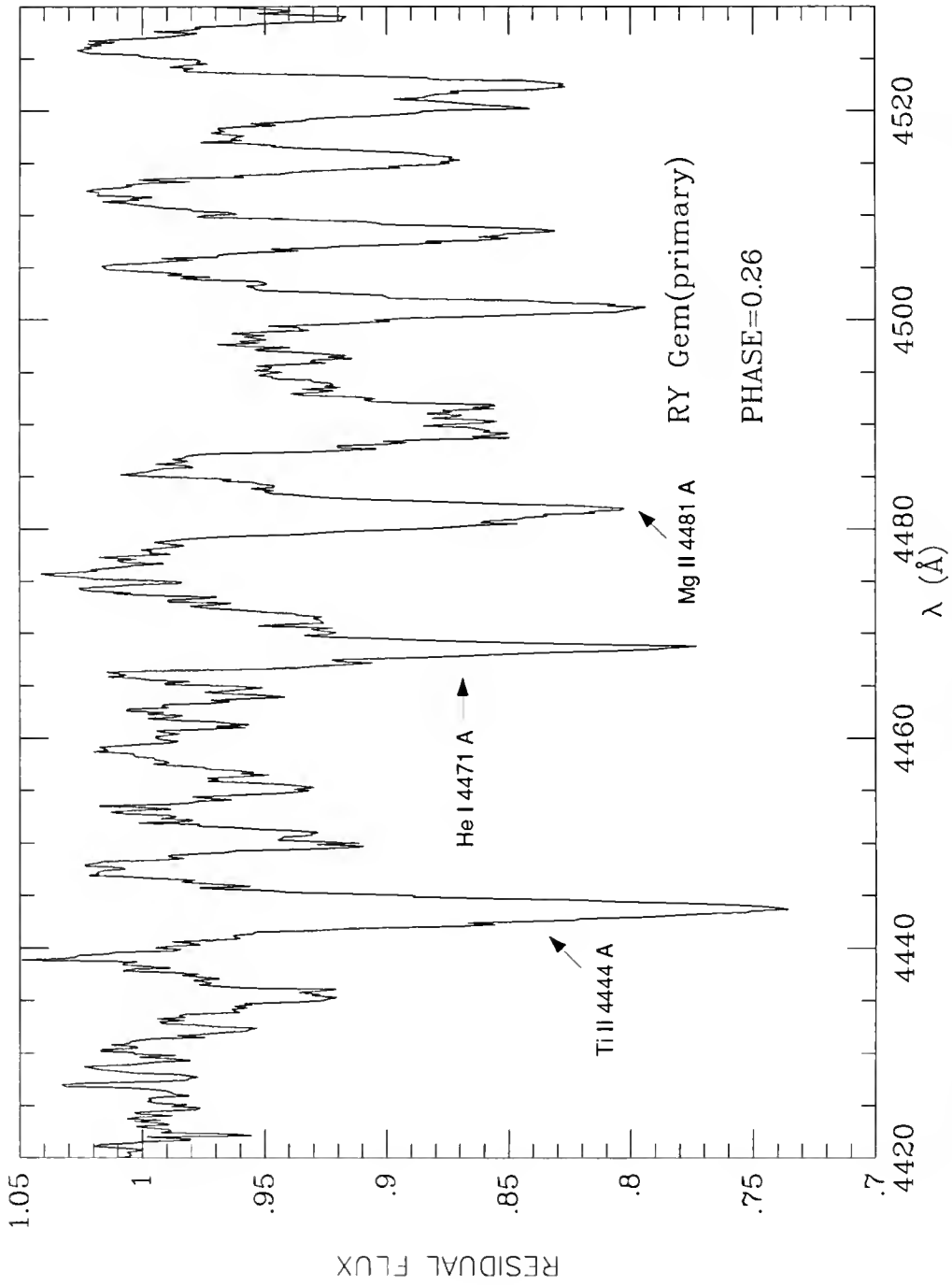
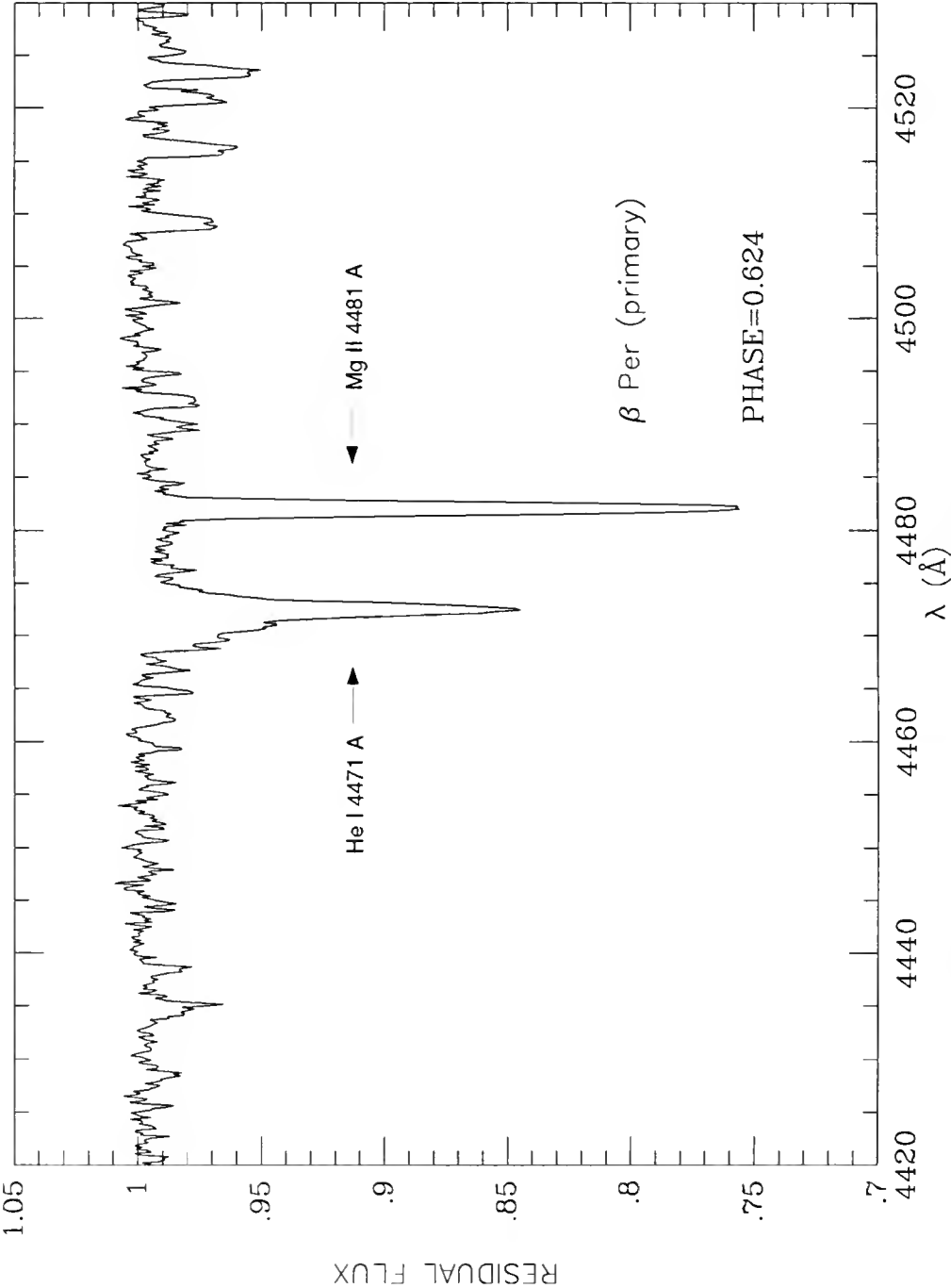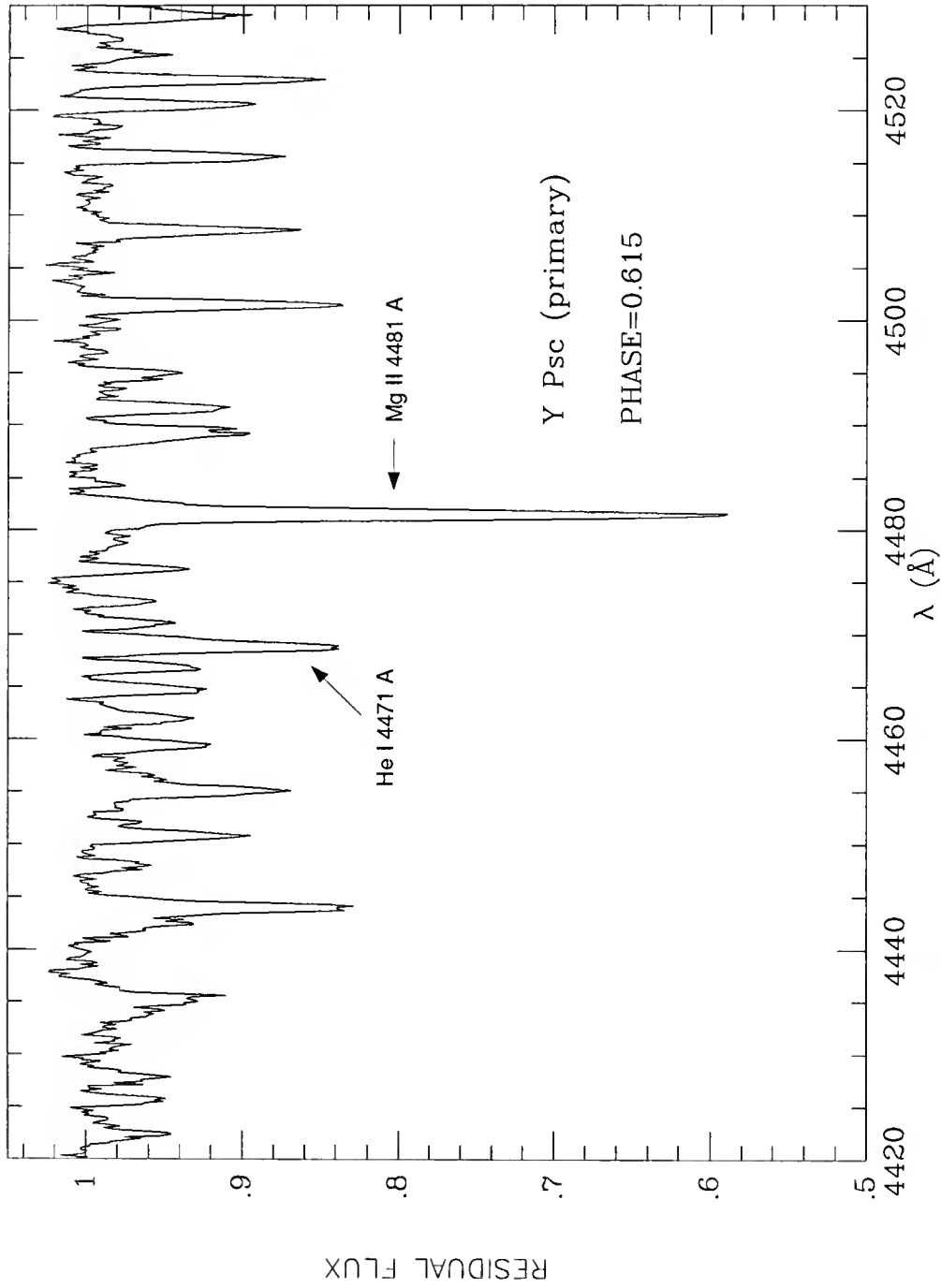Figure 57: Spectrometry of RY Gem over the wavelength range 4420 – 4530 Angstrom Units
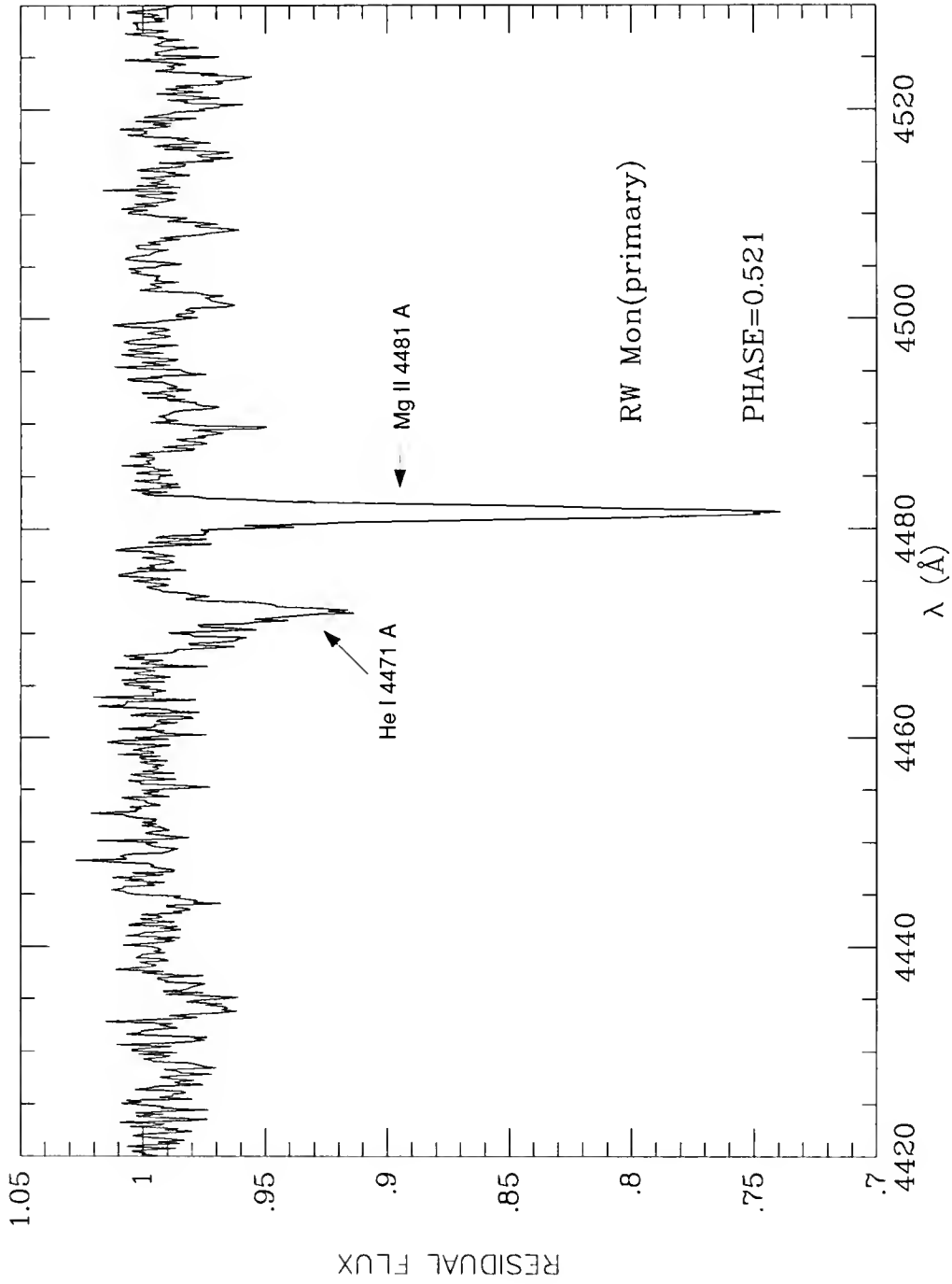
Figure 58: Spectrometry of RW Mon over the wavelength range 4420 – 4530 Angstrom Units

Figure 59: Spectrometry of TU Mon over the wavelength range 4420 – 4530 Angstrom Units

Figure 60: Spectrometry of DM Per over the wavelength range 4420 – 4530 Angstrom Units

Figure 61: Spectrometry of RW Per over the wavelength range 4420 – 4530 Angstrom Units

Figure 62: Spectrometry of RY Per over the wavelength range 4420 – 4530 Angstrom Units

Figure 63: Spectrometry of β Per over the wavelength range 4420 – 4530 Angstrom Units

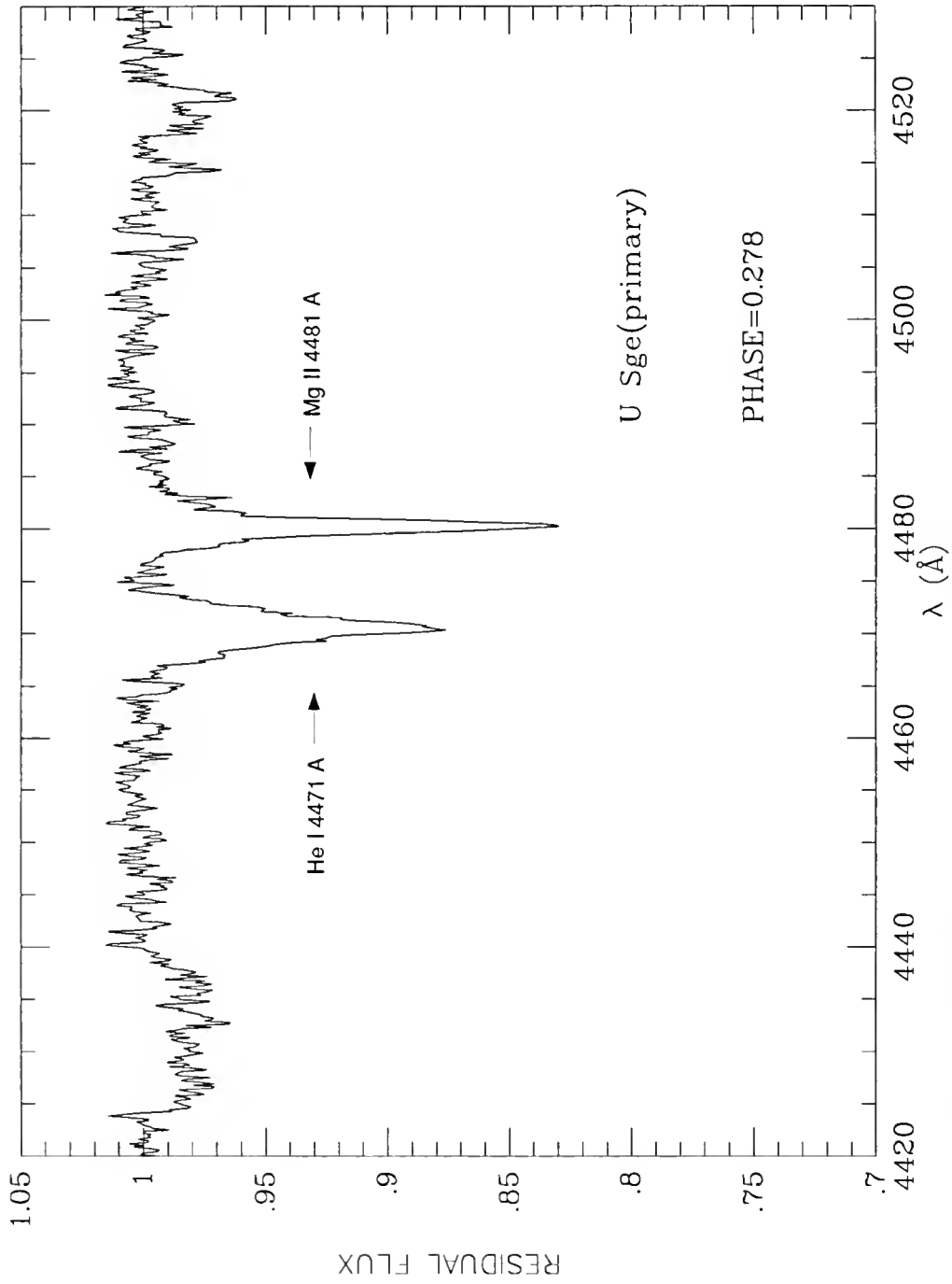Figure 64: Spectrometry of Y Psc over the wavelength range 4420 – 4530 Angstrom Units

Figure 65: Spectrometry of U Sge over the wavelength range 4420 – 4530 Angstrom Units
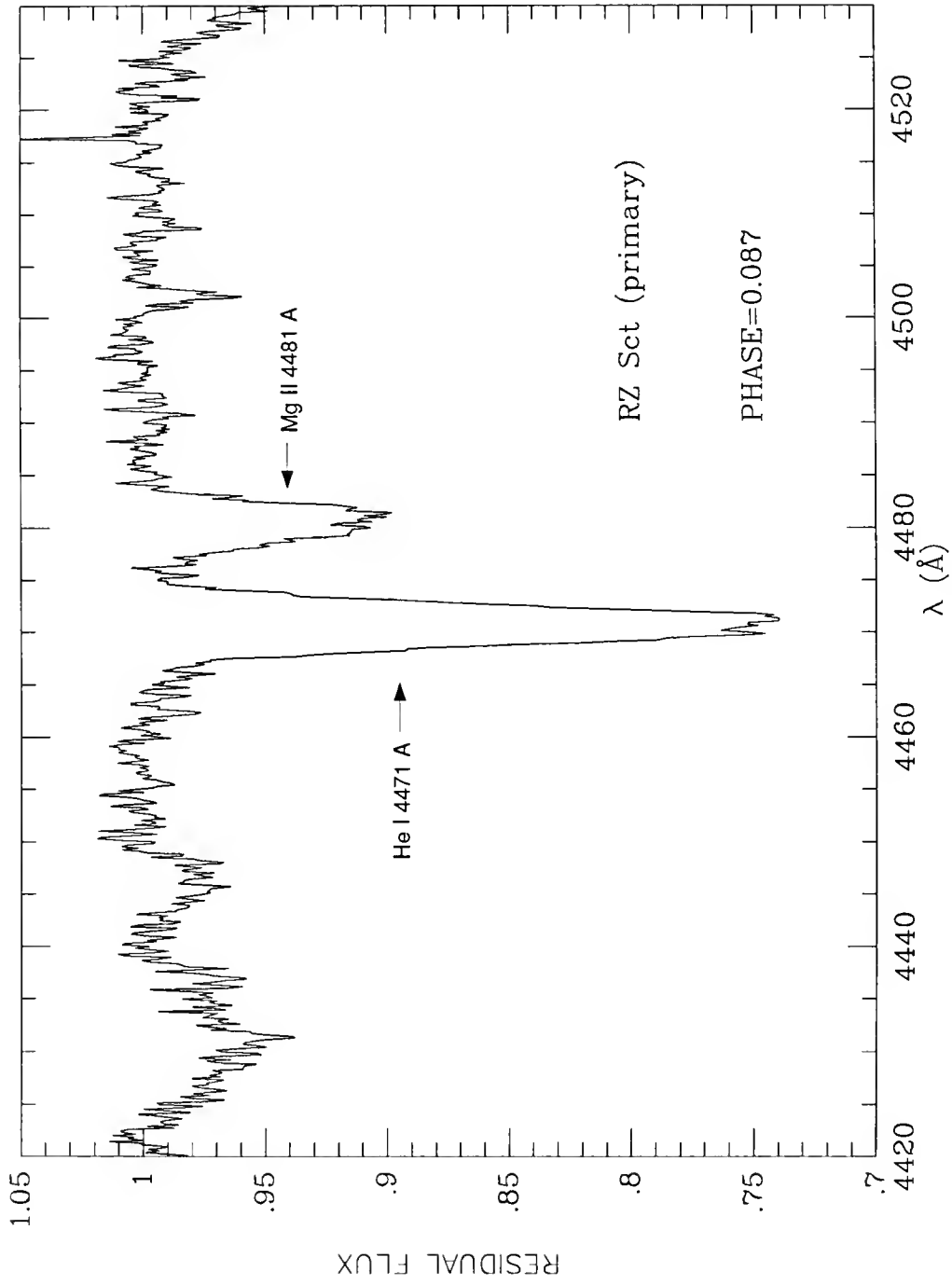
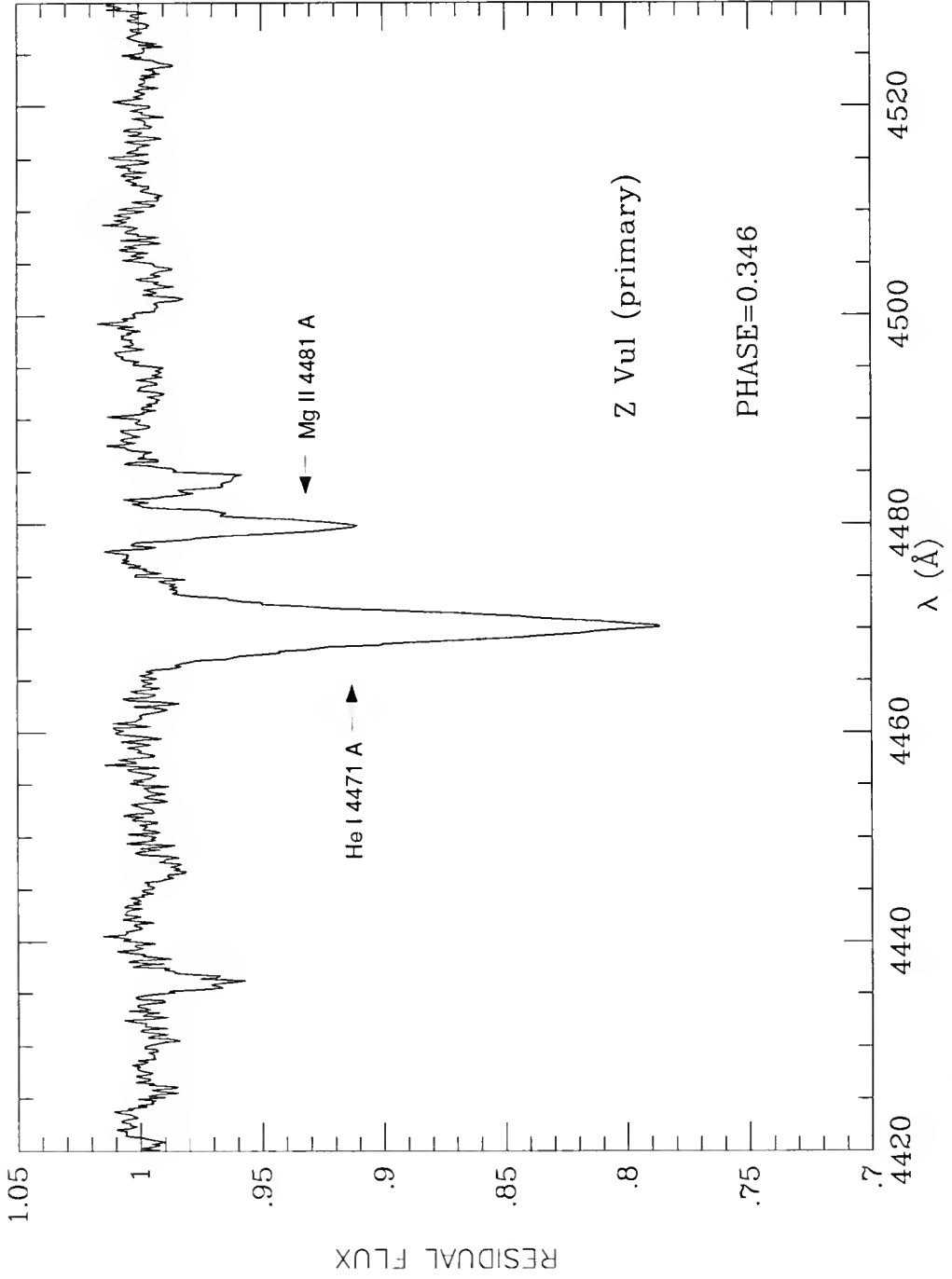Figure 66: Spectrometry of RZ Sct over the wavelength range 4420 – 4530 Angstrom Units

Figure 67: Spectrometry of Z Vul over the wavelength range 4420 – 4530 Angstrom Units

BIBLIOGRAPHY

Aller, L.H. 1963, *Astrophysics, The Atmospheres of the Sun and the Stars* (The Ronald Press Company, New York), 174

Al Naimiy, H.M. 1978, Ap&SS, **53**, 181

Ambartsumian, V.A. 1958, *Theoretical Astrophysics* (Pergamon Press, New York), 134

Anderson, L., & Shu, F.H. 1979, ApJ Suppl. Series., **40**, 667

Batten, J.M., Fletcher, J.M., & MacCarthy, D.G. 1989, *Eighth Catalogue of the Orbital Elements of Spectroscopic Binary Systems* (Dominion Astrophysical Observatory, Victoria, B.C., Canada)

Beckers, J.M. 1980, *Stellar Turbulence*, ed. Gray, D.F., & Linsky, J.L. (Springer-Verlag, New York), 85

Biermann, P., & Hall, D.S. 1973, A&A, **27**, 249

Birney, D.S. 1991, *Observational Astronomy* (Cambridge University Press, Cambridge, England), Chapter 13

Bousquet, P. 1971, *Spectroscopy and its Instrumentation* (Hilger, London), 90

Branham, R.L. Jr. 1990, *Scientific Data Analysis: An Introduction to Overdetermined Systems* (Springer-Verlag, New York), Chapters 4 and 5

Caceci, M.S., & Cacheris, W.P. 1984, Byte, **May 1984**, 340

Carpenter, K.G., Slettebak, A., & Sonneborn, G. 1984, ApJ, **286**, 741

Carroll, J.A. 1933, MNRAS, **93**, 478

Cester, B., Fedel, B., Giuricin, G., Mardirossian, F., & Pucillo, M. 1977, A&A, **61**, 469

Cester, B., Giuricin, G., Mardirossian, F., Mezzetti, M., & Milano, L. 1979, A&AS, **36**, 272

Chambliss, C.R. 1976, PASP, **88**, 22

Chandrasekhar, S. 1947, ApJ, **106**, 145

Colacevich, A. 1950, Mem. Soc. Astron. Ital. **21**, 275

Collins, G.W. II. 1974, ApJ, **191**, 157

Collins, G.W. II. 1989a, *The Fundamentals of Stellar Astrophysics* (W.H. Freeman & Co., New York), 355

Collins, G.W. II. 1989b, *The Fundamentals of Stellar Astrophysics* (W.H. Freeman & Co., New York), 369

Deutsch, A.J. 1945, ApJ, **102**, 433

Dobias, J.J., & Plavec, M.J. 1985, PASP, **97**, 138

Dobias, J.J., & Plavec, M.J. 1987, PASP **99**, 159

Duerbeck, H.W., & Hanel, A. 1979, A&AS, **38**, 155

Elvey, C.T. 1930, ApJ, **71**, 221

Etzel, P.B., & Olson, E.C. 1985, AJ, **90**, 504

Finn, G.D., & Mugglestone, D. 1965, MNRAS, **129**, 221

Frieboes-Conde, H., & Herczeg, T. 1973, A&AS, **12**, 1

Furenlid, I. 1976, In *Abundance Effects in Spectral Classification*, ed. Hauck, B. & Keenan, P.C. (D. Reidel Pub. Co., Dordrecht, Holland), 64

Gehren, T. 1980, In *Stellar Turbulence*, ed. Gray, D.F., & Linsky, J.L. (Springer-Verlag, New York), 103

Gray, D.F. 1976, *The Observations and Analysis of Stellar Photospheres* (Wiley, New York), Chaps. 2 and 12

Gray, D.F. 1988, *Lectures on Spectral Line Analysis: F, G, and K Stars* (Aylmer Express Ltd., Arva, Ontario, Canada), Chapter 3

Hall, D.S. 1969, In *Mass Loss from Stars*, ed. M. Hack (Reidel, Dordrecht), 171

Hall, D.S., Eaton, J.A., Wilson, J.W., & Stuhlinger, T. 1982, Acta Astr., **32**, 411

Hall, D.S., Keel, W.C., & Neuhaus, G.H., 1976, Acta Astr., **26**, 239

Hall, D.S., & Stuhlinger, T. 1978, Acta Astr., **28**, 207

Hansen, K., & McNamara, D.H. 1959, ApJ, **130**, 789

Harris, D.L. III. 1948, ApJ, **108**, 112

Heard, J.F., & Newton, J. 1969, J. R. Astron. Soc. Can., **63**, 208

Hilditch, R.W., Skillen, I., Carr, D.M., & Aikman, G.C.L. 1986, MNRAS, **222**, 167

Hiltner, W.A, 1946, ApJ, **104**, 396

Hjerting, F. 1938, ApJ, **88**, 508

Huang, S.S., & Struve, O. 1960, In *Stellar Atmospheres*, ed. Greenstein, J.L. (University of Chicago Press, Chicago), Chapter 8

Hummer, D.G. 1965, MNRAS, **70**, 1

Kaitchuck, R.H., Honeycutt, R.K., & Schlegel, E.M. 1985, PASP, **97**, 1178

Karetnikov, V.G., & Mecheneva, E.V. 1987, Soviet Astr., **31**, 192

Kim, Ho-Il. 1989, ApJ, **342**, 1061

Kondo, Y., Modisette, J.L., & Morgan, T.H. 1977, IBVS Number **1312**

Kurucz, R.L. 1970, ATLAS: *A Computer Program for Calculating Model Stellar Atmospheres* (Cambridge: Smithsonian Ap. Obs. Rept. No. 309)

McKellar, A. 1949, Publ. Dom. Astrophys. Obs. **8**, 244

McNamara, D.H. 1951, PASP, **63**, 38

McNamara, D.H., & Feltz, K.A., Jr. 1976, PASP **88**, 688

Mezzetti, M., Cester, B., Giuricin, G. & Mardirossian, F. 1980, A&AS, **39**, 265

Mihalas, D. 1978a, *Stellar Atmospheres* (W.H. Freeman and Company, San Francisco), 149

Mihalas, D. 1978b, *Stellar Atmospheres* (W.H. Freeman and Company, San Francisco), 309

Mihalas, D. 1978c, *Stellar Atmospheres* (W.H. Freeman and Company, San Francisco), 310.

Mihalas, D. 1978d, *Stellar Atmospheres* (W.H. Freeman and Company, San Francisco), 313

Mihalas, D. 1978e, *Stellar Atmospheres* (W.H. Freeman and Company, San Francisco), 314

Olson, E.C. 1978, ApJ, **220**, 251

Olson, E.C. 1984, PASP, **96**, 376

Olson, E.C., Schaefer, B.E., Lines, R., Lines, H., & Fried, R.E. 1992, AJ **103**, 256

Packet, W. 1981, A&A, **102**, 17

Piotrowski, S.L., Rucinski, S.M., and Semeniuk, I. 1974, Acta Astr., **24**, 389

Plavec, M.J. 1966, BAC, **17**, 295

Plavec, M. 1967, In *Determination of Radial Velocities and their Application*, ed. Batten, A.H., and Heard, J.F. (Academic Publishers, London), 229

Plavec, M.J. 1980, In *Close Binary Stars: Observations and Interpretation – I.A.U. Symp. No. 88*, ed. Plavec, M.J. (Dordrecht, Holland: D. Reidel. Publ. Co.), 251

Plavec, M.J. 1983, ApJ, **275**, 251

Plavec, M.J., & Koch, R.H. 1978, IBVS, **1482**

Plavec, M.J., Weiland, J.L., & Dobias, J.J. 1982, In *Advances in Ultraviolet Astronomy*, ed. Kondo, Y., Mead, J.L., & Chapman, R.D. (National Technical Information Service, Springfield, Virginia), 550

Popper, D.M. 1957, ApJ, **126**, 53

Popper, D.M. 1967, PASP, **79**, 493

Popper, D. M. 1982, PASP, **94**, 945

Popper, D.M. 1989, ApJS, **71**, 595

Popper, D.M., & Tomkin, J. 1984, ApJ, **285**, 208

Rossiter, R.A. 1924, ApJ, **60**, 15

Rucinski, S.M. 1979, Acta Astr., **29**, 339

Rucinski, S.M. 1992, AJ, **104**, 1968

Shajn, G., & Struve, O. 1929, MNRAS, **89**, 222

Slettebak, A. 1985, In *Calibration of Fundamental Stellar Quantities*, ed. Hayes, D.S., Pasinetti, L.E., & Davis, P.A.G. (D. Reidel Pub. Co., Boston), 163

Struve, O. 1945, ApJ, **102**, 74

Struve, O. 1946, ApJ, **104**, 253

Struve, O., & Elvey, C.T. 1934, ApJ, **79**, 409

Stumpff, P. 1980, A&AS, **41**, 1

Terrell, D., Mukherjee, J., & Wilson, R.E. 1992, *Binary Stars: A Pictorial Atlas.* (Krieger Publishing Company, Malabar, Florida)

Tomkin, J. 1981, ApJ, **244**, 546

Tomkin, J., & Lambert, D.L. 1978, ApJ, **222**, L119

Tremko, J., & Bakos, G.A. 1976, Bull. Astron. Inst. Czech. **28**, 41

Twigg, L. 1979, Ph.D. dissertation, *An Analysis of the Rossiter Effect in Algol-type Eclipsing Binary Systems*, University of Florida, Gainesville

Van Hamme, W., & Wilson, R.E. 1986a, ApJ, **307**, 151

Van Hamme, W., & Wilson, R.E. 1986b, AJ, **92**, 1168

Van Hamme, W., & Wilson, R.E. 1990, AJ, **100**, 1981

Van Hamme, W., & Wilson, R.E. 1993, MNRAS, **262**, 220

Vogt, S.S., Penrod, G.D., & Hatzes, A.P. 1987, **321**, 496

Wilson, R.E. 1979, ApJ, **234**, 1054

Wilson, R.E. 1988, In *Critical Observations Versus Physical Models for Close Binary Systems*, ed. Leung, K.C. (Gordon and Breach Science Publishers, New York), 204

Wilson, R.E. 1989a, Space Science Reviews, **50**, 191

Wilson, R.E. 1989b, Space Science Reviews, **50**, 235

Wilson, R.E., & Biermann, P. 1976, A&A, **48**, 349

Wilson, R.E., & Devinney, E.J. 1971, ApJ, **166**, 605

Wilson, R.E., Liou, J.C., Mukherjee, J., & Terrell, D. 1992, In *Robotic Observatories- Present and Future*, ed. Baliunas, S.L., and Richard, J.L. (Fairborn Press, Mesa, Arizona), 85

Wilson, R.E., & Mukherjee, J. 1988, AJ, **96**, 747

Wilson, R.E., & Plavec, M.J. 1988, AJ, **95**, 1828

Wilson, R.E., & Stothers, R. 1975, MNRAS, **170**, 497

Wilson, R.E., & Twigg, L.W. 1980, In *Close Binary Stars: Observations and Interpretation*, eds. Plavec, M.J., Popper, D.M., & Ulrich, R.K. (Dordrecht, Holland: D. Reidel. Publ. Co.), 263

Wilson, R.E., Van Hamme, W., & Pettera., L.E. 1985, ApJ, **289**, 748

Wlodarcyk, K. 1983, Acta Astr., **34**, 1

Young, A., & Snyder, J.A. 1982, ApJ, **262**, 269
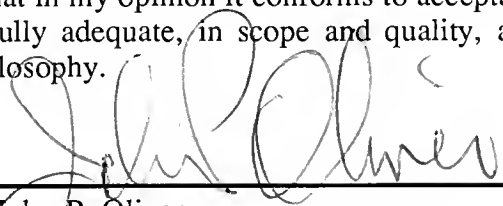
BIOGRAPHICAL SKETCH

Jaydeep Mukherjee was born in Calcutta, India, on October 10, 1961. His family moved to Bombay, India, in 1962, and he graduated from St. Theresa's High School, Bombay in 1977. He earned a B.Sc. in Physics from St Xavier's College in Bombay in 1981 and joined the master's program at Bombay University. He received his M.Sc. degree in physics from Bombay University in 1984. In 1985 he enrolled at the University of Florida, Gainesville. He completed his master's degree in 1988 and will receive his Ph.D. degree in astronomy in December of 1993.

I certify that I have read this study and that in my opinion it conforms to acceptable standards of scholarly presentation and is fully adequate, in scope and quality, as a dissertation for the degree of Doctor of Philosophy.
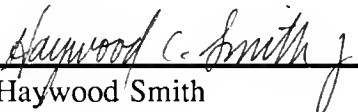
Robert E. Wilson, Chair
Professor of Astronomy

I certify that I have read this study and that in my opinion it conforms to acceptable standards of scholarly presentation and is fully adequate, in scope and quality, as a dissertation for the degree of Doctor of Philosophy.

John P. Oliver
Associate Professor of Astronomy

I certify that I have read this study and that in my opinion it conforms to acceptable standards of scholarly presentation and is fully adequate, in scope and quality, as a dissertation for the degree of Doctor of Philosophy.
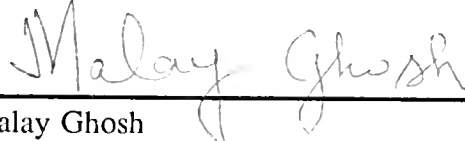
Haywood Smith
Associate Professor of Astronomy

I certify that I have read this study and that in my opinion it conforms to acceptable standards of scholarly presentation and is fully adequate, in scope and quality, as a dissertation for the degree of Doctor of Philosophy.

Stanley Dermott
Professor of Astronomy

I certify that I have read this study and that in my opinion it conforms to acceptable standards of scholarly presentation and is fully adequate, in scope and quality, as a dissertation for the degree of Doctor of Philosophy.

Malay Ghosh

Malay Ghosh
Professor of Statistics

This dissertation was submitted to the Graduate Faculty of the Department of Astronomy in the College of Liberal Arts and Sciences and to the Graduate School and was accepted as partial fulfillment of the requirements for the degree of Doctor of Philosophy.

December 1993

Dean, Graduate School